1980

Concrete railroad viaducts with maintenance free track support system, M.S. thesis, December 1980

Daniel H. Lavanchy

CONCRETE RAILROAD VIADUCTS WITH "MAINTENANCE FREE" TRACK SUPPORT SYSTEM

by

Daniel H. Lavanchy

A Thesis

Presented to the Graduate Committee

of Lehigh University

in Candidacy for the Degree of

Master of Science

in

Civil Engineering

Lehigh University

1980

This thesis is accepted and approved in partial fulfillment of the requirements for the degree of Master of Science.

December 10, 1980

(date)

Professor in charge

Professor in charge

Chairman of Civil Engineering Department

A

ACKNOWLEDGMENTS

The author wishes to express his deep appreciation for the supervision, advice, and review of the manuscript by Drs. Ben T. Yen and J. Hartley Daniels, professors in charge of this thesis. The help provided by Dr. Roger G. Slutter is also sincerely appreciated.

The experimental and analytical study was conducted at Fritz Engineering Laboratory, Lehigh University, Bethlehem, Pennsylvania. Dr. Lynn S. Beedle is Director of Fritz Engineering Laboratory and Dr. David A. VanHorn is Chairman of the Department of Civil Engineering.

The author also wishes to thank Mr. Tom B. Benner of Gannett Fleming Corddry and Carpenter, Inc. and Mr. Don Wolf of the Port Authority Transit Corporation for their help in furnishing the basic data used for this study.

The author is indebted to his colleagues at Fritz Engineering Laboratory. Their many lively and helpful discussions were of great value to the author. In particular, thanks are due to Mr. Robert J. McDermott for his help and advise in conducting the tests.

Thanks are extended to Ms. Barabara Bryan for her great help in the preparation of the manuscript. Thanks go also to Mr. John Gera and Mrs. Sharon Balogh for preparing some of the drawings. And last but not least, many thanks go to Mrs. Dorothy Fielding for her careful typing of this thesis.

TABLE OF CONTENTS

TABLE OF CONTENTS (continued)

TABLE OF CONTENTS (continued)

LIST OF TABLES

LIST OF TABLES (continued)

LIST OF FIGURES

LIST OF FIGURES (continued)

LIST OF FIGURES (continued)

LIST OF FIGURES (continued)

LIST OF FIGURES (continued)

ABSTRACT

Track support systems which require little maintenance in keeping proper grade and alignment are first developed for rails on ground and then are used on viaducts. A review of some of the most important experiments conducted throughout the world is presented in the beginning of this thesis.

The Collingswood and Westmont viaducts in the Philadelphia-Lindenwald Rapid Transit Line are two existing cases of tracks supported directly on concrete viaducts. Finite element models are used in this thesis to evaluate the forces in the rails and the displacements of the viaduct. Differential changes of temperature in the rails and the concrete are found to be the primary cause of undesirable forces and displacements. The rails and the concrete viaduct behave as a composite structure and the anchorage between the rails and the slab is a significant factor.

Brief discussions on different arrangements to avoid some of the undesirable conditions of the Collingswood and Westmont viaducts are made. Possible corrections to the two viaducts are also presented.

1. INTRODUCTION

1.1 Background

1.1.1 Conventional Railway Track Support System (CRTSS)

A conventional railway track support system (CRTSS) consists of rails, tie-plates, wood ties and ballast[1]. The rails are set on the tie-plates to reduce crushing and abrasion of ties. Wood ties are still widely used in the United States. European countries and the Japanese have increased the use of concrete ties in the last few years. The ballast can consist of materials like crushed stone, traprock, slag, etc. The American Railway Engineering Association (AREA) recommends a well-graded gravel for the ballast.

The CRTSS was first developed for use where tracks are supported on soil. An example of arrangement is shown in Fig. 1[1]. The system was then extended for use with concrete railroad viaducts. A conventional concrete railroad viaduct is shown in Fig. 2[2]. For the track on soil a subballast may be necessary between the ballast and some soils of inadequate quality. The subballast may consist of a wide range of materials including well-graded granular materials and stabilized soil.

During construction the track is adjusted to the correct grade and alignment by tamping the ballast. The track will then settle under loading as the railway is in service. This track settlement is due to the consolidation and the degradation of the

ballast. The amplitude of settlement is a function of traffic, loading, drainage, and other track conditions[3]. Continual maintenance work is necessary to correct the deformation of the CRTSS. This work basically consists of retamping at periodic intervals to maintain proper grade and alignment.

The main advantage of the CRTSS is its low construction cost. Construction materials can be found easily almost everywhere. Also the system can be adapted for almost all kinds of soils. The disadvantage is the necessity of continual maintenance which is time consuming and costly. With the development of high speed trains in Japan and Europe, and now in America, close tolerances of track grade and alignment are essential. The required tolerances can no longer be economically maintained with the CRTSS.

1.1.2 "Maintenance Free" Track Support Systems

Several research studies have been performed in search for track support systems which require little or no maintenance to remain within close tolerances of tracks required for high speed trains[4,5,6,7]. Current track research is oriented toward the development of a concrete slab railway track support system with the rails fastened indirectly to the concrete slab. Such a system not only permits establishing and maintaining more precise track grade and alignment, but the continuous support for the rails make it possible to use low profile rail sections. Furthermore, the uniform distribution of loads over the subgrade can in some cases eliminate the need for subballast or the removing of unsuitable

subgrade material. The saving of cost from maintenance and subgrade work may offset the higher initial cost of the concrete slab.

The application of the concrete slab railway track support system for viaducts is much less advanced than its use for tracks on soil. Only a few tests on viaducts have been done[4,8] and there are important problems for which a solution has not yet been found. Can the normal slab of the viaduct be used as a track support system? How should the viaduct be designed so that the interaction between the steel rails and the concrete will not create undesirable effects in the structural components of the viaduct, or in the rails, particularly in the case of continuous rails?

The Collingswood and Westmont viaducts on the Delaware River Port Authority's Philadelphia-Lindenwald Rapid Transit Line employ a concrete slab track support system and continuous rails, and have experienced undesirable displacements since their construction in 1968. These displacements have resulted in slight damage to the two structures, and are probably related to the fracture of insulation joints of the continuous rails at two locations. Preliminary assessments indicated that these undesirable events were induced by responses of the structures to thermal changes.

1.2 Purpose and Scope

The purpose of this thesis is to study the track support system at Collingswood and Westmont viaducts. The study is divided into 3 parts.

1. A review of the concrete slab track support systems recently studied throughout the world to compare them with the features of Westmont and Collingswood viaducts.
2. A theoretical analysis of the Collingswood and Westmont viaducts to examine the behavior of these structures under temperature changes. The distribution of forces in the superstructures was studied to determine how the observed damages could have occurred.
3. A brief discussion of possible arrangements for future concrete railroad viaducts supporting continuous rails so as to avoid some of the difficulties observed on the Westmont and Collingswood viaducts. Through this discussion, possible corrections to the two viaducts are suggested.

Part one consists of Chapters 2 and 3. Chapter 4 and 5 describe the finite element models developed for the analysis; Chapter 6 examines the results of computation and correlates with actual observations. These three chapters constitute the second part of the thesis. The third part is Chapter 7. All the conclusions from these three parts are summarized in Chapter 8.

For the entire thesis, SI units have been adopted. All the dimensions given in the figures are in millimeters (mm) for lengths smaller than 10 meters. For lengths greater than or equal to 10 meters, dimensions are in meters (m).

2. CONCRETE SLAB TRACK SUPPORT SYSTEMS

2.1 Development of Concrete Track Slab

2.1.1 Japanese National Railway (JNR)

(a) Japanese Railroad Association (JRA) Track-Slab

Since 1924 the JNR has tested many kinds of concrete-slab track supports[4]. One of the latest is the JRA track-slab. It consists of a 160 mm thick precast reinforced concrete slab supported and locked in by a 50 mm thick asphalt layer as shown in Fig. 3. The rails are anchored to the slab with a type of compression rail anchor. The rails are continuously supported in the vertical direction.

The construction of this type of track is accomplished in three steps:

1. The slabs are laid temporarily and the rails are fixed.
2. Asphalt is poured under the slabs and into the pockets between the rails.
3. Adjustment of the track is achieved by raising the slabs and injecting quick-hardening fillers.

The tests of these concrete slabs were first conducted for tracks on soil, but with the idea that this kind of construction could also be used on viaducts. A slab on a viaduct structure is also shown in Fig. 3 to indicate the arrangement.

The results of the tests have not yet been published, so the exact behavior of this slab is not known. By observation of the drawing of this track support system it is possible to make the following remarks:

1. The simple design of the slab enables easy construction on soil.
2. The asphalt pockets provide some restraint to possible horizontal movement of the slab with respect to the asphalt layer.
3. The cost of this type of track support system on viaducts may be high because it is necessary to have a viaduct slab under the asphalt layer.
4. There is no connection system to attach the track-slab to the viaduct slab. The relative movement of one slab to the other can create large forces in the rails, and may lead to damages in the track system.

(b) Standard Concrete Slab

There are two kinds of standard concrete slab track support in use on JNR lines, both primarily designed for tunnels[4]. One is a concrete slab into which concrete blocks are embedded as shown in Fig. 4. This is used on straight tracks. The other type, shown in Fig. 5, used wood blocks. This type is used on curves because exact position of the rails is more easily adjusted on wood blocks.

In both kinds of standard track-slab, a rubber pad is inserted under the rail and under the baseplate to provide a spring

constant of about 35,000 N/mm in the vertical direction. That is about the same elasticity as provided by the ballast, and it helps to diminish traffic noise.

The concrete block is anchored to the concrete slab by an anchor bar and the wood block by an anchor bolt as shown in Figs. 4 and 5. This is intended to resist the 100 to 200 N of uplifting force which is likely to occur when the train is running.

The laying of the track has also required several studies[4]. The actual technique used consists of laying out the rails on temporary supports adjusted to the correct line and grade. Then the concrete blocks are suspended from the rails by their fastenings, after the position of the rails has been checked again, the concrete slab is poured. With this technique, the track laying can be completed to an accuracy of 0.5 mm so far as gauge, alignment, track grade and superelevation are concerned.

The standard concrete slab track support has both the advantage of low maintenance and great accuracy in location of the rails. The main disadvantage is the cost of construction. The large volume of concrete involved cannot be placed quickly, and a team of 30 men can complete only 40 m of track in one day, as compared to 500 to 1000 m of conventional ballasted track[4].

(c) Japanese Railroad Maintenance (JRM) Track

Conscious of some disadvantages mentioned for the JRA track-slab, the JNR developed the JRM track-slab[4]. It is composed of

precast concrete supports placed at fixed intervals in a road bed in tunnels or on soil. These supports carry a precast concrete track-slab on which the rails are anchored. The concrete track-slab is prestressed longitudinally and is secured to the supports by springs. Adjustable rubber mats are inserted at joints so that the concrete track-slab is supported by mats vertically, laterally, and longitudinally. A perspective of the JRM track-slab is shown in Fig. 16.

The construction of this track-slab is performed in three steps:

1. The supports are laid in place and secured on the road by the mortar or concrete.
2. The track-slab is temporarily laid on the supports, and after fastening the rails to the slab, the rail alignment is adjusted using jacks on the track-slab.
3. The rubber mats are inserted to maintain position of the track-slab.

This kind of track system is very expensive because of the complexity of the joints. It may still be attractive for use in viaducts because a viaduct slab can be reduced in size or be eliminated totally.

An important fact to note is that the anchorage between the track-slab and the concrete supports is not rigid. This lack of connection can generate large forces in the rails and joints and may lead to damages.

2.1.2 British Railways (BR)

The British Railways' experiments with concrete track-slab started from two observations[5]:

1. In the tests carried out by the JNR, track support is created by assembling precast concrete units. This limits the size of the units and makes it necessary to provide joints between units. The inclusion of joints creates many difficulties. Thus it is considered undesirable to combine a continuous rail with a discontinuous track support.
2. In the last twenty years great developments have been made in road-paving machinery. These machines can lay continuous reinforced concrete roadways to a very high standard of accuracy without the use of side forms.

These two observations led the BR to test a 72 m long reinforced concrete slab laid by machine. A cross-section of the slab is shown in Fig. 7. The rails are directly fixed to the slab by clips which are glued with epoxy into holes drilled in the concrete.

It is necesary for the BR to test their design on a larger scale before making any decision, but some future applications can already be considered. For example, a study is being performed to determine the feasibility of using the direct-laying system on viaducts by placing the reinforced concrete track-slab directly on a structural slab.

The major problem with the BR system is the cost of construction. Significant cost reduction can be expected with new machines and better design.

2.1.3 German Federal Railway (DB)

Several studies have led the DB to the conclusion that the upper speed limit for trains on a conventional railway track support system (CRTSS) may be regarded as 260 km/h[6]. For higher train speeds the DB has formulated six requirements for the design of concrete track-slabs.

1. Connection between individual slabs to be as firm as possible.
2. Prefabrication of components, which must be suitable for fully mechanized tracklaying.
3. A frostproof supporting layer to avoid distortion by frost heave.
4. Generously dimensioned rail fastenings with the possibility of a certain amount of height adjustment.
5. Precise maintenance of gauge at the highest speeds.
6. Minimum maintenance requirements.

Several designs were developed as a joint effort by the DB, the German concrete industry, and Munich Technical University. One of these designs, tested on the high-speed experimental line between Forchheim and Bamberg in the Nuremberg District, is shown in Fig. 8. This design consists of track-slabs prestressed transversely and longitudinally. These slabs are connected by full-load carrying

Thermit steel pipe muff joints to take up transverse and longitudinal forces and bending moments. The 300 mm thick layer of sandy gravel is made to act as low-strength concrete in its upper part by the addition of a small amount of cement.

Technically, this track design creates a continuous support for a continuous rail. It also gives a good distribution of stresses in the soil under the track, especially for high axle-loads, and offers the possibility of building the track with great accuracy.

The main disadvantages are the construction cost (more than twice as high as for the CRTSS) and the difficulties in adapting this design to viaducts.

2.1.4 American Experiments

The first known tests of concrete track-slab in the United States began in 1975 in Kansas with a study of the Santa Fe Railroad. Unfortunately, the slabs were abandoned after the fasteners connecting the rails to the slabs popped out and a significant distortion of the subgrade damaged the slab.

In the summer of 1979 the Long Island Railroad (LIRR) began construction of a mile of "maintenance free" track[7]. This track consists of a 305 mm thick reinforced concrete slab with a rectangular cross-section. The concrete is poured in place and finished with a standard highway screed.

One of the most attractive features of this experiment is that two steel bridges and a reinforced concrete viaduct are included

in the project. On these structures the thickness of the track-slab was reduced from 305 mm to 229 mm to reduce the dead load.

The tests began during the summer of 1980 and no technical results are available. If the tests are successful the trains now traveling over a temporary track will be rerouted to the new slab.

2.2 Application to Railroad Viaducts

2.2.1 The Tokaido Line

In 1971 the JNR made the decision to build a 3 km test segment of elevated viaduct structure with a concrete slab[8]. The objective was to produce a maintenance free road bed. This test segment appears to be the only one undertaken on a large scale that has rails directly anchored to a concrete track-slab on viaducts.

The structure of the track-slab is shown in Fig. 9. A pre-stressed concrete slab 5000 mm by 2340 mm is laid, and cement mortar mixed with asphalt emulsion is poured under it. After the mortar hardens, the rails are fastened to the concrete slab. Posts anchored to the viaduct deck help in positioning of the track-slabs.

No results of the test segment has been published by the JNR, but three disadvantages of such a support system can be mentioned:

1. The relative complexity of the prestressed concrete slab makes this structure expensive.

2. The assembly of the five meter long slabs necessitates joints, creating a discontinuous foundation for continuous rails.
3. The short length of the track-slab makes it necessary to have a viaduct slab with two slabs, one on the other.

2.2.2 The French National Railway

The French National Railway (SNCF) is currently building a new 400 km line between Paris and Lyon which will be open to traffic in 1983. On this line the trains will reach a speed of 300 km/h[9].

The viaducts over the rivers are of cast-in-place prestressed concrete and are constructed by the launching method[10]. A cross section of one of the continuous viaducts is shown in Fig. 10. The concrete box-section supports a layer of ballast on which the concrete/steel ties are placed.

In contrast to the studies done by the DB, the SNCF has found that very high speed can be reached with the conventional railway track support system (CRTSS). The advantages of the ballast are to absorb the noise created by the traffic and to reduce the number of expansion joints in the continuously-welded rails. The use of the CRTSS is justified by the fact that the maximum load on this line will be 170 kN per axle.

The same approach is used for continuous steel-concrete composite bridges, which have a smaller span length than the box

girder viaducts shown in Fig. 10. The cross section of the composite bridges is shown in Fig. 11. The steel I-beams are embedded in the concrete deck. This gives the deck greater rigidity which is necessary to limit the deflection for the high speed traffic. The ballast is laid on the deck. The ties are placed in the same manner as for the box girder viaducts.

From this example two observations can be made: first, the DB and the SNCF studies give different ranges of use of the CRTSS as judged by the maximum speed; second, the ballasted deck viaducts are not out-of-date and in certain cases they can still be considered as the best solution.

3. COLLINGSWOOD AND WESTMONT VIADUCTS

Collingswood and Westmont Viaducts are at the stations with the respective names in the Philadelphia-Lindenwald Rapid Transit Line. Figure 12 is a photograph of the Westmont viaduct looking towards the station. The viaducts use a single layer of concrete slab as support for the continuous rails. The rails are fastened to the slabs. Thus the viaducts can be regarded as among the most advanced "maintenance free" track support systems.

3.1 Characteristics of the Viaducts

Based on the drawings from the designer[11] and on the results of field inspections, the features and characteristics of each viaduct are as described below. The essential information is also summarized in Table 1.

3.1.1 Collingswood Viaduct

A plan of the Collingswood viaduct is shown in Fig. 13. The viaduct is 727.2 m long and is composed of 34 single spans. The first 18 spans are straight, each consisting of 4 prestressed concrete I-beams on hammerhead piers and supporting a 203 mm thick reinforced concrete slab. A typical cross section of the first 18 spans is shown in Fig. 14.

The width of the viaduct gradually increases from pier 18 to pier 25 to accommodate the Collingswood station. The number of

prestressed concrete I-beams increases accordingly from 4 to 6. A cross section of the viaduct in the vicinity of the station is shown in Fig. 15.

The station is situated between the two tracks on spans 25 to 29. The westbound track is straight for the entire length of the viaduct. The eastbound track curves slightly as it passes on the other side of the station as shown in Fig. 13. From pier 29 towards the end of the viaduct, the width of viaduct gradually decreases with the number of I-beams per span.

The dimensions of the I-beams vary from one span to another. Six types of I-beams are used with heights varying from 1.14 m to 1.57 m. The bottom widths of the I-beams vary from 610 mm to 660 mm. The I-beams are prefabricated. The prestress forces are applied through pre-tensioning and varies from 3475 kN to 5695 kN[11]. The prestressing steel consists of 36 to 59 seven-wire strands and the steel areas vary from 26.7 cm^2 to 43.8 cm^2.

The reinforced concrete slab was poured-in-place to create a composite section with the I-beams. The slab is 203 mm thick for the complete length of the viaduct. Its width varies from 7.95 m to 15.00 m according to the width of the viaduct.

The slab reinforcement is the same top and bottom and consists of #5 bars (area 200 mm^2) longitudinally with a spacing of 203 mm and by #6 bars (area 284 mm^2) transversely at 130 mm spacing. The transverse steel is closer to the surfaces of the slab than the longitudinal steel.

An elevation of the first several spans of the Collingswood viaduct is shown in Fig. 16. Figure 17 is a photograph showing one complete span. Each span is a "simple" span with a fixed bearing at one end and an expansion bearing at the other. The fixed bearings of two adjacent spans are located on the same pier. The bearings for all spans less than 25 m consist of 38 mm thick 60 Durometer Neoprene bearing pads. The bearing pads, which vary in width and length, are simply placed between the I-beams and the top of the piers at expansion bearing. There is no provision to maintain the pads in place. At the fixed bearings, each I-beam is anchored to the pier by two 29 mm diameter plain bars through the bearing pad as shown in Fig. 18. At these locations a diaphragm of reinforced concrete is also placed between the exterior beams.

The bearing pads are composed of only one 38 mm thick layer of Neoprene. This is contrary to recommendations requiring the pads to be made up of several layers each with a maximum thickness of 12.5 and separated by bonded metal plates or fabric sheets[12].

For all spans longer than 25 m, the expansion bearings consist of a steel roller of 101.6 mm diameter under each beam. A steel shoe is used at the fixed bearing.

Above the simple-span composite concrete section, the rails are continuous and are anchored to the reinforced concrete slab. Figure 19 is a photograph showing the continuous rails over the joint in the slab between two spans and showing the anchorages of

the rails. The rails are placed on tie plates and elastometric pads which provide an electric insulation of the rails. Figure 20 is a transverse cross section through a rail and the compression rail anchorage. The compression rail clip secure the rail to the tie plate while the tie plate and elastometric pads are bolted to the concrete slab by anchor bolts with insulation. The compression rail clip and the anchor bolts are staggered in position. To achieve proper pressure, the profile of the compression rail clip is adjusted to match that of a template. The anchor bolts are tightened by using a torque wrench.

For the operation of the signaling system fiberglass joints exist on the rails near the station as shown on the photograph of Fig. 21. These joints are near or directly above a joint between the reinforced concrete slabs of two spans. Two fiberglass strips one on each side of the web are bolted to the abutting rails to form an electric insulation joint. Figure 22 shows the dimensions of the fiberglass strips used to create the joint. Each strip of fiberglass has a cross-sectional area of 3630 mm^2. The bolts are 25 mm in diameter.

3.1.2 Westmont Viaduct

The essential components of the Westmont Viaduct are arranged in the same manner as for the Collingswood viaduct. The primary difference is the curvature. The Westmont viaduct is 600 m long with a 3000 m radius curve on the first 350 m and a straight section for the last 250 m as shown in Fig. 23.

The viaduct is composed of 27 simple spans. The first 12 spans each have 4 prestressed concrete I-beams on hammerhead piers and supporting the reinforced concrete slab. The width of the viaduct gradually increases from pier 10 to pier 18 to accommodate the Westmont station and the number of prestressed concrete I-beams per span increases from 4 to 6 as in the case of the Collingswood viaduct.

The dimensions of the prestressed I-beams vary from one span to another. Five types of I-beams are used with heights varying from 1.07 m to 1.52 m. The bottom width of the I-beams measures 610 mm. The pre-tensioning prestress forces vary from 2993 kN to 5605 kN[11]. The prestressing steel consists of 31 to 58 seven-wire strands and its area varies from 23.0 cm^2 to 43.0 cm^2.

The reinforced concrete slab, 203 mm thick, has reinforcement exactly the same as for the Collingswood viaduct slab. The width of the slab varies from 7.95 m at locations with 4 I-beams to 15.00 m at the widest point.

The fixed and expansion bearings are all identical to those of the Collingswood viaduct, except the thickness of the Neoprene pad, the size of the steel roller, and the anchorage dowels at the fixed bearings. For the viaduct the single layer Durometer Neoprene bearing pads are 25 mm thick and the steel rollers are 127 mm diameter. While the dowels are between the beams and the piers at the Collingswood viaduct, the 25 mm diameter plain bar dowels at the fixed bearings of the Westmont viaduct are between the reinforced concrete diaphragms and the piers as shown in Fig. 24.

The diaphragms are placed between and rigidly connected to the exterior beam and the adjacent interior beam at all fixed bearings.

3.2 Comparison with Other Systems

From the features of the Collingswood and Westmont viaducts, it is observed that these viaducts are different from the European and Japanese experimental systems and are similar to that of the Long Island Railroad concrete viaduct. The Tokaido Line viaduct of Japanese National Railway (see Article 2.2.1) has a track-slab over the viaduct slab; the French National Railway viaducts (see Art. 2.2.2) use the conventional railway track support system with ties and ballast. These features do not exist in the Philadelphia-Lindenwald viaducts. The anchorage of continuous rails to the viaduct slab of single spans is unique to these viaducts and the Long Island Railroad (LIRR) viaduct.

While the experiments in LIRR are being conducted, the viaducts at Collingswood and Westmont have had nine years of service life. Results of inspection indicate that, although the railway track support system is by and large maintenance free, it is not without problems. For the evaluation of the problems, a "structural" review of the specific features of these viaducts may help to focus attention on possible causes.

The most outstanding character of the viaducts is the anchorage of the continuous rails to the simple span composite beams-slab. For the purpose of maintaining track position, the

rails are attached to the tie plates by compression rail clips with a predetermined force in the clip bolts. The tie plates and the insulation pads are firmly anchored to the viaduct slab. This anchorage of rails to the slab, although indirect, made the rails "composite" with the concrete viaduct spans. Consequently, the deflection and rotation of any simple span beam-slab in the viaduct affect the behavior of the continuous rails. Also any change of force or displacement of the continuous rails induces change of behavior to the beam-slab spans. This phenomenon is not expected of the Tokaido Line of JNR or the French National Railway viaduct because the anchorage between the track support system and the viaduct slab is either not firm or not provided.

Since the rails were laid after the construction of the spans, the dead weight of the viaduct does not affect the force or displacement of the rails. The response of the viaduct system to live load is not expected to be pronounced because of the relatively light weight of the trains. The live load deflections of the spans are expected to be very small. Furthermore, because of the smoothness of the continuous track rails the dynamic effects of the trains on the viaduct are very low.

The effects of temperature variations, however, could be amplified by the composite nature of the continuous rails. The single span, composite, prestressed-reinforced concrete beam-slabs are subject to change of stresses when temperature changes. With the continuity of the anchored rails and their suspectability to

high change of temperatures, the change of behavior of the viaduct spans could be fairly high or even very high. This unique character of the Collingswood and Westmont viaducts could be the cause of their problems.

3.3 Observed Behavior and Damages

Inspections of the viaducts revealed that there were damages to the structures and fiberglass joints of the rails.

In the Winter of 1975-76 the fiberglass strips of four rails broke at pier 23 of the Collingswood viaduct. Four fiberglass strips of the westbound track of the Westmont viaduct also broke during the same winter. It is only because of the intervention of the maintenance crew that the four fiberglass strips of the eastbound track did not break. The location of these breaks are marked by an "F" in Figs. 13 and 23 for the two viaducts, respectively.

The bearing pads between the prestressed concrete beams and the piers experienced displacements. At pier 1 of the Collingswood viaduct the bearing pads under the two longest beams displaced toward the abutment about 38 mm, and are clearly visible.

Almost all bearing pads of the Westmont viaduct have experienced significant displacements. These displacements act in the longitudinal and transverse direction of the viaduct. The longitudinal motions are always oriented towards the center of the

spans with some measured displacements which exceed 63 mm. The transverse motions of the pads are always towards the exterior of the viaduct. On top of the Neoprene bearing pads some signs of wear can be observed, indicating that the beams are moving relative to the bearing pads.

At all slabs and beams of the two viaducts, no visual damage had been observed except that a corner of a prestressed concrete I-beam, 65 mm by 30 mm, broke off at pier 18 of the Westmont viaduct. Damages are observed at the diaphragm on top of pier 15 in the Westmont viaduct. This pier constitutes a fixed support for two adjacent spans and is built as shown in Fig. 24. The reinforced concrete diaphragm and the top of the pier have spalled such that the 25 mm diameter steel bars are visible. These damages appear on both faces of the pier under both diaphragms of each span. At pier 19 a similar fixed support, the reinforced concrete diaphragm between the two beams under the eastbound track is broken on its entire height. Each piece of the diaphragm is still rigidly connected to a different beam. A relative displacement of about 25 mm between each piece of the diaphragm can be observed in the direction of the viaduct.

No relative displacement is observed between the slab and the beams of the composite structure. Careful examination of the compression rail anchors reveal that there is no relative movement between the rail and the tie plates when trains pass by. However, there are markings on the rails indicating that there exist relative

displacements between them at the ends of spans. The compression rail anchors move toward the center of the spans relative to the rails during cold months of the year. This condition suggests that temperature effects maybe responsible for the movements, and damages. Analysis of the viaduct structures to examine temperature effects is therefore given primary attention.

4. FINITE ELEMENT MODELS

4.1 General Concepts

Because of the complexity of the structures, analyses by finite element models are chosen. All finite element models of this study are made using the SAP IV computer program[14] and the CDC 6400 computer at Lehigh University. To keep within the limitations of the computer and program and to ensure proficiency of computation, all the models are two-dimensional. This simplification provides displacements and stresses in the longitudinal and vertical directions of the viaducts as well as transverse reactional forces at the piers. The three-dimensional characteristics of the viaducts are taken into account in computing the characteristics of the finite elements.

Two models simulate respectively the complete viaduct structures of the Collingswood and the Westmont spans. The third is a one-span model for more detailed examination of the temperature stresses and displacements in the viaduct spans.

4.2 Models of Complete Viaducts

The objectives in developing a finite element model of a complete viaduct are to determine the axial force in the rails at different temperatures and to obtain displacements of the beams-and-slab concrete section for the one-span model.

A number of conditions dictate or strongly influence the modeling. The most critical is the large number of elements necessary for simulating the entire structure and remaining within the capacity of the computer. In this regard the concrete beams-and-slab portion of each span is condensed to a beam of the same cross-sectional properties and is located at the centroid of the concrete portion. The continuous rails are also similarly condensed and placed. Between the centroids of the concrete and the steel parts, the distance is 635 mm and the two parts are connected by beam elements. The resulting model of the Collingswood and the Westmont viaduct have configurations as shown in Fig. 25.

For the Collingswood model each span has 14 nodal points, the Westmont model has 20. The element length within each span varies according to the span lengths. The length of the rail element between spans and directly over the piers is 762 mm long, the distance between rail anchors. This is necessary in order that representative forces in the rails can be computed for these locations.

The anchorage between the rails and the viaduct slab are represented by the vertical beam elements. The bending rigidity of these elements correspond to the reistance against relative movement between the rails and the slab. There is no available information for a direct correlation. Observations showed that at some compression rail anchors slip marks 25 mm long exist on the rails. After several trials, a moment of inertia of 42,000 cm^4

for the connecting elements is chosen. This moment of inertia allows a relative displacement between the rails and the concrete slab about 25 mm when an axial force of 10,000 kN is applied to the rails.

The placing of the concrete elements at the centroid of the concrete section requires that the bearings of the simple spans be also placed at the same level. This may cause errors in the results of computation if the ends of the concrete beams undergo large rotations. Preliminary evaluations showed that the end rotations of the beams were not large.

For Collingswood and Westmont viaducts the locations of the bearing points are defined by the curves of the axis of the viaducts, but the spans are all straight. This condition reflects the actual configuration of the prestressed concrete beams. The Collingswood viaduct is modeled as 34 straight simple spans with continuous rails. The model consists of 647 nodal points. The Westmont viaduct is modeled as 27 straight simple spans and the model consists of 678 nodal points.

For the model of both viaducts the bearings are assumed as fixed at all odd number piers and as expansion bearings at even number piers. This is the condition in the plan of each viaduct. However, because of the observed displacements at the fixed bearings as well as at the expansion ones, an alternate set of bearing conditions is assumed in that all bearings are the expansion

type. This condition of bearing is designated as E-E model in the analysis, and the fixed and expansion condition as E-F model.

At all expansion bearings, the boundary condition for the models are represented by horizontal boundary elements with shear stiffness of the bearing pads. This permits the beam to displace in the longitudinal and the transverse direction of the beam according to forces generated in the viaduct. At fixed bearings, the horizontal stiffness are given a very large value. The vertical stiffness of the bearing pads is adopted for all vertical boundary elements at fixed and expansion bearings. No torsion of the beams is permitted as the piers prevent any rotation of the viaduct superstructure.

4.3 One-Span Model

The objectives in developing a one-span finite element model are to determine the variation of the axial force in the rails within a span at different temperatures, to examine the stresses in the concrete slab and beams, and to evaluate the displacements at the bearings.

The one-span model is shown in Fig. 26. It has 292 nodal points. In this model the length of the elements representing the rails is 762 mm, the distance between two adjacent anchors of the rails to the slab. The reinforced concrete slab is modeled with plane stress elements. These elements are 203 mm high and 381 mm

long. The height is the actual thickness of the slab. The length was chosen to maintain an aspect ratio less than 2.

The vertical beam elements which connect the rail element nodal points to the slab element nodal points are 198 mm long. Their bending rigidity is to simulate the resistance of the anchors to the relative movement between the rails and the slab. A moment of inertia of 42,000 cm^4 is chosen for these vertical beam elements as for the similar elements in the models of the complete viaducts.

The prestressed concrete beams are also modeled with plane stress elements. Each element is 762 mm high and 381 mm long. The height of two elements is the depth of the prestressed concrete beam. The length of the element maintains an element aspect ratio of 2. Because the input to this one-span model is the span-end displacements, determined from the analysis of the Collingswood and Westmont viaduct models, boundary elements are located where the input displacements are applied at the level of the rails at nodal points between the slab and the beams which are nearest to the centroid of the composite slab and beam section and at nodal points nearest to the bearings.

5. EVALUATION OF FINITE ELEMENT MODELS

5.1 Assumed Temperature Variations

Since temperature effects are of primary concern, variations of temperature in the component parts of the viaduct need to be defined. Measurements of temperature at component parts of steel-concrete bridges have shown that the temperatures at the component part are different and also different from the air temperature. Figure 27 is a plot showing the variation of temperature with time for a concrete deck-steel girder bridge during early summer days. Depending on the weather condition, steel temperature rise and decline more than the air temperature does while the response of the concrete is delayed and less prominent. For the viaducts of the Philadelphia-Lindenwald Line, the steel rails are above the slab thus the differential change in temperature between the rails and the concrete beams are even more drastic.

There are no measurement data of temperature variations in the component parts of the viaducts. Record of construction and weather data indicate that the average air temperature on the day of laying the rails was 20° C (15). Based on the data of Fig. 27 and on information obtained on or near the site[16], two variations of temperature are arbitrarily assumed for the further analysis. These variations of temperature are defined as follows:

1. The Summer Conditions with an increase of

   temperature of: + 20° C for the rails

   + 7° C for the concrete

2. The winter conditions with a decrease of

   temperature of: - 38° C for the rails

   - 32° C for the concrete

In addition to the seasonal changes of temperature, daily fluctuations also cause differential temperatures in the component parts. The amplitudes of daily thermal changes are less than those of the annual changes, but the character of their effects on the viaduct structure is the same. For the evaluation of the models, the assumed annual changes are used.

5.2 Comparison between Viaduct and One-Span Models

As explained in Section 4.3 the one-span finite element model is developed to carry a finer analysis of the forces and stresses in single spans which compose the viaducts. The input for the one-span model are the displacements computed from the viaduct models. For this reason it is important to assure the existence of compatibility between the one-span model and the viaduct models. Direct comparison of the displacements computed by these models are made.

Figure 28 shows the absolute longitudinal displacements of the rails along span 6 of Collingswood viaduct as computed by the E-E viaduct model. For the assumed equivalent rigidity of the rail anchors and decrease of temperature in the component parts, the displacements of the rails are very small, in the order of a millimeter. In other words, the rails remain practically in position with respect to the ground.

By applying the boundary displacements of span 6 of the Collingswood E-E viaduct model to the one-span model and incorporating the same decreases in temperature, the longitudinal displacements of the rails in the one-span model are computed. Figure 29 shows the results. The rail displacements at both ends of the span are equal to those of the complete viaduct model. Within the span, the displacement curve has the same pattern as that in Fig. 28. This agreement is also confirmed for the concrete displacement. Figure 30 shows the longitudinal displacements of the concrete section in span 6 of Collingswood viaduct computed by the E-E viaduct model under the winter conditions. The variation of magnitude of longitudinal displacements of the concrete centroid along span 6 is almost linear. The two ends of the concrete portion move toward the center of the span and other cross sections move proportionally. Under decreasing temperatures, there is a contraction of the concrete section.

The corresponding longitudinal displacements of the concrete component computed by the one-span finite element model are

given in Fig. 31. The bottom of the slab is the nearest point to the centroid of the entire concrete section in the one-span model thus its longitudinal displacements are compared. The variation of the magnitude of the displacements given by the one-span model is almost linear between the ends, just as it is obtained from the E-E model.

From the above comparison of displacements, it can be concluded that there is compatibility between the one-span finite element model and the E-E model of the viaducts. The validity of the computational results from the one-span model must be evaluated against actual measurements at the viaducts to insure accuracy.

5.3 Comparison with Measured Displacements

In order to gain insight of the concrete slab displacements due to temperature changes, brass plugs 9 mm in diameter and 13 mm long were inserted into the slabs in pairs above a number of piers at both viaducts. These plugs are located midway between the rails and each pair of plugs serve as gage targets for a mechanical extensometer. The change of plug distance is the relative displacement between two adjacent slabs over a pier.

There are eleven pairs of plugs over six piers at the Collingswood and Westmont viaducts. Measurements of plug distances were made four times: in the morning and early afternoon of an early summer day (L_1 and L_2), at about the hottest time of a year in August (L_3), and during a cool morning in midfall (L_4). The

results of measurements are summarized and compared in Tables 2, 3 and 4.

In Table 2, the first column gives the location of the measurements. The first letter indicates the viaduct, C for Collingswood and W for Westmont; the number refers to the number of the pier over which the plugs were placed; and the last letter indicates location on the slab, E between the eastbound track rails and W between the westbound track rails. The second column gives the distance L_1 between the pairs of plugs measured early in the morning of June 29, 1980. The third column gives the corresponding distance L_2 measured later in the afternoon. The fourth column shows the difference ΔL between the two measurements, which is the relative displacement between the two plugs of each pair. The last column gives the average of ΔL at each pier, which represents the relative slab displacement at that pier. The suffix E and and F indicates the bearing condition being expanded or fixed.

Similar comparisons are tabulated in Tables 3 and 4 for a large increase of temperature $(L_3 - L_1)$ and a large decrease of temperature $(L_4 - L_2)$, respectively. The air temperature measured above the concrete slab at the level of the rails, are also given in the tables for each time when the relative slab displacements were measured. The significance of these results will be discussed later in Chapter 6. The main reason of presenting these data here is to evaluate the finite element models.

A comparison between the relative displacements given by the E-F finite element models, the E-E finite element models, and the measurements taken in-situ is shown in Table 5. The first column gives the locations where the displacements are compared. The second column gives the relative displacements at the centroid of the concrete segment as computed by the E-F model of the Collingswood and Westmont viaducts. These displacements are computed for the assumed summer increases of temperature as defined in Section 5.1 and listed in the table. The third column of Table 5 gives the corresponding relative displacements by the E-E viaduct models. The fourth column is the last column of Table 2. This is the average of the relative slab displacements measured at each pier.

The temperature difference was + 11.1^{o} C in the air for the measured displacements in the fourth column of Table 5. This change is comparable to the increases of temperature in the rails and the concrete which have been used to obtain the results of the E-F and E-E viaduct models in the second and third columns. Therefore, comparison of relative displacements can be made among the results. By comparing the second column with the fourth column, it can be seen that the relative displacements computed by the E-F finite element models are very different from those measured on the viaducts. This is particularly the case for the fixed bearings where the computed relative concrete displacements are zero and the measured relative slab displacements vary between 1.54 mm to 2.46 mm contraction.

On the other hand, the computed relative displacement by the E-E models are quite agreeable with those measured values, as it is evident from comparing the third and the fourth column. The fitth column of Table 5 gives the algebraic difference between the relative displacements computed by the E-E viaduct models of column 3 and the measured relative displacements of column 4. The last column gives the corresponding percent difference between the computed and the measured values, using the latter as a basis. The differences are within 18%. One of the causes for these differences is the assumed temperature change. The uniformity of the percentage nevertheless shows the validity of the E-E finite element model of the viaducts.

The measured change of air temperature between noon of a mid-summer day and the morning of a fall day was -32.2^{o} C. The measured relative slab displacement at the piers are listed in Table 4 and in the fourth column of Table 6. The slabs are moving away from each other during the cold months of the year. The columns of Table 6 are arranged in the same format as for Table 5. The air temperature change is again comparable to that assumed for the rails and the concrete segment. As for the case of Table 5, the E-E finite element models give results comparable with the field measurements. The last column of Table 6 shows that the differences in computed and measured relative displacements are acceptable, considering that the actual changes of temperature in the rails and the concrete were unknown for the computations.

Therefore, the E-E finite element model of the viaducts are used with the one-span models for analysis of the viaduct spans.

6. ANALYSIS OF RESULTS FROM COMPUTATION

6.1 Forces in Rails

Because there were fractured rail joints, the first items to be analyzed using the finite elements models are the forces in the rails. For the viaducts, factors affecting the rail forces include temperature changes, the rigidity of the rail anchoring device, and train loads. The effects of temperature is examined first.

6.1.1 Effects of Temperature Changes

In evaluating the finite elements models earlier, it has been shown that the ends of adjacent slabs move away from each other when temperature decreases. This generates tension in the rails over the piers. By applying the assumed decreases of temperature in Winter to the E-E viaduct models of the Collingswood and Westmont viaduct, the rail forces are computed. Figure 32 shows the calculated variation of forces in the rails on the Collingswood viaduct. The tension forces in the rails on the Collingswood viaduct. The tension force varies from 10,000 kN in the rail segment over a pier to 3500 kN at the middle of the spans. These forces are computed for 6 rails (of type 132 RE with the dimensions shown in Fig. 33). The maximum axial tension stress in each rail is 200 MPa (29 ksi). The tension stress at midspan is only 70 MPa (10 ksi).

For the Westmont viaduct under the same decreases of temperature, the computed variation of forces in the rails is presented in Fig. 34. The tension force varies from 8700 kN in the rail segment over a pier to 3700 kN at the middle of the spans. The maximum tension stress in the rails is 174 MPa (25 ksi). The tension stress at midspan is 74 MPa (11 ksi).

When the temperatures in viaduct components increase, the gap between ends of concrete slabs decrease and cause compression in the rails. Figure 35 shows the computed variation of forces in the rails on the Collingswood viaduct under the assumed increase of temperature in summer. The compression force varies from -5200 kN in the rail segment above a bearing to -3100 kN at the middle of the spans. These axial forces produce computed compressive axial stresses in the rails which vary from -104 MPa (15 ksi) to -62 MPa (9 ksi). In the case of the Westmont viaduct, the computed compression forces vary from -4600 kN in the rail segment above the bearings to -3000 kN at the middle of the spans. The corresponding axial compression stresses in the rails vary from -92 MPa (13 ksi) above the bearings to -60 MPa (9 ksi) at the middle of the spans.

These computed forces and stresses are summarized in Table 7. Also listed in the table are the change of temperature and the corresponding change of forces and stresses between the assumed extreme conditions of hot summer days and cold winter nights. Since the actual temperature in the rails and in the concrete are not certain, these computed forces and stresses may not be accurate.

However, results of measuring air temperature, as reported in Section 5.3, indicate that the assumed temperature changes are quite reasonable. Therefore, the computed changes of forces and stresses can be used as references for further discussions.

6.1.2 Comparison with Strength of Rails

The temperature-induced forces and stresses must be compared with the strength of the rails. Under severe decreases of temperature, the tensile stresses in the rails should not exceed the allowable stress. During hot summer days, the rails should not buckle because of high compressive forces.

The total tension in a rail is the sum of that due to temperature change and due to wheel loads of trains. The stresses caused by the dead weight of the rails are very small and can be ignored.

The rails under train loads can be treated as continuous beams subjected to concentrated wheel loads. The span of these continuous beams is 762 mm, the distance between two compression rail anchors. The wheel loads are at least 2286 mm apart for the railroad cars of this line, as furnished by the Port Authority Transit Corporation (PATCO). Therefore, the maximum bending moment can be approximated by placing a single wheel load at midspan of an equal-spanned continuous beam.

$$M = \frac{10}{64} PL \qquad (1)$$

where P is the wheel load and L the span length. The PATCO cars

have 8 wheels and weight 334 kN. Thus, P = 41.8 kN and M = 5 kN·m. The maximum bending stresses in the rails (with the cross section of Fig. 33) are 14 MPa (2 ksi). This is also quite low when compared to the highest computed tensile stress of 200 MPa (29 ksi) over the piers under winter conditions as listed in Table 7. Even if a dynamic factor of 2 is applied to the live load stress, it is only about 28 MPa (4 ksi). The maximum total tensile stress is then less than 200 + 28 = 228 MPa (33 ksi).

The allowable tensile stress is specified by the American Railway Engineering Association (AREA) to be $0.55\ F_y$[13]. For the 132 RE rails, the specified minimum yield point is F_y = 534 MPa (77.5 ksi)[17]. Therefore the allowable tensile stress is 294 MPa (42.6 ksi). This is higher than the maximum computed stress value of 214 MPa (31 ksi). The rails are not expected to have any problem in tension due to the effects of temperature changes.

During hot summer days, the total compressive stresses in the rails are the sum of the temperature-induced stresses and the bending stresses from the wheel loads. The maximum compressive stress from Table 7 is 104 MPa (15 ksi), and the wheel load stress is 28 MPa (4 ksi) including the contribution of dynamic effects. The total maximum compressive stress is 104 + 28 = 132 MPa (19 ksi).

Rails subject to high compressive stresses could buckle laterally. The rails are laterally supported at equal distances by compression rail anchors at both sides. Conservative estimates can be made by assuming that each segment of a rail between anchors is a

simple column subjected to combined axial forces and bending[18]. The AREA requirement[13] for combined axial and bending stress is

$$\frac{f_a}{F_a} + \frac{f_b}{F_b\left[1 - \frac{f_a}{200 \times 10^6}\left(\frac{KL}{r}\right)^2\right]} \leq 1.0 \qquad (2)$$

where

f_a = computed axial stress

F_a = axial stress that would be permitted if axial forces alone existed

f_b = computed compressive bending stress at the point under consideration

F_b = compressive bending stress that would be permitted if bending alone existed

$\frac{KL}{r}$ = ratio of the effective length to the radius of gyration of the compression member

For the segment of rail above a support at the Collingswood viaduct under the assumed summer increase of temperature:

f_a = 104 MPa (15 ksi)

f_b = 28 MPa (4 ksi)

F_b = 294 MPa (42.6 ksi) as computed earlier for the winter condition

KL = L = 762 mm (30 in.)

r = 66.3 mm (2.6 in.)

The value of F_a may be determined through strength curves for axially loaded columns. Figure 36 shows some strength curves. The curves are from results of studies at Lehigh University[19,20] and by the European Convention for Construction Steel Work (ECCS)[21,22] and are summarized in a Guide of Structural Stability Research Council (SSRC)[23]. These curves are for columns which have shapes and manufacturing conditions closest to those for 132 RE rails. The curve gives the ratio of the maximum strength P_{max} to the yielding strength P_y as a function of the nondimensional slenderness ratio λ:

$$\lambda = \frac{KL}{\pi r}\sqrt{\frac{F_y}{E}} \qquad (3)$$

where KL/r and F_y are as defined before and E is the Young's Modulus equal to 200,000 MPa (29,000 ksi). By using these numerical values, λ is found to be 0.417 and the two curves give P_{max}/P_y ratios, 0.96 and 0.94 respectively. By taking the smaller ratio and applying to the allowable stress, the allowable axial stress if F_a = 0.94 x 294 = 276 MPa (40 ksi).

When all the values are substituted into Eq. 2 (in U.S. units) it results in

$$\frac{15}{40} + \frac{2}{42.6\left[1 - \frac{15}{200 \times 10^6}\left(\frac{30}{2.6}\right)^2\right]} = 0.42 < 1.0$$

Therefore, the rails in the Collingswood and Westmont viaducts have sufficient safety margin against lateral buckling even under the most severe condition of assumed summer temperature.

The actual condition of the rails is such that no distress has been reported. The problem was the fracture of some fiberglass joints of the rails. This is discussed in the next section.

6.2 Fiberglass Joints of the Rails

The fiberglass joints of the rails are subjected to the same forces as are the rails. Since all such joints are at or near the piers, all are subjected to high forces. From the results of analysis, the forces in the joints are estimated to be 10,000 kN and 8700 kN for the Collingswood and Westmont viaduct joints, respectively, during the winter weather conditions (see Table 7).

The configurations of the fiberglass joints are shown in Figs. 21 and 22. Each joint has two fiberglass strips. Each strip has a gross cross-sectional area of 3630 mm^2. Thus the stresses in the strips are approximately 230 MPa (33 ksi) and 200 MPa (29 ksi). At the bolt holes, the cross-sectional area is about 2661 mm^2 per strip. Therefore, the average tensile stresses are estimated to be 313 MPa (45 ksi) and 272 MPa (40 ksi). Furthermore, stress concentration at the holes may cause the stresses to be higher than the average value, with the increase depending on the clamping forces from the bolts[24,25].

The strength of the fiberglass joints is governed by the mmterial properties of the fiberglass, the geometrical conditions of the joints, and the nature of the loading, among other factors[25]. No information has been received concerning the properties of the fiberglass material. In order to have some references for evaluation, four prismatic bars 250 mm (10 in.) or longer were cut from a fiberglass strip in the direction of the rail joints and tested under tension. Figure 37 shows a photograph of the specimens after failure.

These fiberglass bar tests show that the load-elongation relationship is linear from the onset of loading to the termination of testing. Termination, unfortunately, was due to failure at the gripping portion at the end of the bars, not at the middle of the length. Nevertheless, the results are listed in Table 8. Specimens 1 and 2 had short gripping lengths and failure occurred early. Specimens 3 and 4 were longer and did a little better, with a maximum tensile stress of 337 MPa (49 ksi) and 323 MPa (47 ksi), respectively. The "ultimate stress" for this material should be higher. Because the load-elongation relationship is linear, the modulus of elasticity can be computed. It is approximately 27,600 MPa (4000 ksi), being less than one-seventh of that for the steel rails.

By comparing the computed winter stresses in the fiberglass strips to the strength from bar tests, it is seen that the ultimate strength of the fiberglass material probably is not exhausted under winter conditions. On the other hand, experience from bolted joints

has indicated that joints sometimes fail because of geometrical conditions[25]. The "unbottuning" of end bolts of a long joint is an example. Each of the fiberglass strips has six bolts in a line, three for each abutting rail. The joints are fairly long. Thus it is likely that transfer of forces from the rails to the fiberglass strips is not even among the bolts.

Again, in order to gain information on the behavior of the fiberglass strips, a small specimen was made and tested. The specimen, as shown in Fig. 38, has two fiberglass strips with all dimensions one fourth those of the actual fiberglass strip. The fiberglass strips are bolted with 6.3 mm (1/4") diameter high strength bolts both sides of two steel plates which represents the rail. Tension is applied at the end of the steel plates. The specimen was pulled to fracture.

Figure 39 shows the fiberglass strips after testing. The first bolt has torn the end of the fiberglass stips completely. The second and third bolts are broken and they have also torn the fiberglass strips. Careful examination revealed two tearing lines connected the bolt holes parallel to the direction of applied force. The distance between one line and the other is the diameter of the holes. The maximum tension force applied to the specimen was 96.5 kN (21.7 kips). The corresponding net section stress in the strips was 307 MPa (44 ksi). This is less than the average tensile stress of 313 MPa (45 ksi) computed in the fiberglass joint on Collingswood viaduct under winter temperature changes.

strongly suggests that the geometry of the fiberglass joints has a profound influence on their failure in the Collingswood and Westmont viaducts.

Other factors which could affect the behavior of the fiberglass joints include the differential change of length between the fiberglass and the steel rails, the mechanical properties of the fiberglass in low temperature, and the low cycle fatigue characteristics of the strips. It is necessary to know all these relevant data, as well as the exact temperature in the viaduct and the corresponding displacements and forces of the rails, before the exact phenomenon of fiberglass failure can be reconstructed. Based on the results of computer analysis by finite element model, it appears that the most important conclusion is to place the fiberglass joints away from the slab joints over the piers.

6.3 Effects of Rail Anchorage

The arrangement of compression rail anchors and the slab anchor bolts of the viaducts is analogous to the use of shear connectors between the component parts of composite beams. Studies on steel-concrete composite beams have shown that the number of shear connectors influence the composite action[25]. Sufficient number of shear connectors permits the development of complete interaction between the component parts of the beam, and insufficient shear connectors is accompanied by partial interaction. There is

relative displacement between the component parts in the case of incomplete interaction.

For the Collingswood and Westmont viaducts, it has been observed that during cold months the compression rail anchors move toward the center of the spans relative to the rails. Figure 40 shows an example of the computed relative displacements between the rails and the slab of span 6 in the Collingswood viaduct. This condition is analogous to that of incomplete interaction in composite beams. Therefore an examination of the rigidity of the compression rail anchors will provide information on the relative displacements between the rails and the concrete slab.

In the finite element models of analysis, the rigidity of the elements connecting the rails to the concrete slab is assumed to be constant. A moment of inertia 42,00 cm^4 has been chosen by trial and error such that the computed relative displacements at ends of concrete slabs correspond to the maximum observed movement of about 25 mm. By increasing and decreasing the rigidity of the connection elements, the effects of rail anchorage rigidity can be evaluated.

Three values of moment of inertia for the connecting elements are used: 42×10^{10} cm^4, 42,000 cm^4, and 42 cm^4. The first represents a very rigid anchorage, the second is as explained above, and the third simulates the case when the compression rail anchors are only slightly tightened. These three values are used with the E-E viaduct models.

Figure 41 shows the computed axial force in the rails in spans 5, 6 and 7 of Westmont viaduct under the same assumed decreases of temperature for winter conditions. For very rigid connections between the rails and the concrete slab, the forces in the rails are constant in the span but above a pier the rail tension force increases to 10,800 kN. This corresponds to a tension stress of 216 MPa (31.3 ksi). By contrast, if the connection between the rails and the concrete slab is minimal. The axial force is uniformly 4500 kN over the piers and in the spans throughout the entire length of the viaduct. The corresponding tension stress is 90 MPa (13 ksi) in all segments of the rails. For the intermediate case of rigidity, the rail force over a pier is 8700 kN and decreases gradually to a lowest value towards the center of spans (see Fig. 34 for this case of rigidity). The tensile stress in the rail over the piers is 174 MPa (25 ksi).

The tensile forces and stresses in the rails over the piers for the three element rigidities are summarized in Table 9. Obviously, the more rigid the compression rail anchorage, the higher the forces and stresses in the rails over a pier. From the point of view of reducing the rail forces, it is then advisable not to use a too high bolt force in the compression rail clip bolts.

Because reducing clip bolt forces is equivalent to the condition of insufficient shear connectors in composite beams, the possible occurrence of large relative displacements between the rails and the concrete slabs over the piers should be examined. These

displacements are listed in Table 10 for the Collingswood viaduct under the assumed winter decreases of component temperature. For the anchorage rigidity simulating the existing compression rail clip condition, the displacement is computed to be 2.26 mm. When low clip bolt force is used, the relative displacement only increases to 3.77 mm. This latter value is approximately only twice of that for very rigid anchoring conditions.

Since the relative displacements are highest at ends of simple span beams and decrease to zero towards the center of spans, no computed relative displacement is expected to be more than 3.77 mm for the Collingswood viaduct. The maximum computed value for the Westmont viaduct is slightly less. If such magnitudes of relative displacements are considered tolerable for the viaducts, then the clip bolt forces may be reduced so as to reduce the forces in the rails over the piers.

6.4 Rotation and Displacement of Beams at Piers

All the computed rail forces and relative displacements have been made using the E-E viaduct models and the one-span model. It has been indicated that the condensing of concrete portions of the viaducts as beam elements along their centroid may introduce in the results of computation if the ends of the concrete beams undergo large rotations. It has also been shown that the E-E viaduct models give relative displacements between ends of slabs

which correlate well with measured values. The E-E model has been adopted regardless of the rotations at beam ends.

For the simple spans in the viaducts, the rotations at span ends are induced by the changes of beam curvature responding to the changes of temperature in the component parts. Thus, the rotations for spans of the same geometry are the same for an assumed temperature change. Table 11 shows the computed rotations at span 6 of the Collingswood viaduct under both the winter condition of decreasing temperature and summer condition of increasing temperature. The one-span finite element model permits evaluation of the rotation of the slab and of the beam separately. The I-beam rotate less than the slab because the I-beams have higher moments of inertia. For comparison with the rotation from the E-E viaduct model, the rotation of the straightline connection, the top of the slab to the bottom of the I-beams is given in the third column of the table. The corresponding values from the viaduct model are about half of those from the one-span model. Regardless of how much the one-span model results are better than the E-E model values, the order of magnitude of the rotations indicate that these rotations should not be ignored in examining the behavior of the viaducts.

Rotations of vertical cross-sections at span ends are accompanied by longitudinal displacements of the component parts. These displacements must be superimposed to the shortening or lengthening of the entire viaduct spans due to the change of temperature. In the analysis by the one-span model, the

superposition is handled by taking the absolute longitudinal displacements at the rails and at the centroid of the concrete portion from the E-E model as input. The output are absolute displacements, including the contributions from the curvature of the beams. Examples of computed longitudinal displacements are given in Figs. 42 to 45.

Figure 42 shows the longitudinal displacements at one end of span 6 of Collingswood viaduct under the winter temperature change computed by the one-span model. This end of span is over pier 5. The bottom of the I-beams move 7.72 mm in the direction of the mid-span. The variation of the longitudinal displacement is linear across the depth of the prestressed concrete I-beam corresponding to the rotation of the cross section. There is no slippage between the concrete slab and the prestressed I-beams thus the displacement is identical. The difference of displacement between the rails and the top of slab is the relative displacement discussed earlier and listed in Table 10. The longitudinal displacement of the rails is minimal because of its continuity over the pier. The computed longitudinal displacement of 7.72 mm is relative to the top of the pier.

Figure 43 shows the longitudinal displacements of the same cross section under the summer temperature change. The bottom of the I-beam moves (expands) 2.1 mm away from the span. Characters of results such as linear variation of the longitudinal

displacements of the I-beams and relative displacement between the rails and the slab are all as pointed out above.

The total longitudinal displacement at the bearing of I-beams due to temperature changes between the cold nights of the winter and the hot days of the summer can be estimated by summation. At Pier 5, the bottom of I-beams of span 6 has a computed total movement of 9.82 mm. This corresponds to a temperature change of 58°C for the rails and 39°C for the concrete portion. If the temperature changes are different, the displacements are proportional to the total. Figure 44 shows the displacement of the same span end due to a change of temperature midway between that assumed for the summer and for the winter. The resulting beam displacement at pier top is also midway between the corresponding values. Figure 45 depicts this condition and the linearity of beam displacement at bearings with respect to temperarure. The results as shown in this plot can serve as a guide for evaluation of the bearing performance in the Collingswood viaduct. The accuracy of the plot, because of the various assumptions made, must be examined through physical measurements of beam movements at piers.

One of the assumptions is the rail anchoring system rigidity. It is important to know the influence of the rigidity on the beam displacement at a pier. Figure 46 shows the longitudinal displacements corresponding to those of Fig. 42 but with different characteristics for the vertical elements. By comparing the displacements among the three cases in these two figures, it can be noted that that

if the rigidity of the connection between the rails and the slab is release, the longitudinal displacement of the bottom of the I-beams decreases from 7.72 mm to 3.90 mm. If the rigidity of the connection is increase, then the longitudinal displacement increases from 7.72 mm to 8.15 mm. Rigid connection between the rails and the slab causes more interaction between the rails and the concrete portion and consequently move rotation and displacement at the ends of beams. A connection between the rails and the slab with little resistance to movement in the longitudinal direction permits the rail to slide with respect to the slab. The concrete beam can expand or contract according to temperature change without induction of curvature and rotation. The vertical cross sections of the slab-and-beam portion remain practically vertical even under conditions of large change in component temperature.

6.5 Effects of Viaduct Curvature

So far only displacements and forces in the longitudinal direction have been examined. Both viaducts have horizontal curves. Although all of the I-beams are straight between bearings, the positioning of the bearing points along curves leads to transverse reactions and displacements. In modeling the viaducts, boundary elements with the stiffness of the bearing pads are employed to represent the support conditions.

At each pier where there is a reinforced concrete diaphragm between I-beams the stiffness of the boundary element in

the transverse direction is given a very high value because almost no displacement is considered likely to occur. At each end of the spans the reaction and the displacement in the longitudinal and transversal direction are obtained from the boundary elements.

Table 12 shows the reactions and displacements at the top of the piers of Collingswood viaduct computed by the E-E viaduct model under the assumed condition of winter temperature change. The transversal reactions are equal to zero on the first twelve piers of Collingswood viaduct. It is only near where the width of the deck begins to increase for the Collingswood Station, that some transversal reactions are beginning to be generated. The transverse reactions are fairly high at some bearings and the transverse displacements are all very small.

Table 13 shows the reactions and displacements at the top of the piers of Westmont viaduct computed by the E-E viaduct model under the same assumed winter temperature changes. The transversal reactions are higher than those of the Collingswood viaduct because of the sharper curve described in the Westmont viaduct. The maximum transversal reaction is equal to 372 kN at Pier 7 where there are four prestressed concrete I-beams and a reinforced concrete diaphragm (as shown in Fig. 24). The transverse displacements are small but are higher than those of the Collingswood viaduct.

In the longitudinal direction, Tables 12 and 13 give the displacements which occurs at the centroid of the composite concrete section, not the displacements of the bottom of the prestressed

concrete I-beams. The displacement of the bottom of the I-beam at a pier is affected by rotation and the rigidity of the rail anchors as it has been pointed out earlier. For a given rail anchor rigidity the absolute longitudinal displacement at a pier is the sum of that due to rotation and that of the centroid of the composite section. Since displacements due to rotation is about the same for spans of the same geometry and under the same temperature change, the displacement of the centroid is an indication of the longitudinal displacement of the beams at bearings.

By comparing Tables 12 and 13 it can be noted that on Westmont viaduct all the longitudinal displacements from Span 1 to Span 17 are positive and all the longitudinal displacements from Span 23 to 27 are negative. On Collingswood viaduct the longitudinal displacements are alternatively positive and negative for low number and high number spans. Examples of this result from the computer analysis are shown in Figs. 30, 47, 48 and 49.

Figures 30 and 47 show, respectively, the longitudinal displacements of the concrete centroid in Span 6 and Span 31 of Collingswood viaduct computed by the E-E viaduct model under the winter temperature changes. In both spans the variation of the longitudinal displacements is linear, as it is represented by the straight lines. However, the points of zero longitudinal displacement are at different locations in the spans. In Span 6 this point is in the right half of the span, in Span 31, in the left half of the span.

This shifting of the straight line confirms that there are two different phenomena of longitudinal displacement as it has been discussed earlier. First, the response of the concrete in the span under winter temperature change causes the ends of the span to move toward the midspan. This response is practically identical for the two spans which are of about the same length. Second, the contraction of the entire viaduct under the same temperature changes creates the motion of the entire exterior span toward the "mid of the viaduct". This phenomenon is the response of the total viaduct to temperature change. It is induced by the existence of the anchored continuous rails, and is affected by the horizontal curve of the viaduct.

In the Collingswood viaduct the response of individual spans is more prominent because the horizontal curve is gentle. In the middle of the viaduct, where the effects of horizontal curvature are not very small, the entire beam element displace towards the station. In Westmont viaduct the second phenomenon of overall response is more prominent than the response of individual spans. The results is that individual spans at ends of the viaduct move toward the station. Figure 48 shows the longitudinal displacements of the concrete centroid in Span 6 of Westmont viaduct computed by the E-E viaduct model. Figure 49 shows the corresponding displacements in Span 25. In Span 6 the longitudinal displacements are all positive, on Span 25 they are all negative.

In Figs. 30, 47, 48 and 49 the sloops of the variation of the longitudinal displacements in the span are the same. This implies that for each individual span, the responses to temperature changes are almost the same in both viaducts. It is so because all force spans are similar and are straight. The sharper curve of the Westmont viaduct induces more severe overall longitudinal displacement than in the Collingswood viaduct. This situation is a possible explanation for some of the problems encountered with the bearing pads on Westmont viaduct.

6.6 Stresses in Concrete Sections

The temperature-induced stresses in the concrete portion of the viaduct spans need to be examined. The computation of stresses are presented only for one typical span (Span 6) of the Collingswood viaduct subjected to the assumed temperature changes for winter. As it has been pointed out earlier, the individual spans appear to behave similarly in that the rail forces and displacements are all similar. Therefore examination of one span is sufficient. The assumed winter temperature changes are chosen because they are more severe, and the Collingswood viaduct has higher induced forces in the rails.

Span 6 was chosen because it is far enough from the end of the finite element viaduct model not to be influenced by some possible boundary effects created by the bearing conditions at the last segment of rails. Span 6 was chosen also because it has the smallest concrete cross-section, which is shown in Fig. 50.

The computations of the stresses in the concrete are given in Appendix A. The temperature induced boundary displacements of Span 6 from the E-E viaduct model and the assumed temperature changes are applied to the one-span finite element model to find the internal forces in the midspan section. These internal forces are shown in Fig. 51. By using these forces and assuming a 15% loss of prestressing force per beam[11], the stresses at various points of the cross section are computed. The effects of the weight of the beams and the slab and a dead load on the slab are taken into consideration. The computed stresses are + 165 kPa (0.024 ksi) tension at the top of the slab and - 15.5 MPa (-2.25 ksi) compression at the bottom of the prestressed concrete I-beams under the assumed winter changes of temperature. These computed stresses are below the maximum allowable tension stress[27] of 595 kPa (0.086 ksi) and the maximum allowable compression stress of -24.8 MPa (-3.6 ksi), respectively.

The computation of stresses above is made assuming that the concrete can take no tension stress. Study has shown that for reinforced concrete slabs subject to tension forces, a 60% participation of the concrete can reasonably be assumed[26]. In this case the stress at the top of the slab is -503 kPa (-73 psi) compression the stress at the bottom of the slab is +703 kPa (+102 psi), and the stress in the reinforcing steel is +199 MPa (+28.9 ksi). These stresses are all lower than the respective allowable values.

6.7 Possible Causes of Damages at Piers

The results of computations presented heretofore have shown that the bottom of the concrete beams over the piers move a measurable amount in the longitudinal direction due to the assumed temperature changes in winter and summer. When temperature decreases, the displacement of the beams is toward the center of the span. If temperature increases, the movement reverses the direction. This repeated annual displacement, as well as the daily displacements of smaller magnitudes, must be absorbed by the Neoprene pads at the expansion bearings.

The longitudinal displacement which can be absorbed by a bearing pad in the Collingswood and Westmont viaducts is given by the formula[28]

$$e = \frac{Tt}{Wb\ G} < \frac{t}{2} \qquad (4)$$

where

e = longitudinal displacement

T = shearing force at bearing

W = width of bearing pad

b = length of bearing pad

G = shear modulus of elasticity of Neoprene

From the E-E viaduct model the computed longitudinal reactions at ends of beams are at the level of the centroid of the concrete portion, not at the bottom of the beams. Therefore the longitudinal displacements associated with the shearing of the pad are not known.

Comparisons have to be made on the basis of maximum permissible displacement of t/2.

The estimated total longitudinal movement of I-beams at the expansion bearings of Span 6 in the Collingswood viaduct is in the order of 10 mm. About eighty percent of the total (7.72 mm) is toward the center of the span. The bearing pads in this viaduct are single layer with a thickness of 38 mm. The maximum permissible displacement is 19 mm. Therefore the expansion bearing at Span 6 and at similar spans, should not have problems. Examination of Table 12 shows that the maximum computed centroidal displacement of the concrete beam is 9.83 mm at Pier 24. By assuming conservatively that the displacement associated with beam rotation of Span 25 is about 25% higher than that of Span 6 proportional to span length, the estimated winter displacement of beams at Pier 24 is about 14 mm. This amount is within the capacity of the bearing pad.

At Pier 1 of the Collingswood viaduct, the bearing pads under two longer beams of Span 1 are pushed out toward the center of the span. The configuration of the pad under one beam is sketched in Fig. 52. Because the pier is skewed, the computed displacements from the two-dimensional finite element model can not be considered adequate for evaluation. It can only be reasoned that the longer beams in this span undergo larger displacements at the bearing. Why were the bearing pads pushed out can only be explained when more information is known with regard to forces and displacements at these points as well as to the characteristics

of the pads against sliding. Judging by the markings on the face of the bearing pads, it is evident that the displacement of the pad is caused by the annual thermal displacement of the beam. It appears that the pad moves with the beam toward the center of span in the winter, but does not return with the beam during the summer. Once the pad protrudes beyond the edge of the concrete support, it expands and cannot move back.

For the Westmont viaduct almost all bearing pads moved. In the longitudinal direction all displacements of the pads are toward the center of the spans. The confirmation of the displaced bearing pads and the markings on their surface indicate that the phenomenon is identical to that at Pier 1 of the Collingswood viaduct.

Comparison of the computed longitudinal displacements of the Collingswood viaduct (in Table 12) with those of the Westmont viaduct (in Table 13) reveals that the centroidal displacements of the Westmont viaduct beam-slab system are higher. Consequently, the beam displacements at the piers are also higher. But the bearing pads of the Westmont viaduct are only 25 mm thick and have only one layer. Therefore, the possibility of exceeding the capacity of bearing pads is higher. For example, the estimated beam displacement at Pier 12 is about 12 mm including the contributions from rotation and centroidal displacement. This is about equal to the capacity of these 25 mm thick bearing pads. Once sliding takes place, the beams move to relieve the horizontal forces at the bearings. Since there are transverse forces, transverse

displacements of the beams induce transverse movement of the bearing pads.

At the fixed bearings, the beams are anchored to the piers directly (as in Fig. 18) for the Collingswood viaduct, or indirectly (as in Fig. 24) for the Westmont viaduct. Displacement is thus prevented and horizontal reactions develop. The longitudinal and transverse horizontal forces at the fixed bearings are listed in Tables 14 and 15. These are computed results from the E-F finite element models of the viaducts. Although the computed displacements between the concrete slabs do not agree well with the measured values, the computed reactions can be used for comparison. For the Collingswood viaduct, the maximum horizontal reactions by computation are at Piers 19 and 25. For the Westmont viaduct the maximum are at Pier 21, with high reactions also at adjacent piers. The magnitude of maximum longitudinal reactions in the two viaducts do not differ much, but the transverse reactions are very much higher for the Westmont viaduct. The combination of high magnitude of reaction in both longitudinal and transverse directions could cause the damage at Piers 15, 18 and 19 of the Westmont viaduct.

7. DISCUSSION

7.1 Continuous Rails on Simple Spans

From the analysis of the Collingswood and Westmont viaducts some insight has been gained on the behavior of this type of "maintenance free" track support system. Basically the system consists of individual composite beams supporting continuous rails. The individual spans of the viaduct has a concrete slab in composite action with concrete I-beams or steel girders. Each span is simple supported. The rails are continuous throughout the length of the viaduct and are anchored to the concrete slab.

Besides dead load and live loads, temperature variation is the primary cause of forces, stresses, and displacements in the viaduct structure and the rails. The significant influencing factors are the rigidity of the anchorage between the rails and the concrete deck and the conditions of the bearings. The rigidity controls the interaction between the rails and the concrete slab. Very rigid anchorage assures the "maintenance free" nature in keeping the rails in position. The consequence is the complete interaction between the rails and the individual simple span, and the joining of the individual spans by the continuous rails to form a continuous superstructure. The rails need to be sufficiently strong at the junction of spans. The conditions of the bearings must be

compatible with the forces and displacements of the continuous system. The situation of the Collingswood and Westmont viaducts are of this nature.

If the anchors between the rails and the concrete slab provides resistance to transverse displacement but permits longitudinal movement of the rail, the position of the rails are maintained, yet no interaction takes place between the rails and the spans. The bearings need not be specially designed. The imminent question to be answered is what anchoring system for the rails will provide sufficient resistance to displacement in the lateral and vertical direction without restricting the relative displacement of the rails in the longitudinal direction. Information with regard to this must be developed.

7.2 Continuous Rails on Continuous Spans

Since part of the problem of continuous rails on simple spans is the discontinuity of the simple spans, employment of continuous spans will eliminate this part of the problem. The rails and beams, anchored together, perform as a continuous composite viaduct. Information on continuous composite beams subjected to temperature changes can be applied to this system. The condition that a continuous rail over a joint, however, remains at the ends of the viaduct if the rails are rigidly anchored to the supporting system beyond the viaduct.

As an example the Collingswood viaduct configuration is used as a continuous viaduct with continuous rails for analysis. The composite I-beams are assumed continuous throughout the entire length with one fixed bearing in the middle of the viaduct. All other bearings are assumed to be the expansion type. The finite element mode has vertical connection elements with moment of inertia 42,000 cm^4. For the assumed winter temperature changes of the Collingswood viaduct, the variation of rail forces in one part of this continuous viaduct is shown in Fig. 53. The increase of rail forces near the end of the viaduct is analogous to that which occurs between two simple spans.

One possible arrangement to reduce the sharp increase of rail forces at the end of the continuous viaduct is to place an expansion joint in the rail at or near the ends of the viaduct. The expansion joint must be compatible with the behavior of the continuous composite viaduct. This and other possible arrangements must be analyzed and designed for each track-supporting viaduct. To avoid placing expansion joints in the rail in the viaduct, the Long Island Railroad is testing a series of short slab sections at the abutments of the viaduct. These slab sections are between 3 m and 1.50 m long. The results from this study will be very helpful in assessing the merit of such an arrangement.

7.3 Collingswood and Westmont Viaducts

For the Collingswood and Westmont viaducts with the existing difficulties of fiberglass joints and bearing pad displacements, corrections must be undertaken. Based on the results of analysis presented earlier, three suggestions are presented below.

First, the replacements of broken fiberglass joints are to be placed away from the ends of viaduct spans. The forces in rails are lower in the spans than over the piers. Thus the forces in the fiberglass joints will be lower if the joints are located toward the middle of spans. The strength of the fiberglass joints needs to be evaluated more precisely before actual installation can be modified.

Second, the clip bolt forces may be reduced so as to reduce the compressive forces between the curved spring anchors and the rails. A study needs to be conducted to establish the relationship among the clip bolt forces, the forces in the rails, and the displacement of the rail with respect to the concrete slab. Low forces in the clip bolts will allow the rails to slide on the tie plates. This condition will permit the reduction of rail axial forces through the permission of incomplete composite action between the rails and the concrete viaduct.

Third, it is suggested to replace displaced bearing pads with new bearings which permit movements and are not being pushed out. Simple metal bearing plates anchored to the piers and to the bottom of the I-beams, respectively, will be adequate. At fixed

bearings where displacements have taken place and concrete spalled, repair can be free of the fixity and modifying the bearing plates as stated above. These suggested corrections to the bearings require major interruption of the rapid transit line operation. If the first two suggestions are adopted, there appears no need of considering the third.

In any event, continued monitoring of the behavior of the Collingswood and Westmont viaducts are recommended.

8. SUMMARY

The conclusions from the review and analyzis of "maintenance free" track support viaducts are summarized below.

1. "Maintenance Free" track support systems for railroad viaducts has many forms. The Tokaido Line of the Japanese National Railroad anchors the rails to short concrete slabs which are adhered to the concrete viaduct slab. The French National Railway uses concrete box girders and concrete slabs with encased steel I-beams with ballast and tie. The Long Island Railroad adopts a reinforced concrete slab over the slab of two short steel bridges and as an integral part of a reinforced concrete viaduct. Study of the Long Island Railroad system is current with results anticipated in the near future.

2. The Collingswood and Westmont viaducts in the Philadelphia-Lindenwald Rapid Transit Line use the structural slab of the simple spans as support for the continuous rails. Each span is a multi-beam composite concrete member simple span with fixed bearing at one end and expansion bearing at the other end. The viaducts are curved horizontally, with higher curvature for the Westmont viaduct. The rails are firmly anchored to the viaduct slabs. Broken pieces have been found at some fiberglass insulation joints of the rails, Neoprene bearing pads are observed to have moved from under the beams, and concrete spalled at a number of fixed bearings.

These damages are preliminary assessed as being induced by differential temperature changes.

3. Two-dimensional finite element models are employed to represent the complete viaducts and a single span for analysis of forces and displacements. The sizes of the elements, thus the accuracy of the models, are controlled by the capacity of the computer. The geometrical characteristics of the models are determined from the actual viaducts.

4. The validity of the models are evaluated through examination of computer output under assumed temperature changes. The magnitudes of temperature change are arbitrarily assumed considering the locality of the viaducts. The computed displacements from the viaduct models are found compatible with those from the one-span model, and the estimated relative displacements between slabs agreed fairly well with actual measured values taken at the viaducts.

5. Results of computation show that forces in the rails vary with changes of temperature. During cold nights high tension exists in rails above the junctions of concrete slabs directly over the piers. In summer days high compressive forces are produced there. The magnitude of these forces are much lower towards the middle of the span.

6. The strength of the rails are found to be adequate against the estimated tension and compression, as well as against lateral buckling of the rails between anchors.

7. The fiberglass joints, however, appear to be inadequate for the high tensile forces in the rails directly over the piers. Testing of small fiberglass joints produced premature failures. Study of the fiberglass joint strength is suggested.

8. The anchoring of the rails to the concrete slabs produce interaction between the rails and the viaduct spans. More rigid connection between the rails and the slab introduce higher degree of composite action. It is confirmed as expected that higher degree of complete interaction generates higher rail forces over the piers. Less rigid anchorage of the rails reduces these forces but induces relative displacements between the rails and the slab. These relative displacements are not very large.

9. The interaction between rails and viaduct also induce rotation of cross sections of the viaduct and displacements at piers. These rotations and displacements are linearly influenced by the change of temperature. The rotations and displacements are also strongly affected by the rigidity of the rail anchorage.

10. Curvature of a viaduct causes transverse reactions at the piers. Sharper curves have higher transverse reactions. Curves of the rails also cause the centroid of the individual spans to move along the direction of the viaduct. Therefore, during the winter, the end spans of a viaduct with sharp curve displace toward the middle of the viaduct more than the spans of a viaduct with gentle or no curve.

11. The stresses on the concrete composite beams of the viaducts are computed to be fairly low.

12. The cause of all damages in the Collingswood and Westmont viaducts are believed to be temperature changes. The bearing pads appear to displace with the bottom of I-beams in winter but do not recover as temperature increases. Westmont viaduct sustained more bearing pad displacement because of the larger movement of the I-beams. The spalling of concrete at fixed bearings is interputed as relieving of high longitudinal and transverse reaction forces at these piers.

13. There appears to be two basic types of track supporting viaduct systems for continuous rails. One is the use of continuous rails on individual spans, the other is to place the rails on continuous viaduct spans. For the first, low rigidity of anchoring system against longitudinal displacement is probably better. For the continuous span system, the forces in the rails at the ends of the viaduct must be adequately analyzed and properly dispensed.

14. To the damaged fiberglass joints in the Collingswood and Westmont viaducts, replacements should be located in the spans away from the piers. The clip bolt forces could be released after a study of the behavior of the anchorage system. The pushed out bearing pads may be replaced by simple bearing plates attached to the piers and the bottom of the I-beams, respectively, and the damaged fixed bearings may be converted to expansion bearings.

TABLE 1 PRINCIPAL CHARACTERISTICS OF THE VIADUCTS

	COLLINGSWOOD	WESTMONT
General Aspects		
Length	727.2 m	600 m
Number of Spans	34	27
Length of spans	21.34 m - 27.98 m	19.01 m - 27.43 m
Number of 4 I-Beams Spans	20	12
Number of 5 I-Beams Spans	8	7
Number of 6 I-Beams Spans	6	8
Prestressed Beams		
Number of Different Types	6	5
Height of Beams	1.14 m - 1.57 m	1.07 m - 1.52 m
Width of Beams	61 - 66 cm	61 cm
Initial Prestress Force	3475 - 5695 kN	2993 - 5605 kN
Number of Seven-wire Strands	36 - 59	31 - 58
Area of Prestressing Steel	26.7 cm^2 - 43.8 cm^2	23.0 cm^2 - 43.0 cm^2
Reinforced Concrete Slab		
Thickness	20.3 cm	20.3 cm
Width	7.95 - 15.00 m	7.95 - 15.00 m
Bearing Pads		
Thickness of Fix Support	38 mm	25 mm
Thickness at Expansion Support	38 mm	35 mm

TABLE 2 MEASUREMENTS OF THE DISTANCE BETWEEN THE PAIRS OF PLUGS SEALED IN THE SLAB ON JUNE 29, 1980

Location of the Measurements	Distance Between Plugs on June 29, 1980 at 7:00 a.m. L_1 (mm)	Distance Between Plugs on June 29, 1980 at 12:45 p.m. L_2 (mm)	$\Delta L = /L_2-L_1/$ (mm)	Average ΔL at each Pier (mm)
C 12 E	254.88	253.43	- 1.45	- 1.58 E
C 12 E	253.46	251.75	- 1.71	
C 13 E	254.52	253.28	- 1.24	- 1.63 F
C 13 W	254.45	252.44	- 2.01	
C 23 E	255.08	253.00	- 2.08	- 1.96 F
C 23 E	255.74	253.91	- 1.83	
W 10 E	254.50	253.41	- 1.09	- 1.30 E
W 10 W	253.18	251.40	- 1.50	
W 11 E	253.18	251.40	- 1.78	- 1.54 F
W 11 W	252.31	251.02	- 1.29	
W 15	259.78	257.32	- 2.46	2.46 F
Air Temperature	21.0°C (70°F)	32.2°C (90°F)		

Measurements $\pm$ 0.08 mm

TABLE 3 MEASUREMENTS OF THE DISTANCE BETWEEN THE PAIRS OF PLUGS SEALED IN THE SLAB, LARGE INCREASE OF TEMPERATURE

Location of the Measurements	Distance Between Plugs on June 29, 1980 at 7:00 a.m. L_1 (mm)	Distance Between Plugs on August 7, 1980 at 3:00 p.m. L_3 (mm)	$\Delta L = /L_3 - L_1$ (mm)	Average ΔL at each Pier (mm)
C 12 E	254.88	250.87	- 4.01	
				- 3.85 E
C 12 W	253.46	249.57	- 3.89	
				- 2.48 F
C 13 E	254.52	251.91	- 2.61	
				- 4.44 F
C 13 W	254.45	252.11	- 2.34	
C 23 E	255.08	250.49	- 4.60	
				- 4.44 F
C 23 W	255.74	251.48	- 4.27	
W 10 E	254.50	250.92	- 3.58	
				- 3.46 E
W 10 W	254.32	250.99	- 3.33	
W 11 E	253.18	250.16	- 3.03	
				- 2.95 F
W 11 W	252.31	249.44	- 2.87	
W 15	259.78	255.11	- 4.67	
Air Temperature	21.1°C (70°F)	37.8°C (100°F)		

Measurements $\pm$ 0.08 mm

TABLE 4 RELATIVE DISPLACEMENTS OF THE PAIRS OF PLUGS SEALED IN THE SLAB, LARGE DECREASE OF TEMPERATURE

Location of the Measurements	Distance Between Plubs on Aug. 9, 1980 at 3:00 p.m. L_3 (mm)	Distance Between Plugs on Nov. 16, 1980 at 10:00 a.m. L_4 (mm)	$\Delta L = L_4 - L_3$ (mm)	Average ΔL each Pier (mm)
C 12 E	250.87	256.81	5.94	7.08 E
C 12 W	249.57	257.79	8.22	
C 13 E	251.91	258.64	6.73	6.52 F
C 13 W	252.44	258.74	6.30	
C 23 E	250.49	258.97	8.48	8.36 F
C 23 W	251.48	259.71	8.23	
W 10 E	250.92	260.95	10.03	9.95 E
W 10 W	250.99	260.85	9.86	
W 11 E	250.16	256.53	6.37	6.36 F
W 11 W	249.44	255.69	6.25	
W 15	255.11	263.85	8.74	8.74 F
Air Temperature	37.8°C (100°F)	5.6°C (42.6°F)		

Measurements $\pm$ 0.08 mm

TABLE 5 COMPARISON BETWEEN THE DISPLACEMENTS GIVEN BY THE FINITE ELEMENT MODELS AND THE MEASUREMENTS IN-SITU, INCREASE IN TEMPERATURE

Location of the Displacements	Relative Displacements of the Ends of the Slab at some Joints			Algebraic Difference Between Column 3 and Column 4	Relative Difference Between Column 3 and Column 4
Pier No.	Computed by E - F Viaduct Models (mm)	Computed by E - E Viaduct Models (mm)	Measurements Column 5 of Table 2 (mm)	(mm)	(%)
C 12	-3.21	-1.86	-1.58 E	0.28	15%
C 13	-0.0	-1.86	-1.63 F	0.23	12%
C 23	-0.0	-1.92	-1.96 F	- 0.04	- 2%
W 10	-3.04	-1.60	-1.30 E	0.30	18%
W 11	0.0	-1.73	-1.54 F	0.19	10%
W 15	0.0	-2.00	-2.46 F	- 0.46	-18%
Temperature Change					
Rails	+ 20°C	+ 20°C			
Concrete	+ 7°C	+ 7°C			
Air			+11.1°C		

TABLE 6 COMPARISON BETWEEN THE DISPLACEMENTS GIVEN BY THE FINITE ELEMENT MODELS AND THE MEASUREMENTS IN-SITU UNDER DECREASE OF TEMPERATURE

Location of the Displacements	Relative Displacements of the Ends of the Slab at some Joints				
	Computed by E-F Viaduct Models	Computed by E-E Viaduct Models	Measurements Columns 5 of Table 4	Algebraic Difference Between Columns 3 and 4	Relative Difference Between Columns 3 and 4
Pier No.	(mm)	(mm)	(mm)	(mm)	(%)
C 12	11.79	6.83	7.08	0.25	3
C 13	0.00	7.85	6.52	- 0.33	- 5
C 23	0.00	6.98	8.36	1.38	16
W 10	12.43	7.13	9.95	2.82	28
W 11	0.00	7.14	6.36	- 0.78	- 12
W 15	0.00	8.16	8.74	0.58	7

Temperature Change

Rails	- 38°C	- 38°C	
Concrete	- 32°C	- 32°C	
Air			- 32.2°C

TABLE 7 COMPUTED FORCES AND STRESSES IN RAILS

Change of Temperature		COLLINGSWOOD				WESTMONT			
		Over Piers		At Midspan		Over Piers		At Midspan	
		Force (kN)	Stress (MPa)	Force (kN)	Stress (MPa)	Force (kN)	Stress (MPa)	Force (kN)	Stress (MPa)
WINTER:	Rails $-38^{\circ}C$	10,000	200	3,500	70	8,700	174	3,700	74
	Concrete $-32^{\circ}C$								
SUMMER:	Rails $+20^{\circ}C$								
	Concrete $+7^{\circ}C$	- 5,200	- 104	- 3,100	- 62	- 4,600	- 93	- 3,000	- 60
RANGE:	Rails $\pm 58^{\circ}C$	15,200	304	6,600	132	13,300	266	6,700	134
	Concrete $\pm 39^{\circ}C$								

Connection Elements I = 42,000 cm^4

TABLE 8 RESULTS OF THE TENSION TEST ON FOUR FIBERGLASS BARS

Specimen	Area (mm^2)	Maximum Force (kN)	Maximum Stress (MPa)	Maximum Stress (ksi)	Modulus of Elasticity (MPa)
1	438.7	93.4	213	41	27,250
2	403.2	108.5	269	39	22,250
3	403.2	135.6	337	49	27,600
4	403.2	130.3	323	47	27,600

TABLE 9 EFFECTS OF RAIL ANCHOR RIGIDITY ON RAIL FORCES*

Anchorage Conditions	Elements Moments of Inertia (cm^4)	Rail Force (kN)	Rail Stress (MPa)	Rail Stress (ksi)
Rigid	42×10^6	10,800	216	31
Intermediate	42,000	8,700	174	25
Low Clip Bolt Force	42	4,500	90	13

*Computed by Westmont Model

Notes: Rails $\Delta T = -38^{\circ}C$
Concrete $\Delta T = -32^{\circ}C$

TABLE 10

EFFECTS OF RAIL ANCHOR RIGIDITY ON RELATIVE DISPLACEMENT BETWEEN RAILS AND SLABS OVER PIERS*

Anchorage Condition	Element Moment of Inertia (cm^4)	Relative Displacement (mm)
Rigid	42×10^6	1.80
Intermediate	42,000	2.26
Low Clip Bolt Force	42	3.77

*Computed by Collingswood E-E Model

Notes: Rails T = - 38°C
Concrete T = - 32°C

TABLE 11

ROTATION AT ONE END OF SPAN 6 OF COLLINGSWOOD VIADUCT

Rotations	One-Span Model		E-E Viadict Model	
	Winter Conditions (°)	Summer Conditions (°)	Winter Conditions (°)	Summer Conditions (°)
Slab	0.27	- 0.073		
I-Beams	0.13	- 0.036		
Concrete Portion	0.15	- 0.04	0.075	- 0.021

TABLE 12

REACTIONS AND DISPLACEMENTS AT THE TOP OF THE PIERS OF COLLINGSWOOD VIADUCT COMPUTED BY THE E-E VIADUCT MODEL UNDER WINTER TEMPERATURE CHANGE

Pier No.	Span No.	Longitudinal		Transversal	
		Reactions (kN)	Displacements (mm)	Reactions (kN)	Displacements (mm)
Abt	1	- 7.47	4.24	- 24.33	0.0
1	1	- 18.73	- 4.04	0.0	0.0
1	2	- 12.01	2.59	0.0	0.0
2	2	- 13.61	- 2.95	0.0	0.0
2	3	- 16.50	3.56	0.0	0.0
3	3	- 13.75	- 2.97	0.0	0.0
3	4	- 13.75	3.76	0.0	0.0
4	4	- 12.86	- 2.77	0.0	0.0
4	5	- 18.37	3.96	0.0	0.0
5	5	- 11.88	- 2.57	0.0	0.0
5	6	- 19.35	4.19	0.0	0.0
6	6	- 10.90	- 2.36	0.0	0.0
6	7	- 20.37	4.39	0.0	0.0
7	7	- 9.88	- 2.13	0.0	0.0
7	8	- 21.44	- 4.62	0.0	0.0
8	8	- 8.81	- 1.90	0.0	0.0
8	9	- 22.55	4.88	0.0	0.0
9	9	- 7.70	- 1.65	0.0	0.0
9	10	- 23.71	5.13	0.0	0.0
10	10	- 6.49	- 1.40	0.0	0.0
10	11	- 24.95	5.38	0.0	0.0
11	11	- 5.25	- 1.14	0.0	0.0
11	12	- 26.24	5.69	0.0	0.0
12	12	- 3.96	- 0.86	0.0	0.0

TABLE 12 (CONTINUED)

Pier No.	Span No.	Longitudinal Reactions (kN)	Longitudinal Displacements (mm)	Transversal Reactions (kN)	Transversal Displacements (mm)
12	13	- 27.67		0.0	0.0
13	13	2.54	- 0.56	- 0.03	0.0
13	14	- 29.14	6.30	- 0.17	0.0
14	14	- 1.02	- 0.22	0.0	0.0
14	15	- 30.74	6.65	0.0	0.0
15	15	0.62	0.13	- 0.93	0.0
15	16	- 32.47	7.04	- 4.72	0.0
16	16	2.36	0.51	0.0	0.0
16	17	- 34.34	7.44	0.0	0.0
17	17	4.23	0.92	- 25.18	0.0
17	18	- 36.39	7.87	-142.6	0.0
18	18	6.32	1.37	- 0.03	0.0
18	19	- 39.06	8.43	- 0.47	- 0.10
19	19	8.76	1.90	50.18	- 0.03
19	20	- 41.55	8.99	-174.01	- 0.09
20	20	11.30	2.44	- 0.02	- 0.03
20	21	- 43.28	9.35	0.0	- 0.20
21	21	11.43	2.46	54.27	- 0.05
21	22	- 43.46	9.40	- 31.00	0 0.21
22	22	11.43	2.48	0.00	- 0.05
22	23	- 43.59	9.42	0.02	- 0.24
23	23	11.52	2.49	108.40	- 0.07
23	24	- 43.82	9.47	-167.96	- 0.19
24	24	11.61	2.51	0.16	- 0.01
24	25	- 45.46	9.83	0.11	- 0.25
25	25	3.71	0.81	143.41	- 0.02
25	26	- 38.92	8.41	134.29	- 0.17

TABLE 12 (CONTINUED)

Pier No.	Span No.	Longitudinal Reactions (kN)	Longitudinal Displacements (mm)	Transversal Reactions (kN)	Transversal Displacements (mm)
26	26	- 2.89	- 0.63	0.01	0.02
26	27	- 32.29	6.98	0.00	- 0.04
27	27	- 9.41	- 1.82	57.07	0.01
27	28	- 27.12	- 5.87	45.28	0.00
28	28	- 13.52	- 2.92	0.00	0.00
28	29	- 22.06	4.78	0.00	0.03
29	29	- 18.77	- 4.06	83.00	- 0.02
29	30	- 17.04	3.68	72.91	0.07
30	30	- 23.84	- 5.16	0.00	- 0.10
30	31	- 10.76	2.34	0.00	0.05
31	31	- 21.35	- 4.62	-13.88	- 0.09
31	32	- 11.57	2.49	-61.96	0.03
32	32	- 20.42	- 4.42	0.00	- 0.05
32	33	- 12.72	2.74	0.00	0.03
33	33	- 19.17	- 4.14	- 9.78	- 0.05
33	34	- 12.41	2.69	-13.03	- 0.02
Abt	34	- 19.08	- 4.14	0.00	- 0.04

Positive Force = Compression

TABLE 13

REACTIONS AND DISPLACEMENTS AT THE TOP OF THE PIERS OF WESTMONT VIADUCT COMPUTED BY THE E-E VIADUCT MODEL UNDER WINTER TEMPERATURE CHANGE

Pier No.	Span No.	Longitudinal		Transversal	
		Reactions (kN)	Displacements (mm)	Reactions (kN)	Displacements (mm)
Abt	1	- 39.72	8.38	0.01	1.55
1	1	8.04	1.70	327.08	0.30
1	2	- 37.85	8.08	146.30	1.37
2	2	6.27	1.32	0.02	0.23
2	3	- 37.14	7.95	- 0.02	1.22
3	3	5.83	1.24	- 144.70	0.18
3	4	- 36.61	7.82	- 13.37	1.19
4	4	5.16	1.12	0.0	0.18
4	5	- 35.85	7.67	0.0	1.17
5	5	5.29	1.14	162.09	0.18
5	6	- 36.16	7.75	70.19	1.12
6	6	4.80	1.03	0.01	0.15
6	7	- 36.12	7.75	0.0	1.04
7	7	4.80	1.03	3.78	0.14
7	8	- 36.30	7.77	372.00	1.04
8	8	4.89	1.07	0.04	0.13
8	9	- 37.05	7.98	- 0.02	0.86
9	9	4.45	0.97	- 134.83	0.10
9	10	- 37.3]	8.03	227.79	0.86
10	10	4.58	0.99	0.03	0.10
10	11	- 37.68	8.13	- 0.01	0.71
11	11	4.94	1.07	- 95.41	0.10
11	12	- 38.12	8.20	210.71	0.71
12	12	5.29	1.14	0.02	0.09

TABLE 13 (CONTINUED)

Pier No.	Span No.	Longidudinal Reactions (kN)	Longidudinal Displacements (mm)	Transversal Reaction (kN)	Transversal Displacements (mm)
12	13	- 37.63	8.13	- 0.01	0.76
13	13	4.85	1.07	- 82.11	0.08
13	14	- 36.92	7.98	192.12	0.58
14	14	3.43	0.74	0.02	0.05
14	15	- 34.83	7.52	0.0	0.41
15	15	1.07	0.23	- 137.54	0.01
15	16	- 38.88	8.38	120.19	0.43
16	16	6.01	1.30	0.0	0.07
16	17	- 36.79	7.95	0.0	0.38
17	17	0.71	0.15	- 47.95	0.01
17	18	- 31.45	6.81	- 9.39	0.33
18	18	- 1.38	- 0.29	0.0	- 0.01
18	19	- 27.62	5.97	0.0	0.28
19	19	- 4.94	- 1.07	2.27	- 0.05
19	20	- 21.97	4.75	- 1.33	0.23
20	20	- 6.23	- 1.35	0.0	- 0.06
20	21	- 23.04	4.98	0.0	0.23
21	21	- 17.88	- 3.86	- 3.43	- 0.18
21	22	- 13.97	3.02	- 23.75	0.14
22	22	- 26.64	- 5.84	0.0	- 0.25
22	23	- 3.16	0.69	0.0	0.03
23	23	- 30.29	- 6.55	- 114.99	- 0.30
23	24	2.14	- 0.46	229.22	- 0.01
24	24	- 35.76	- 7.72	0.0	- 0.21
24	25	6.14	- 1.32	0.0	- 0.04
25	25	- 39.32	- 8.51	- 49.91	- 0.23
25	26	6.98	- 1.51	192.25	- 0.03
26	26	- 40.43	- 8.74	0.0	- 0.15
26	27	9.43	- 2.04	0.0	- 0.03
Abt	27	- 41.68	- 9.02	49.69	- 0.15

TABLE 14

REACTIONS AND DISPLACEMENTS AT THE TOP OF THE PIERS OF COLLINGSWOOD VIADUCT COMPUTED BY THE E-F MODEL UNDER THE WINTER CONDITIONS

Pier No.	Span No.	Longitudinal		Transversal	
		Reactions (kN)	Displacements (mm)	Reactions (kN)	Displacements (mm)
Abt	1	- 12.58	7.19	0.0	0.0
1	1	-10,227.40	0.00	0.0	0.0
1	2	- 6,924.50	0.00	0.0	0.0
2	2	- 23.62	- 5.11	0.0	0.0
2	3	- 27.98	6.05	0.0	0.0
3	3	- 6,667.44	0.00	0.0	0.0
3	4	- 7,721.22	0.00	0.0	0.0
4	4	- 27.22	- 5.89	0.0	0.0
4	5	- 27.22	5.89	0.0	0.0
5	5	- 7,564.20	0.00	0.0	0.0
5	6	- 7,549.10	0.00	0.0	0.0
6	6	- 27.22	- 5.89	0.0	0.0
6	7	- 27.22	5.89	0.0	0.0
7	7	- 7,564.20	0.00	0.0	0.0
7	8	- 7,560.20	0.00	0.0	0.0
8	8	- 27.22	- 5.89	0.0	0.0
8	9	- 27.22	5.89	0.0	0.0
9	9	- 7,560.20	0.00	0.0	0.0
9	10	- 7,560.20	0.00	0.0	0.0
10	10	- 27.22	- 5.89	0.0	0.0
10	11	- 27.22	- 5.89	0.0	0.0
11	11	- 7,560.20	0.00	0.0	0.0
11	12	- 7,560.20	0.00	0.0	0.0
12	12	- 27.22	- 5.89	0.0	0.0

TABLE 14 (CONTINUED)

Pier No.	Span No.	Longit udinal		Transversal	
		Reactions (kN)	Displacements (mm)	Reactions (kN)	Displacements (mm)
12	13	- 27.22	5.89	0.0	0.0
13	13	- 7,560.20	0.00	- 0.01	0.0
13	14	- 7,560.20	0.00	- 0.06	0.0
14	14	- 27.22	- 5.89	0.00	0.0
14	15	- 27.22	5.89	0.00	0.0
15	15	- 7,559.30	0.00	- 0.33	0.0
15	16	- 7,559.30	0.00	- 1.67	0.0
16	16	- 27.22	- 5.89	0.00	0.0
16	17	- 27.22	5.89	0.00	0.0
17	17	- 7,576.20	0.00	- 8.94	0.0
17	18	- 7,536.60	0.00	- 55.83	0.0
18	18	- 27.22	- 5.89	- 0.01	0.0
18	19	- 27.22	5.89	- 0.32	- 0.08
19	19	- 7,479.70	0.00	-117.66	0.0
19	20	- 8,126.50	0.00	- 59.87	0.0
20	20	- 27.22	- 5.89	0.05	0.06
20	21	- 27.22	- 5.89	- 0.01	- 0.14
21	21	- 7,930.30	0.0	- 36.70	0.0
21	22	- 8,515.70	- 0.00	- 57.47	0.0
22	22	- 29.27	- 6.35	0.00	0.14
22	23	- 29.54	6.38	0.02	- 0.16
23	23	- 8.047.70	0.00	- 45.46	0.0
23	24	- 9,918.20	0.00	- 17.48	0.0
24	24	- 28.74	- 6.22	0.19	15.72
24	25	- 38.21	8.25	0.10	- 0.20
25	25	-11,021.40	0.00	- 37.05	0.0
25	26	-12,616.00	0.00	105.50	0.0

TABLE 14 (CONTINUED)

Pier No.	Span No.	Longitudinal Reactions (kN)	Longitudinal Displacements (mm)	Transversal Reactions (kN)	Transversal Displacements (mm)
26	26	- 37.59	- 8.13	0.01	0.17
26	27	- 35.32	7.65	0.01	- 0.04
27	27	-12,415.90	0.00	149.20	0.00
27	28	-12,004.40	0.00	60.18	0.00
28	28	- 35.50	- 7.67	0.00	0.00
28	29	- 35.90	7.77	0.00	0.04
29	29	-12,315.30	0.00	98.35	0.00
29	30	-10,837.60	0.00	16.73	0.00
30	30	- 36.92	- 7.98	0.00	- 0.15
30	31	- 28.87	6.25	0.00	0.12
31	31	- 9,727.80	0.00	6.00	0.00
31	32	- 8,125.60	0.00	- 88.34	0.00
32	32	- 29.49	- 6.38	0.00	- 0.07
32	33	- 29.27	6.35	0.00	0.07
33	33	- 8,318.18	0.00	40.21	0.00
33	34	- 6,712.40	0.00	13.48	0.00
Abt	34	- 29.94	- 6.48	0.00	- 0.06

TABLE 15

REACTIONS AND DISPLACEMENTS AT THE TOP OF THE PIERS OF WESTMONT VIADUCT COMPUTED BY THE E-F MODEL UNDER WINTER CONDITIONS

Pier No.	Span No.	Longitudinal		Transversal	
		Reactions (kN)	Displacements (mm)	Reactions (kN)	Displacements (mm)
Abt	1	- 32.21	6.83	0.07	1.22
1	1	- 2,529.70	0.00	- 6,503.70	0.00
1	2	- 9,039.20	0.00	2,408.70	0.00
2	2	- 27.58	- 5.89	- 0.67	- 0.85
2	3	- 27.67	5.92	0.67	0.76
3	3	- 7,945.40	0.00	- 5,624.30	0.00
3	4	- 7,790.20	0.00	5,923.70	0.00
4	4	- 27.89	- 5.99	- 0.62	- 0.79
4	5	- 27.09	5.82	0.58	- 0.76
5	5	- 7,695.40	- 0.00	- 5,832.50	- 0.00
5	6	- 7,893.80	0.00	5,778.20	0.00
6	6	- 27.76	- 5.97	- 0.67	- 0.71
6	7	- 27.76	5.97	0.67	0.67
7	7	- 7,909.80	0.00	- 5,068.70	0.00
7	8	- 8,086.40	0.00	6,192.40	0.00
8	8	- 27.71	- 5.94	- 0.49	- 0.69
8	9	- 28.82	6.20	0.58	0.53
9	9	- 8,413.40	0.00	- 3,699.60	0.00
9	10	- 8,618.40	0.00	4,904.20	0.00
10	10	- 28.82	- 6.20	- 0.42	- 0.58
10	11	- 28.87	6.22	0.44	0.46
11	11	- 8,548.60	0.00	- 4,282.10	0.00
11	12	- 8,936.90	0.00	4,477.60	0.00
12	12	- 28.96	- 6.25	- 0.35	- 0.48

TABLE 15 (CONTINUED)

REACTIONS AND DISPLACEMENTS AT THE TOP OF THE PIERS OF WESTMONT VIADUCT COMPUTED BY THE E-F MODEL UNDER WINTER CONDITIONS

Pier No.	Span No.	Longitudinal		Transversal	
		Reactions (kN)	Displacements (mm)	Reactions (kN)	Displacements (mm)
12	13	- 29.54	6.38	0.30	0.41
13	13	- 8,551.30	0.00	- 7,700.30	0.00
13	14	- 9,099.30	0.00	7,836.40	0.00
14	14	- 29.98	- 6.48	- 0.26	0.41
14	15	- 30.29	6.55	0.23	0.30
15	15	- 8,944.90	0.00	- 2,080.40	0.00
15	16	- 9,633.90	0.00	2,882.40	0.00
16	16	- 29.27	- 6.32	- 0.12	- 0.30
16	17	- 32.78	7.09	0.12	0.30
17	17	- 9,435.60	0.00	- 4,868.10	0.00
17	18	- 9,497.40	0.00	1,600.00	0.00
18	18	- 29.94	- 6.48	- 0.22	- 0.26
18	19	- 29.54	6.38	0.02	0.30
19	19	- 7,898.30	0.00	- 8,674.00	0.00
19	20	- 8,573.10	0.00	- 4,644.40	0.00
20	20	- 24.90	- 5.38	- 0.05	- 0.24
20	21	- 36.20	7.82	0.17	0.33
21	21	-10,791.40	0.00	8,162.90	0.00
21	22	-11,979.90	0.00	-17,569.10	0.00
22	22	- 35.50	- 7.67	- 0.24	- 0.31
22	23	- 29.22	6.32	0.13	0.27
23	23	-10,219.80	0.00	14,848.70	0.00
23	24	8,651.80	0.00	11,766.00	0.00

TABLE 15 (CONTINUED)

REACTIONS AND DISPLACEMENTS AT THE TOP OF THE PIERS OF WESTMONT VIADUCT COMPUTED BY THE E-F MODEL UNDER WINTER CONDITIONS

Pier No.	Span No.	Longitudinal		Transversal	
		Reactions (kN)	Displacements (mm)	Reactions (kN)	Displacements (mm)
24	24	- 30.74	- 6.65	- 0.08	- 0.16
24	25	- 29.67	6.40	0.09	0.15
25	25	- 9,773.60	0.00	71.04	0.00
25	26	- 8,371.10	0.00	779.77	0.00
26	26	- 30.47	- 6.60	- 0.04	- 0.10
26	27	- 28.65	6.17	0.05	0.10
Abt	27	-10,601.00	0.00	519,10	0.00

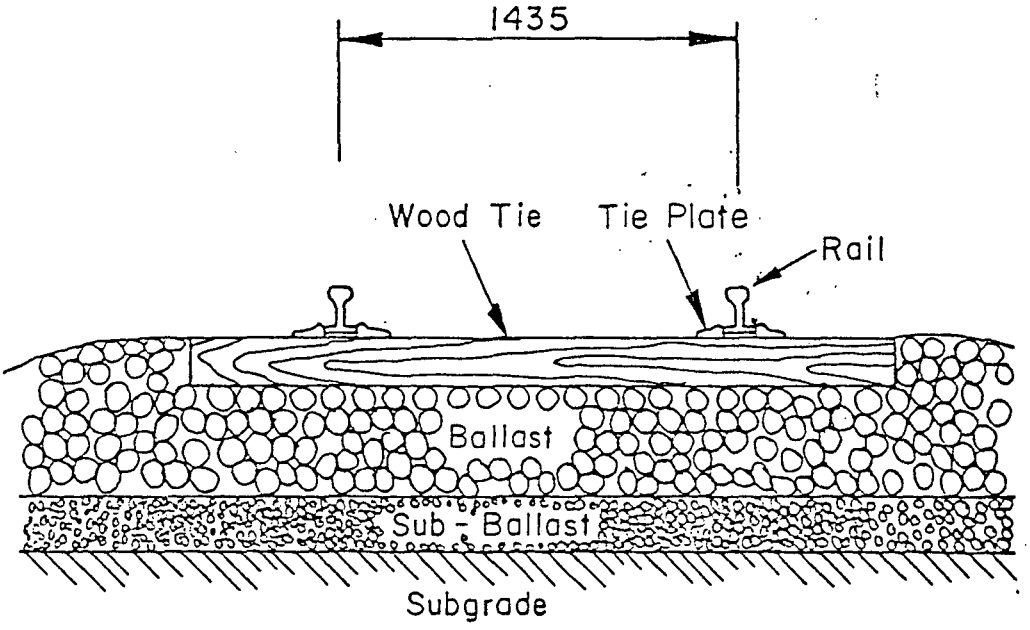

Fig. 1 Conventional Railway Track on Soil

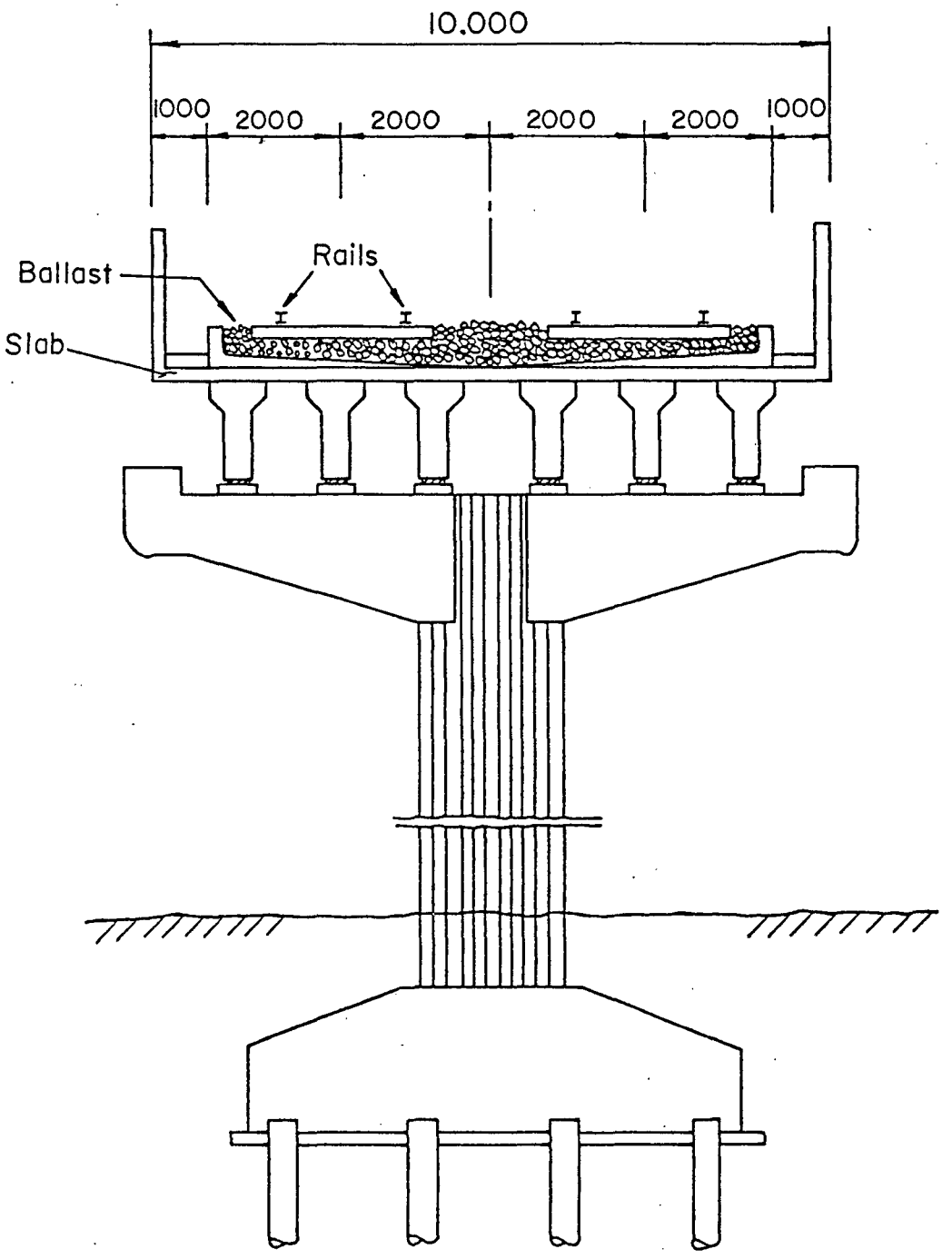

Fig. 2 Conventional Concrete Railroad Viaduct

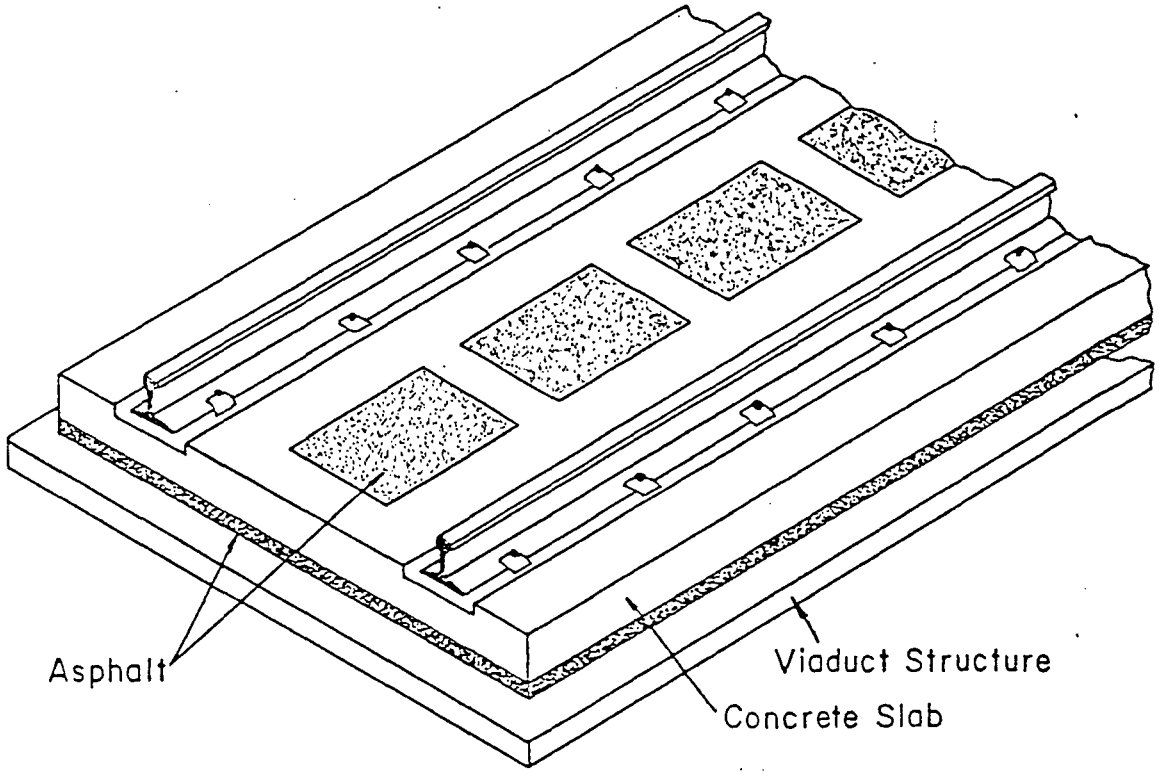

Fig. 3 Japanese Railroad Association Track (JRA)

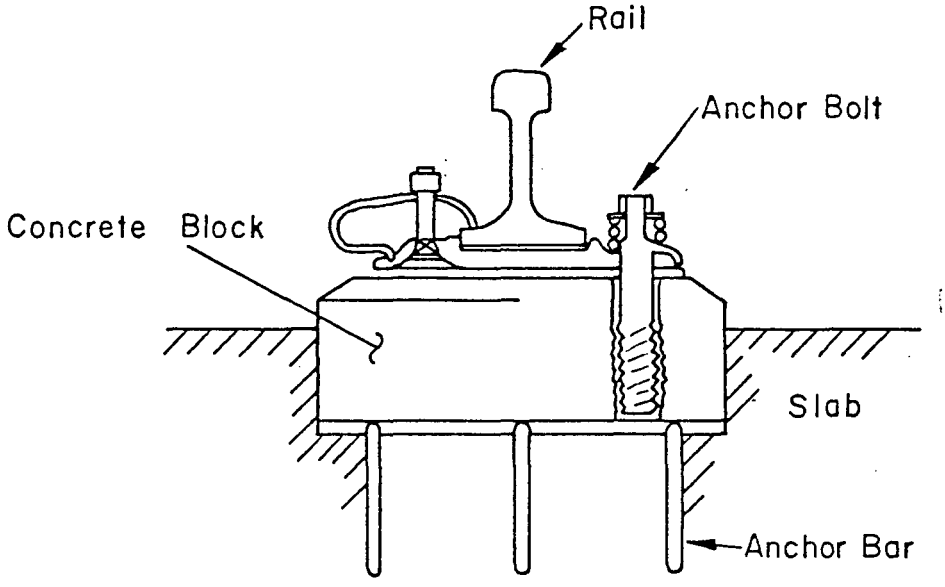

Fig. 4 Concrete Block Embedded in Concrete Slab

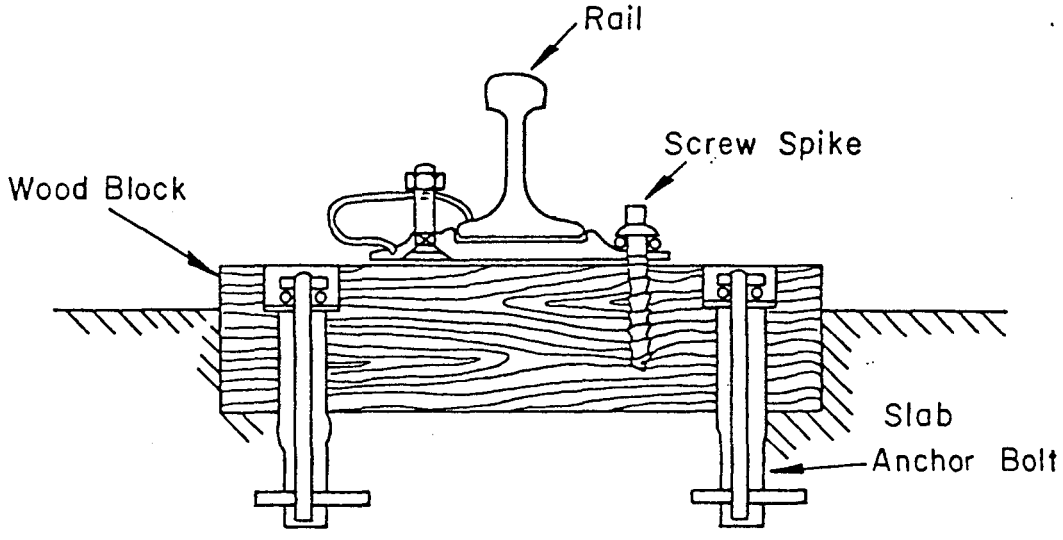

Fig. 5 Wood Block Embedded in Concrete Slab

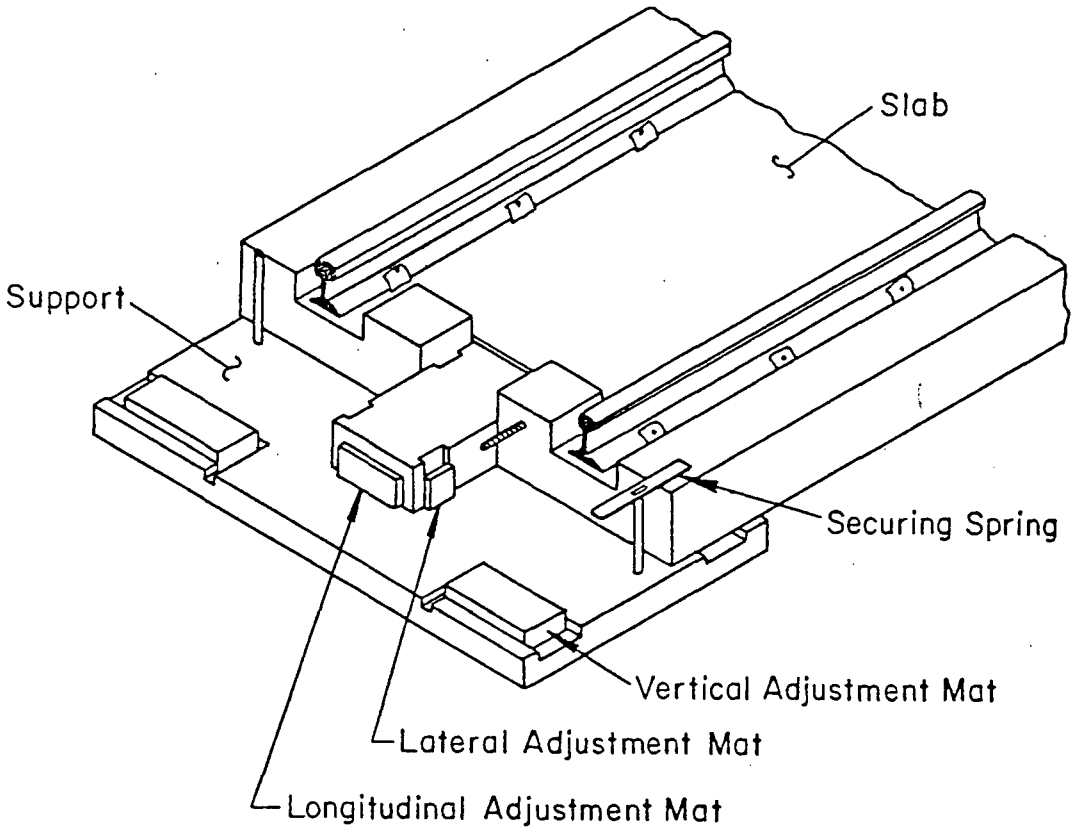

Fig. 6 Japanese Railroad Maintenance Track Slab (JRM)

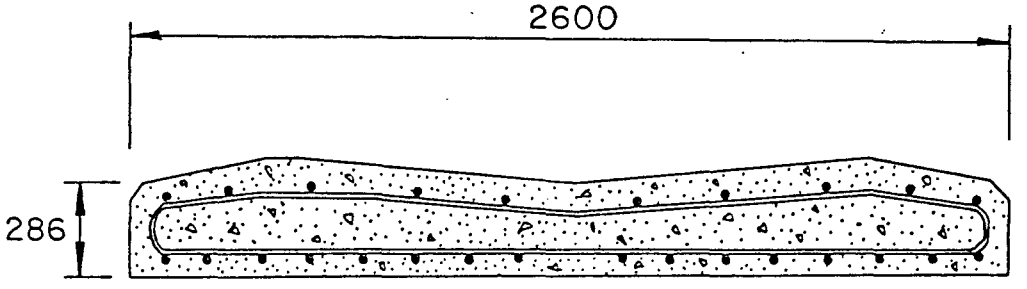

Fig. 7 Cross-Section of the Slab Tested by the British Railways (BR)

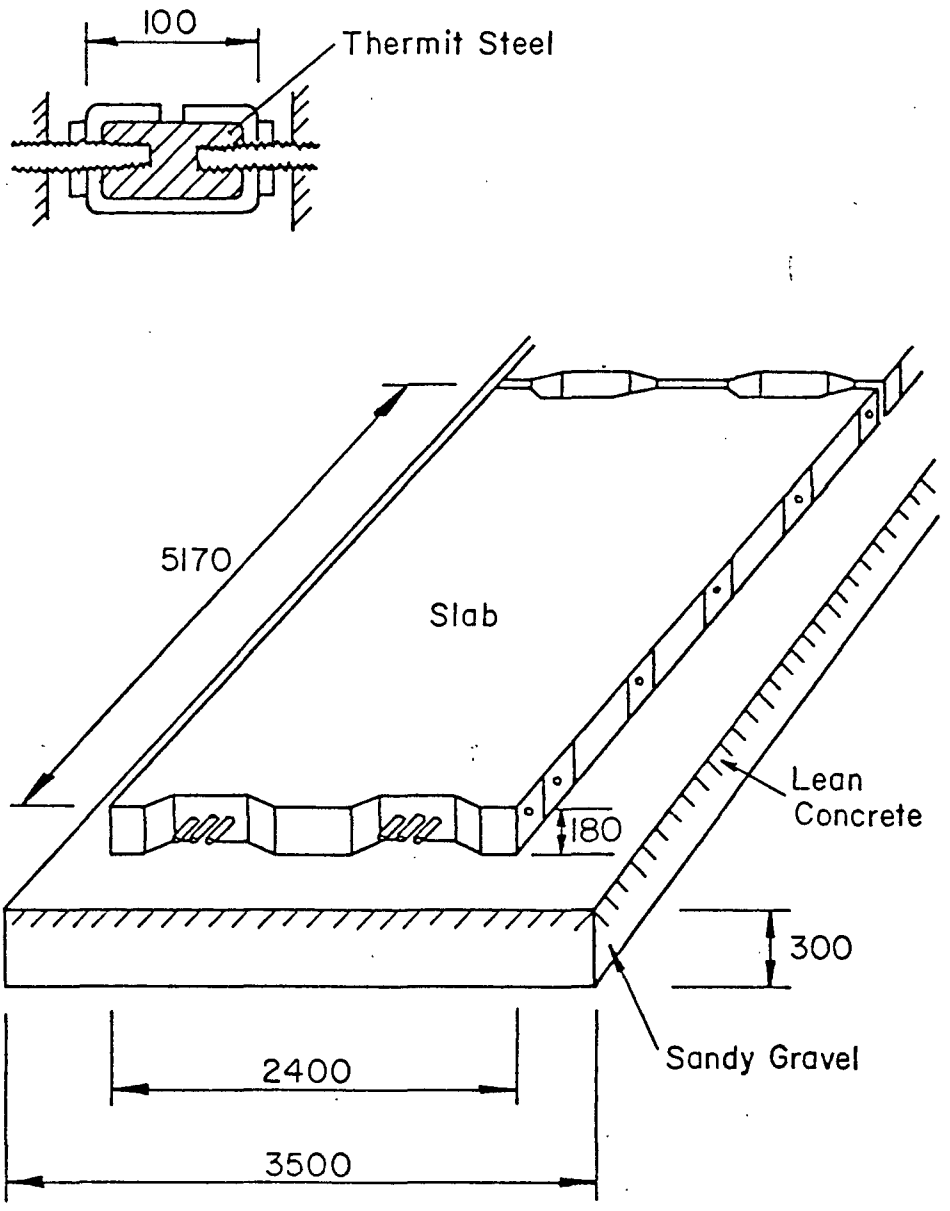

Fig. 8 Concrete Slab Tested by the German Federal Railways (DB)

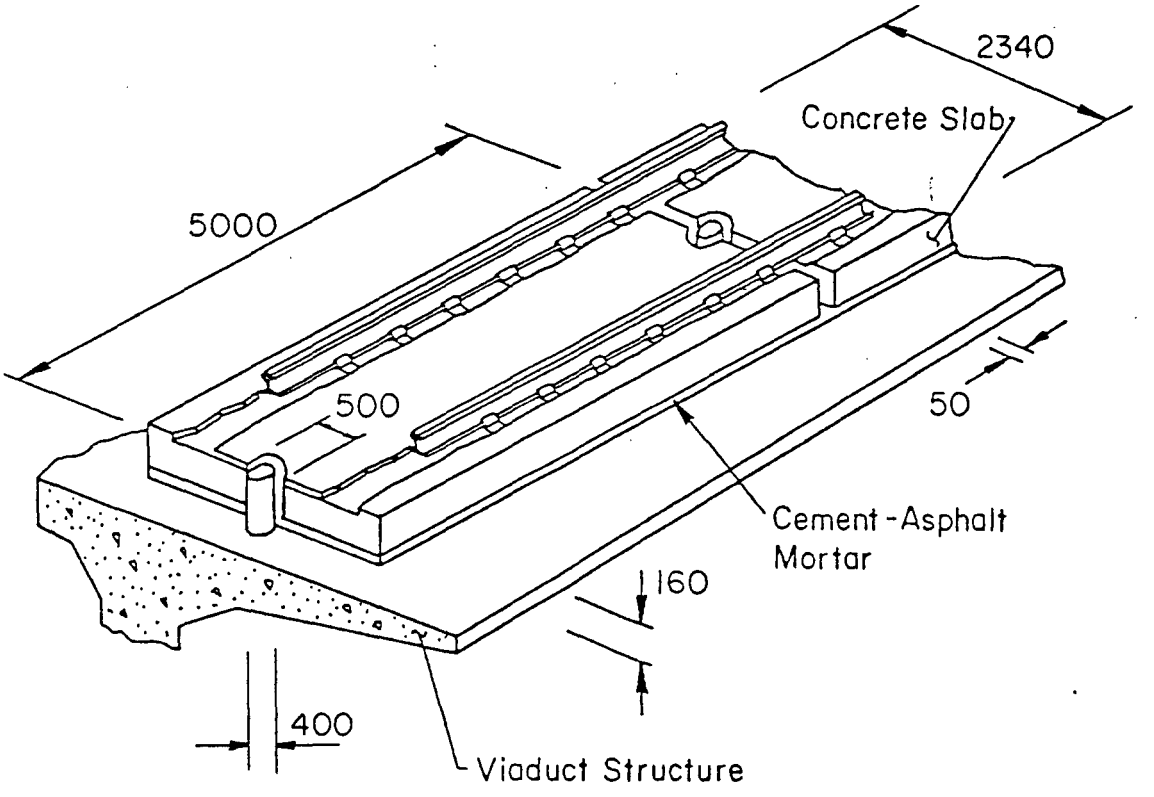

Fig. 9 Track on Concrete Slab on Elevated Structure Tested by the Japanese National Railways - The Tokaido Line

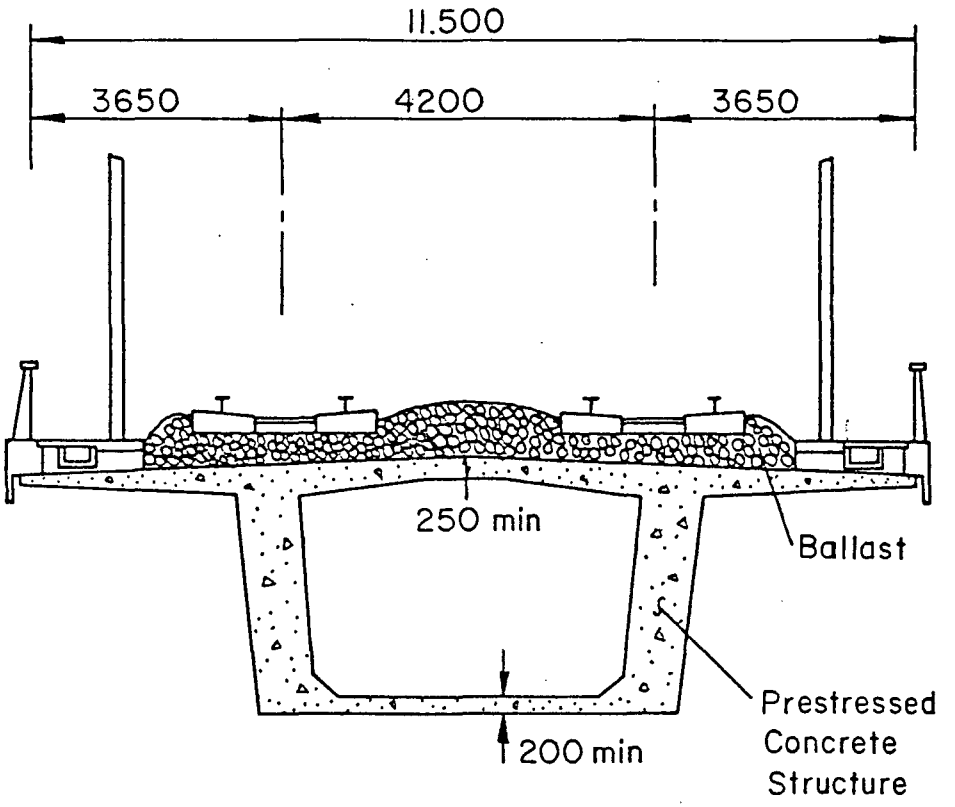

Fig. 10 Cross-Section of a Continuous Viaduct Built by the French National Railways (SNCF)

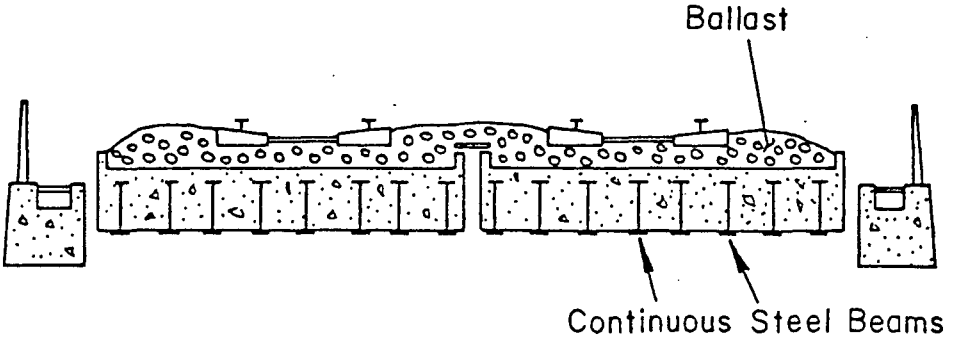

Fig. 11 Composite Concrete/Steel Bridge Built by the French National Railways (SNCF)

Fig. 12 Westmont Viaduct Looking towards the Station

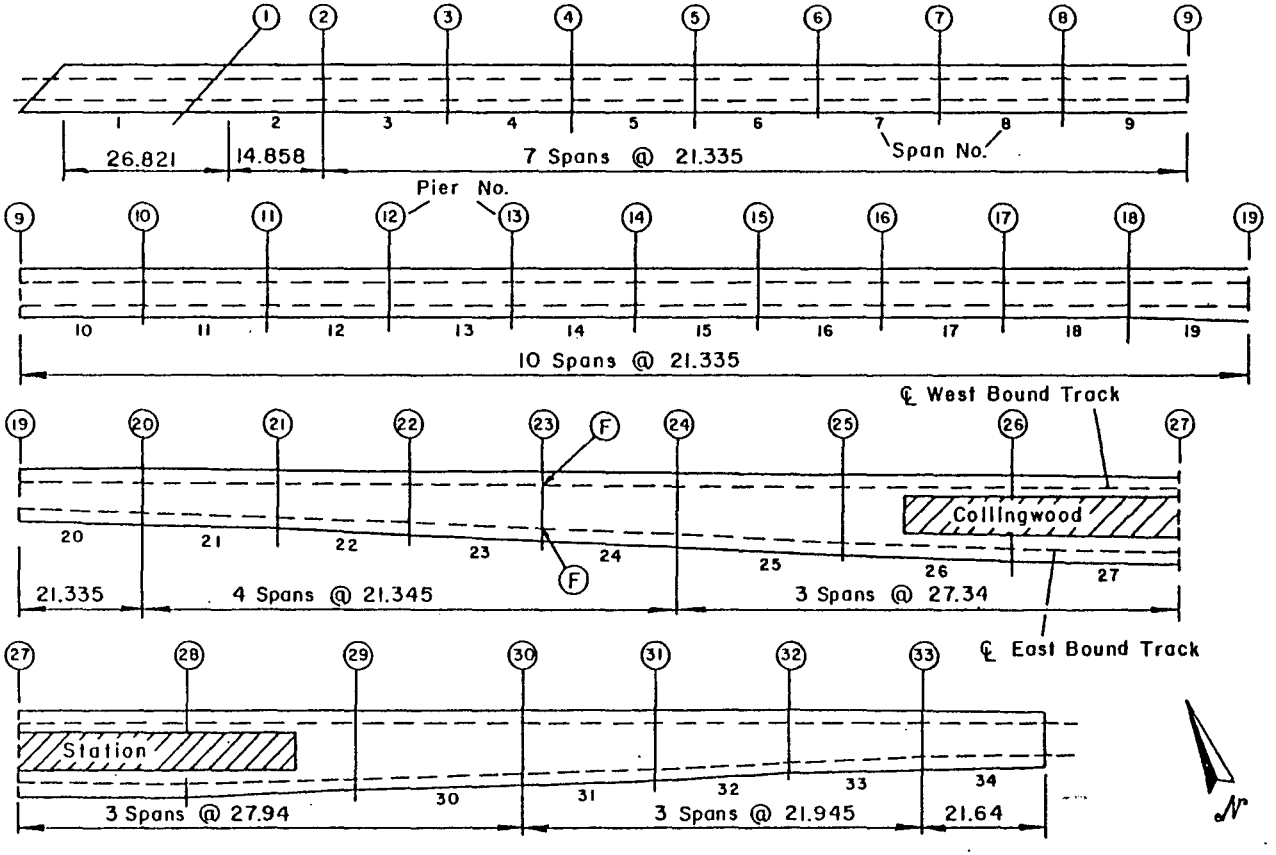

Fig. 13 Plan of the Collingswood Viaduct

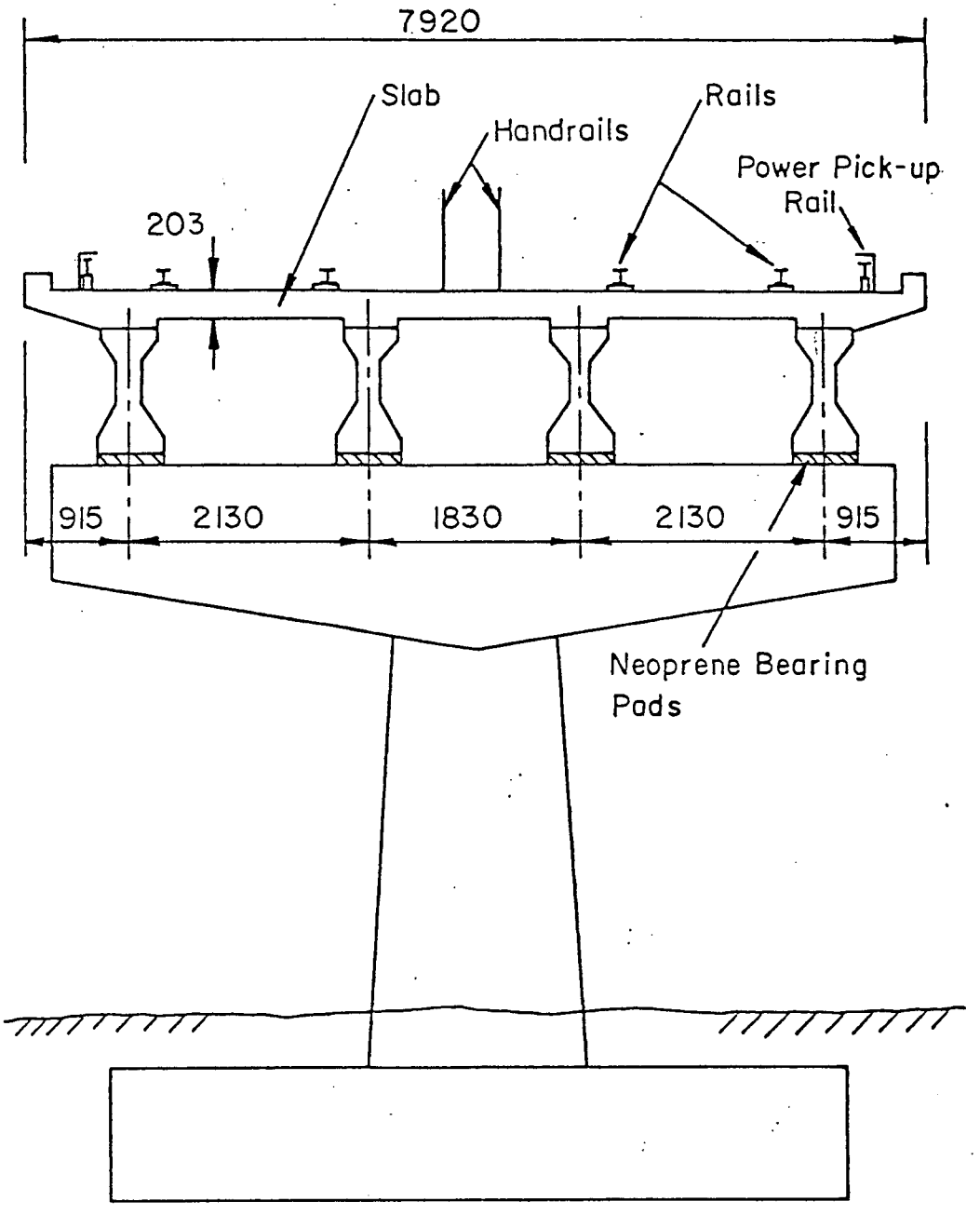

Fig. 14 Typical Cross-Section of the 4 I-Beam Span of the Collingswood and Westmont Viaducts

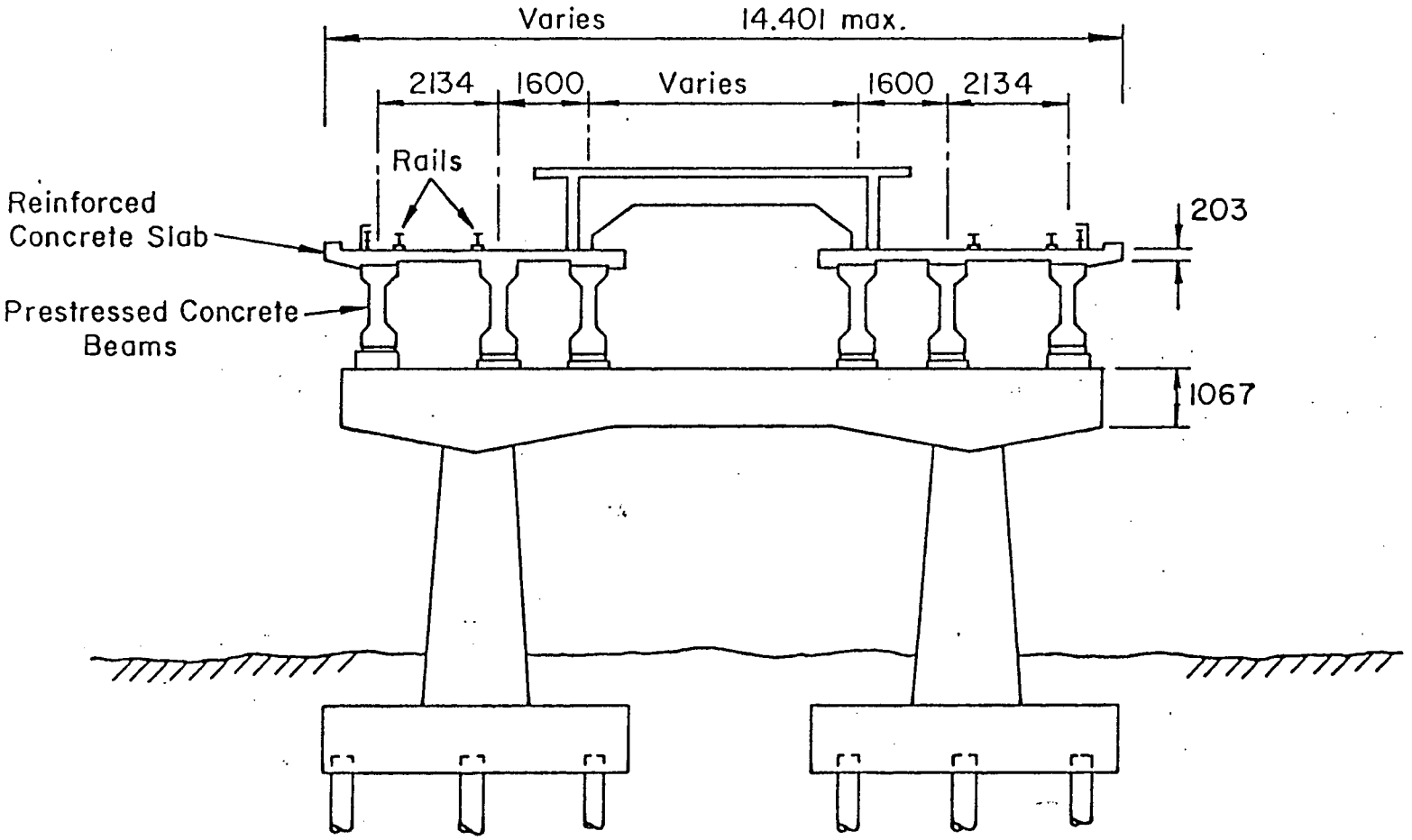

Fig. 15 Cross-Section of the Collingswood and Westmont Viaducts in the Vicinity of the Station

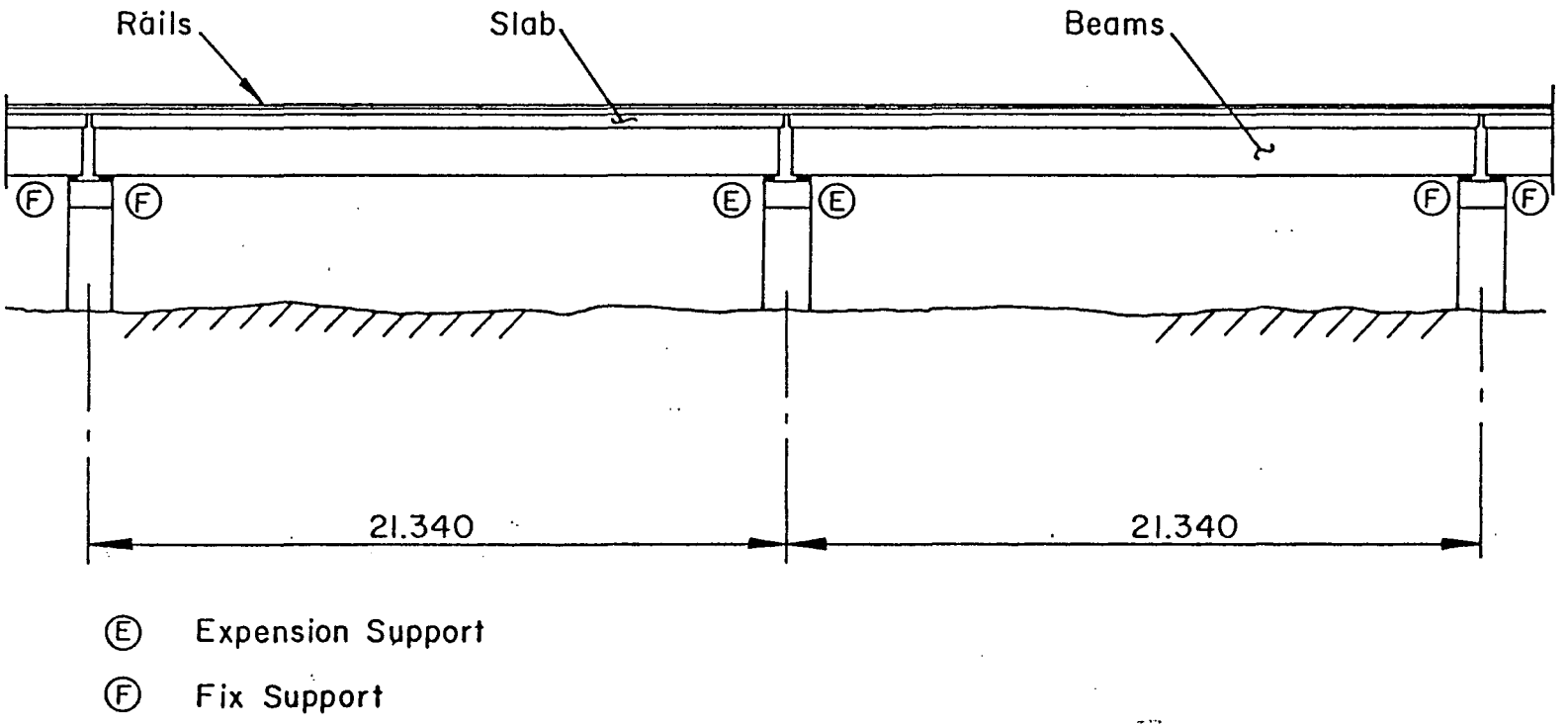

Fig. 16 Typical Elevation of the Collingswood and Westmont Viaducts

Fig. 17 One Complete Span of Collingswood Viaduct

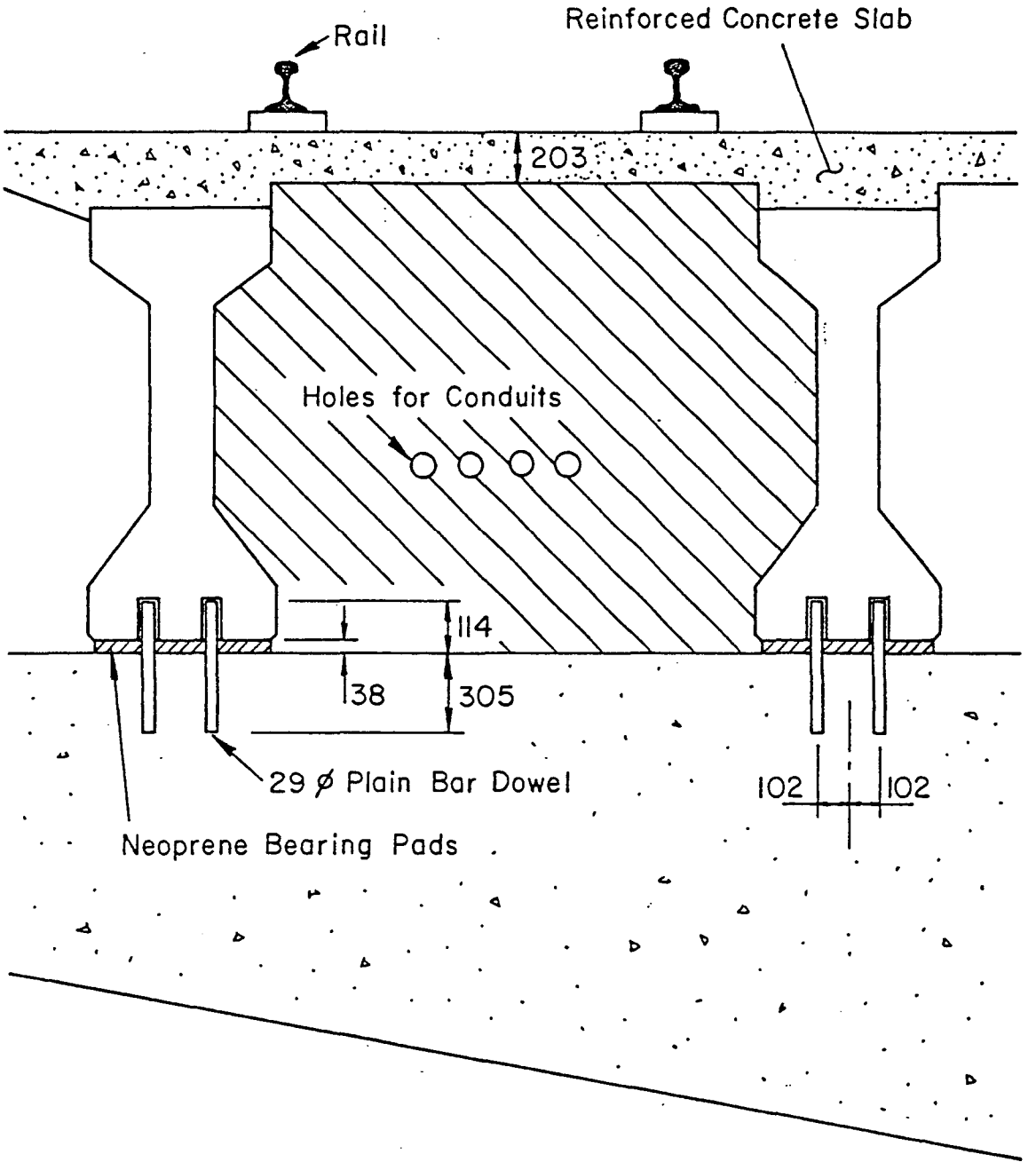

Fig. 18 Anchorage Details at the Fixed Bearings of the Collingswood Viaduct

Fig. 19 Continuous Rails over the Joint in the Slab and Anchorages of the Rails

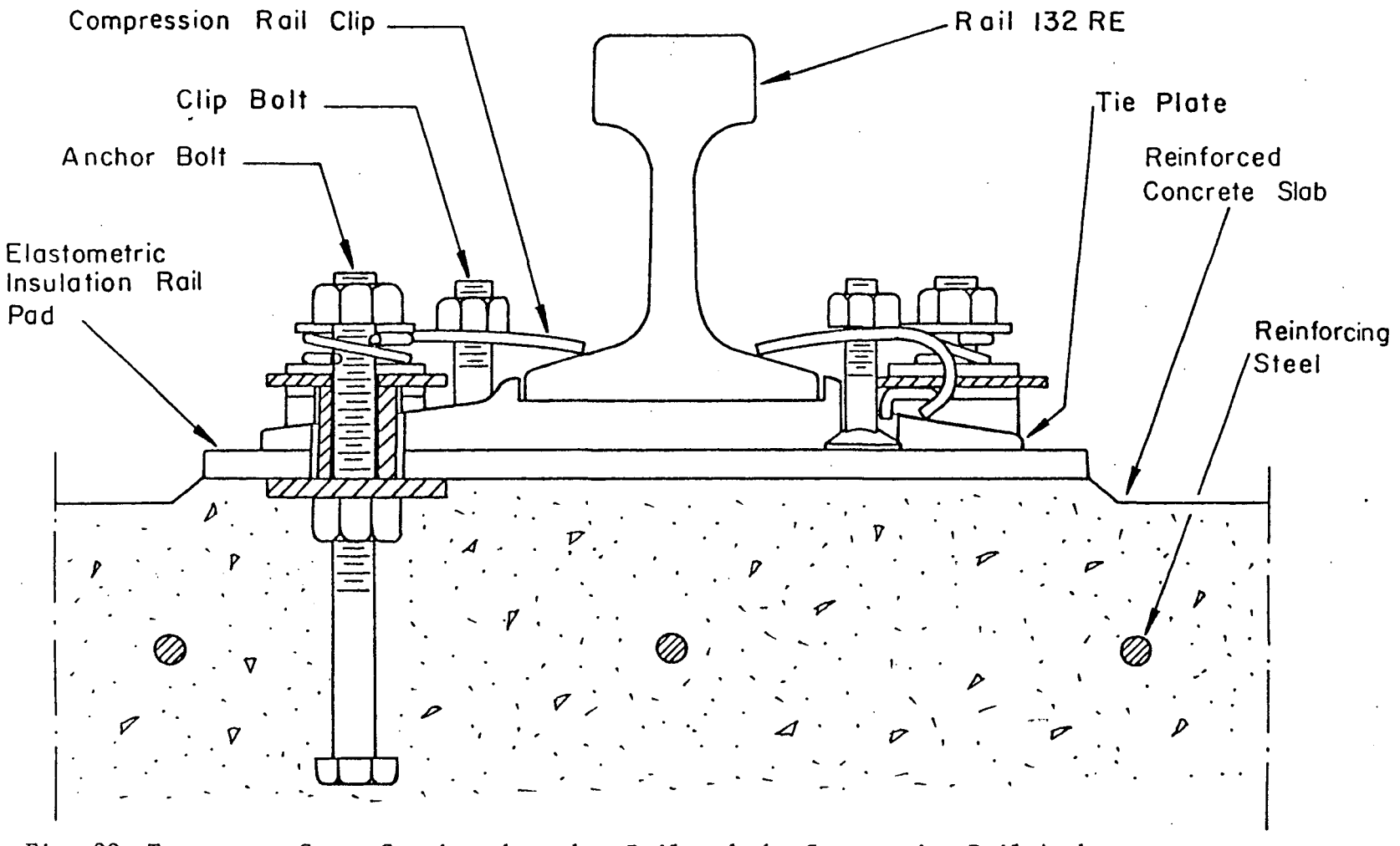

Fig. 20 Transverse Cross-Section through a Rail and the Compression Rail Anchorage

Fig. 21 Fiberglass Joint on the Rails near the Station

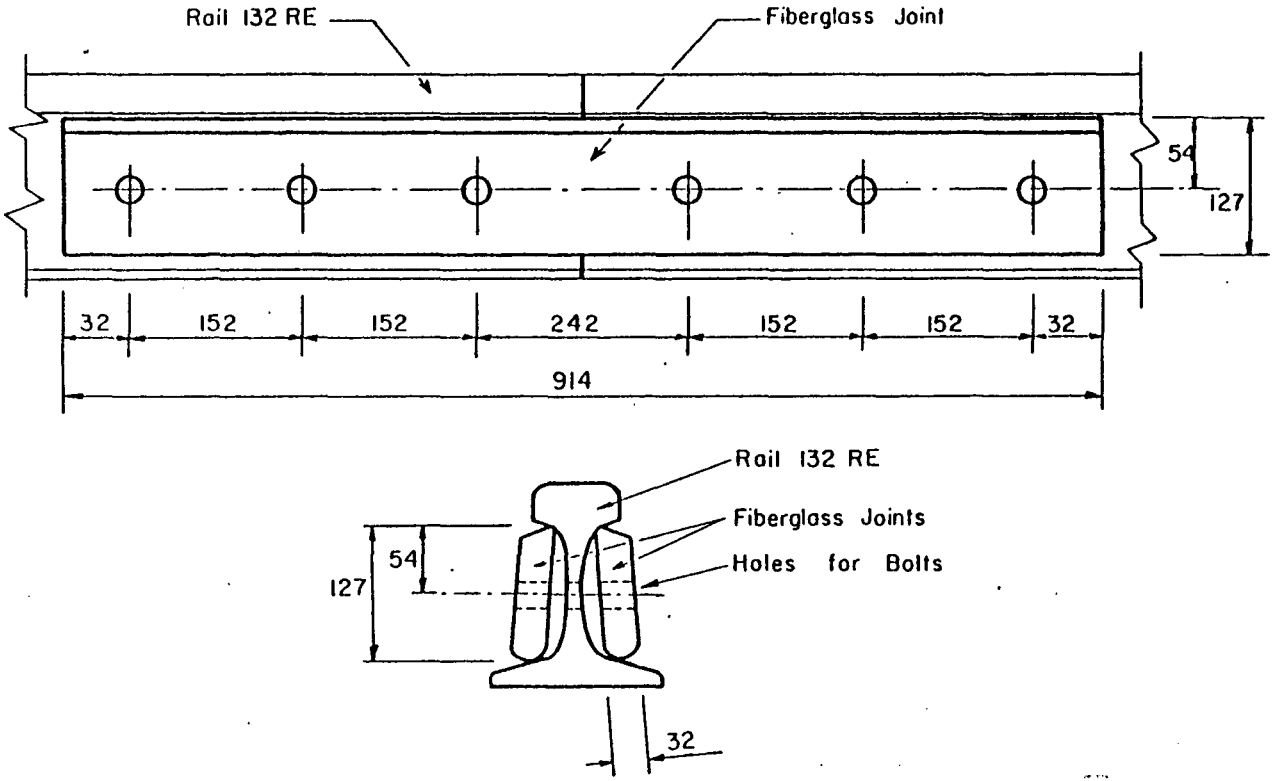

Fig. 22 Fiberglass Strips used to Create the Electric Insulation Joint on the Rails

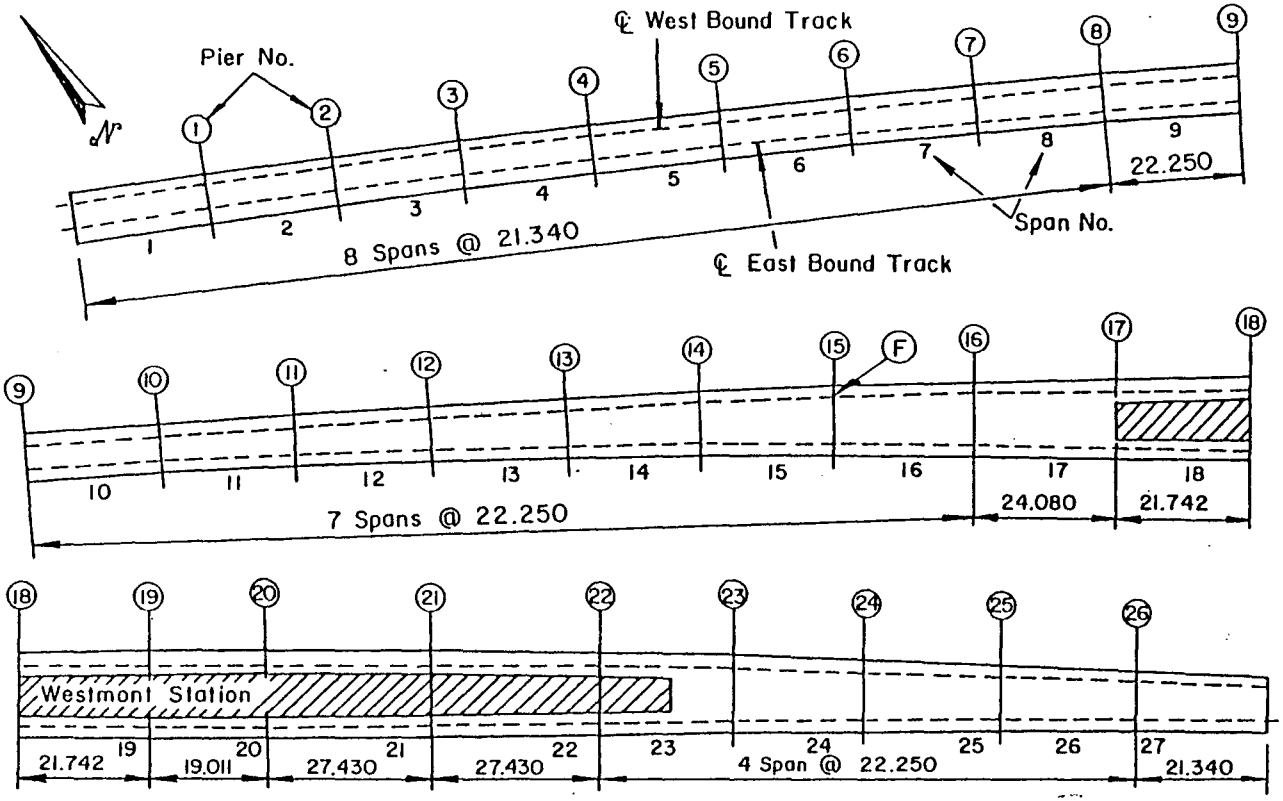

Fig. 23 Plan of the Westmont Viaduct

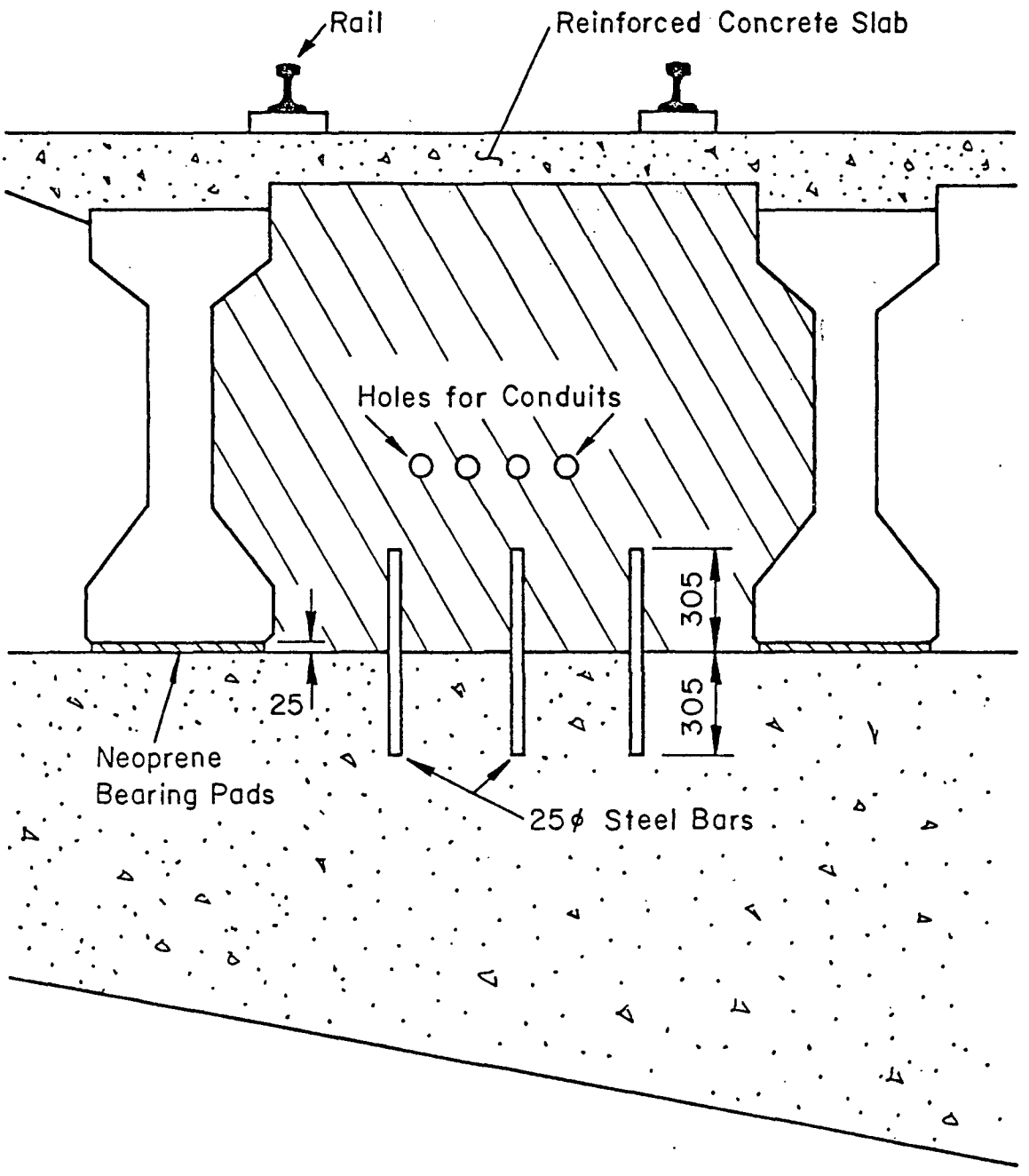

Fig. 24 Anchorage Details at the Fixed Bearings of the Westmont Viaduct

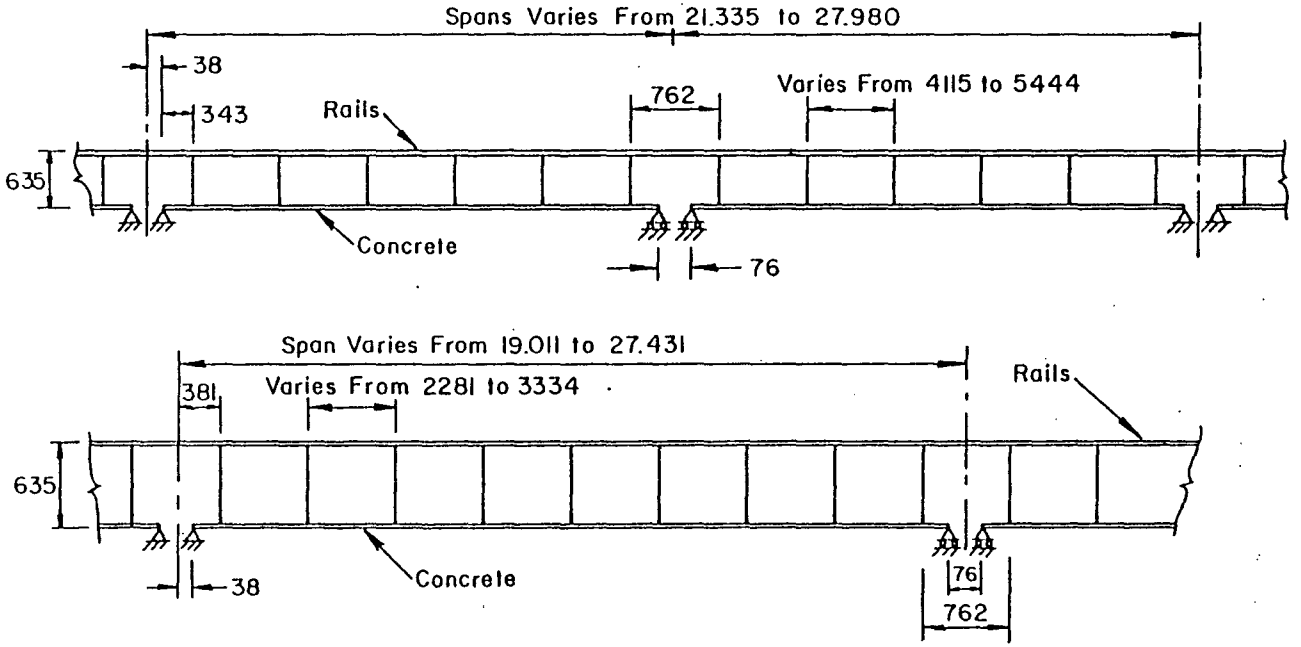

Fig. 25 Collingswood and Westmont Finite Element Models

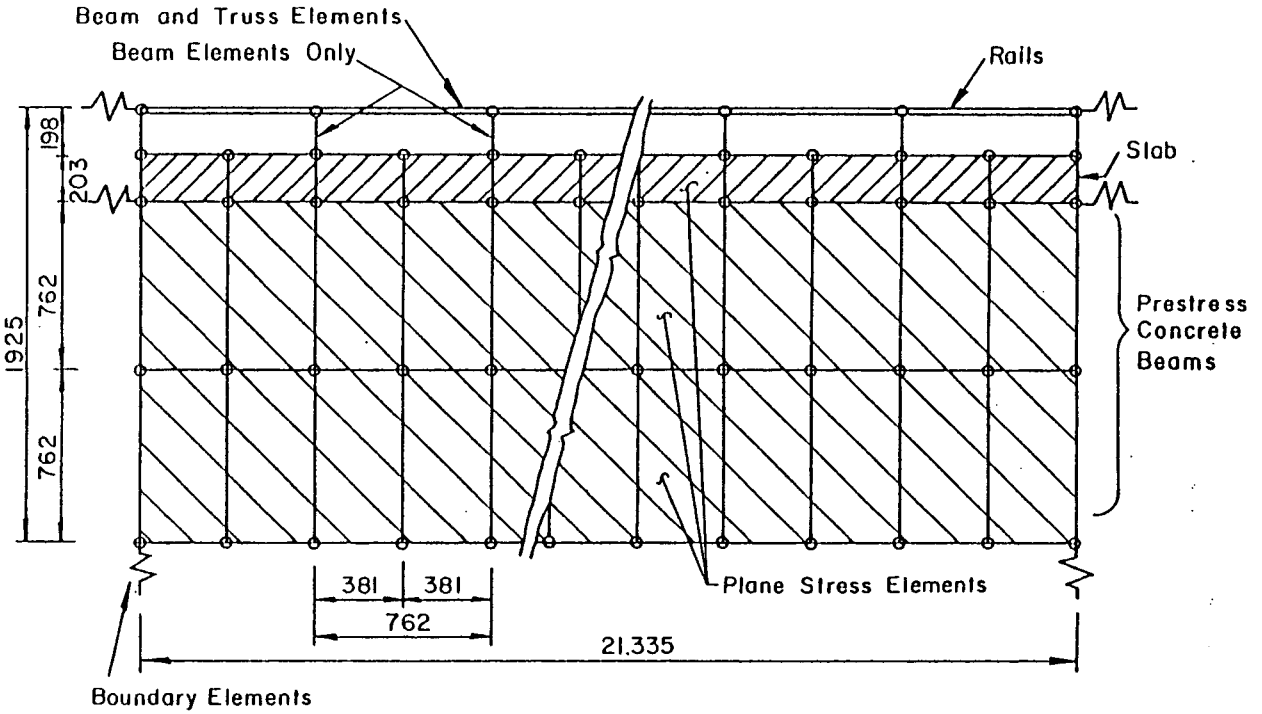

Fig. 27 One-Span Finite Element Model

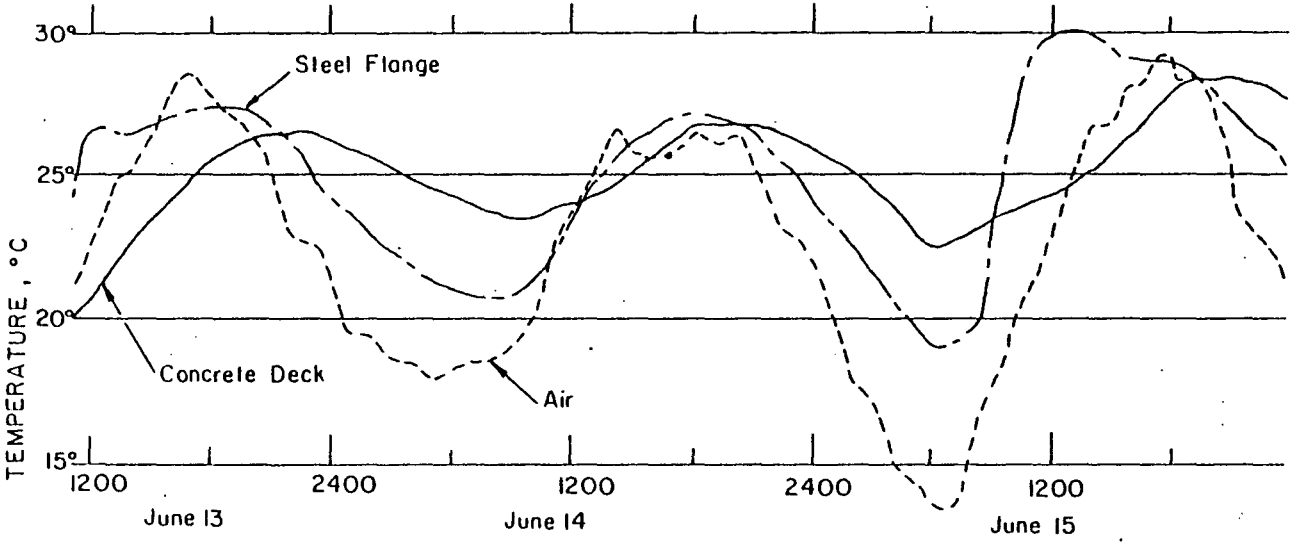

Fig. 27 Temperature Variation for a Concrete Deck-Steel Girder Bridge

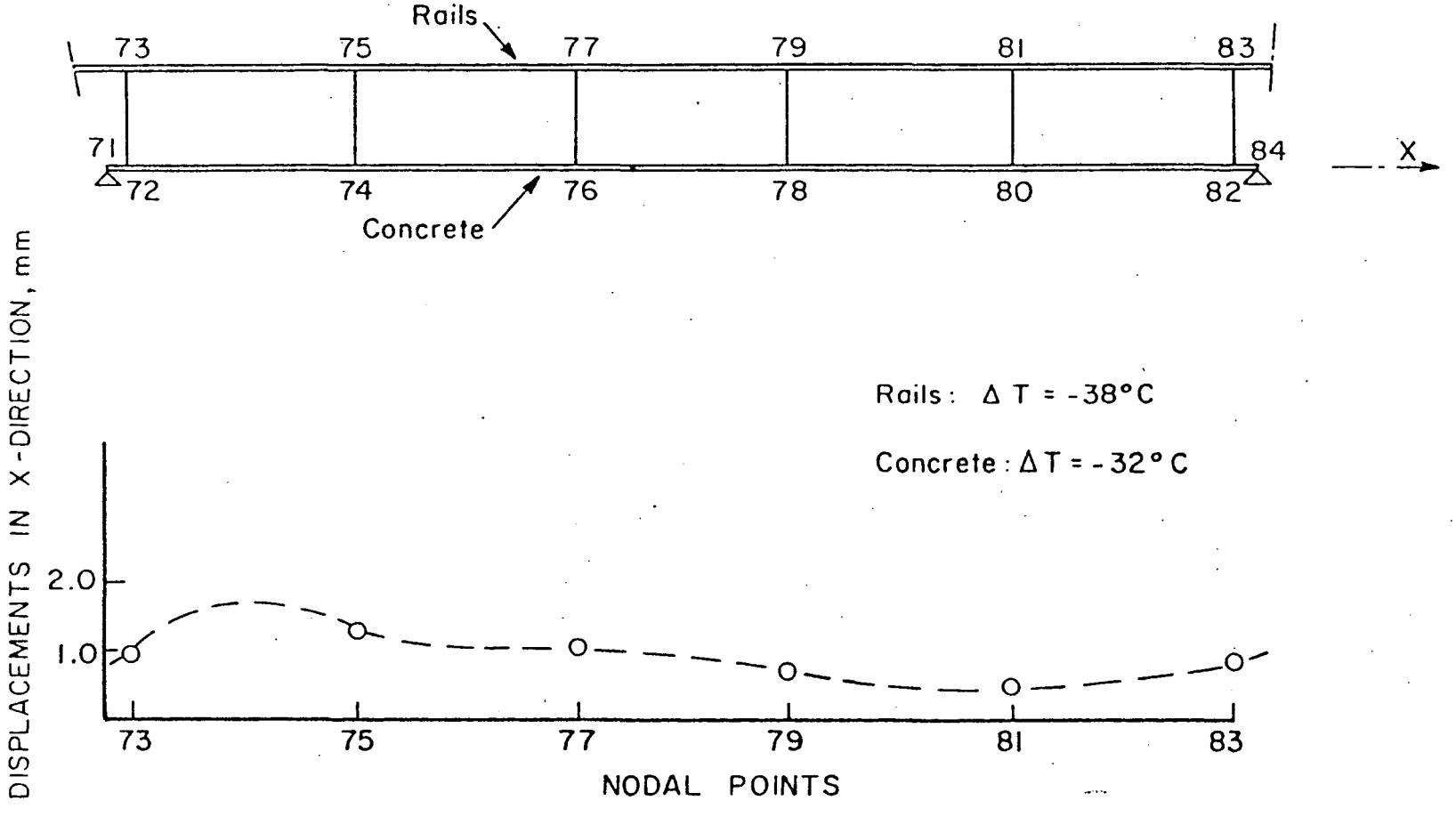

Fig. 28 Longitudinal Displacements of the Rails in Span 6 of Collingswood Viaduct as Computed by the E-E Viaduct Model

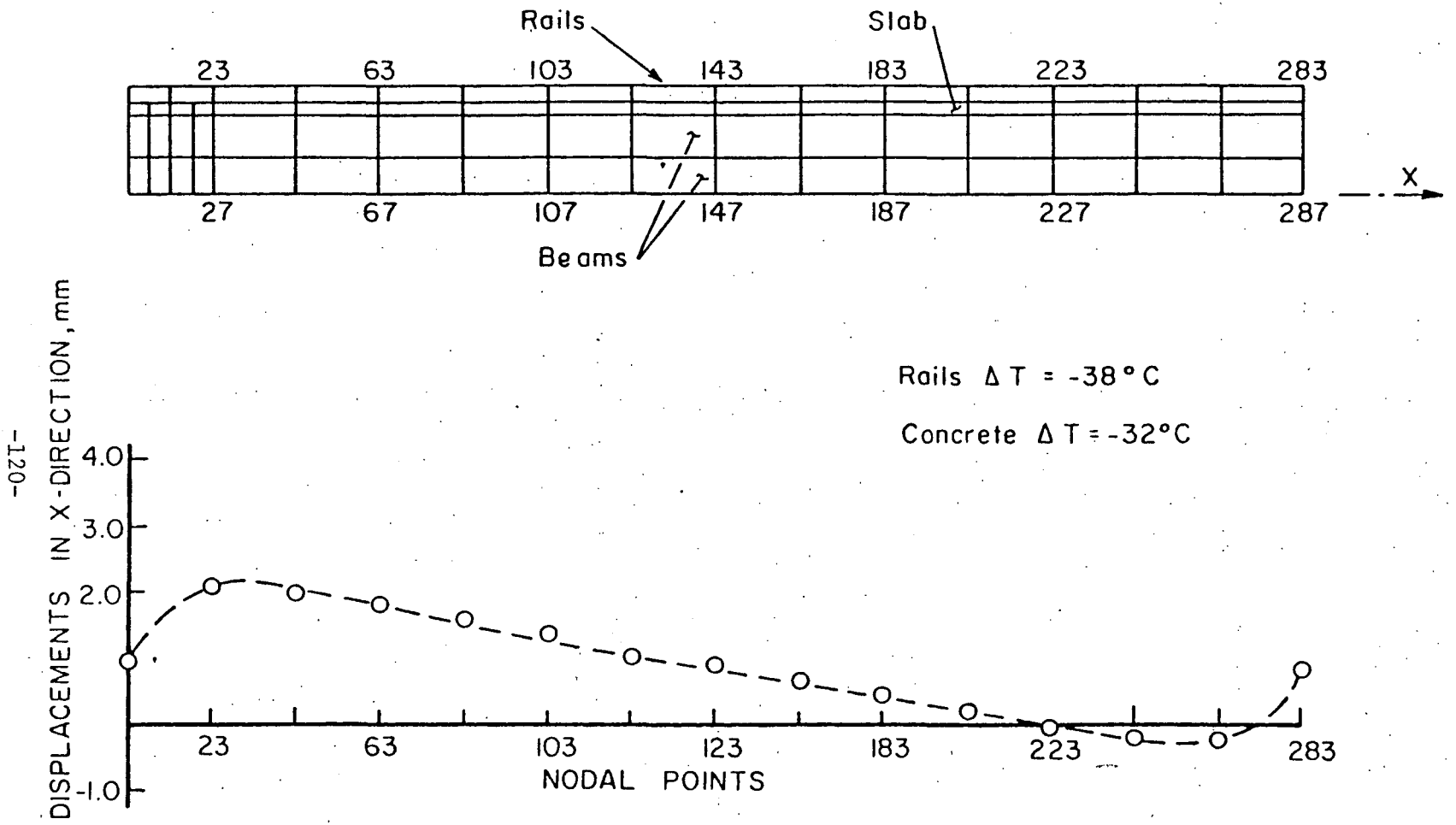

Fig. 29 Longitudinal Displacements of the Rails in Span 6 of Collingswood Viaduct as Computed by the One-Span Model

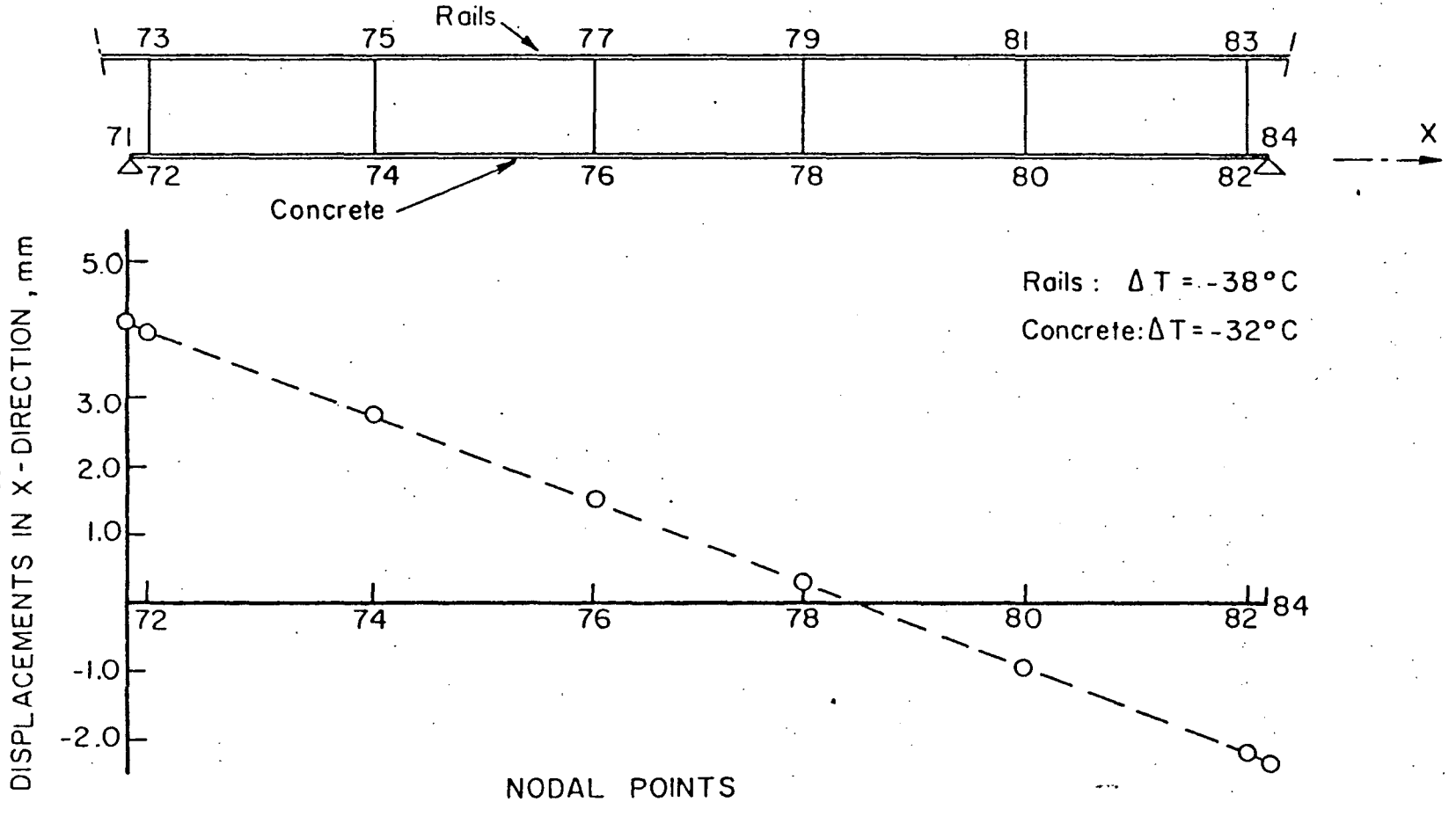

Fig. 30 Longitudinal Displacements of the Concrete Section in Span 6 of Collingswood Viaduct as Computed by the E-E Viaduct Model

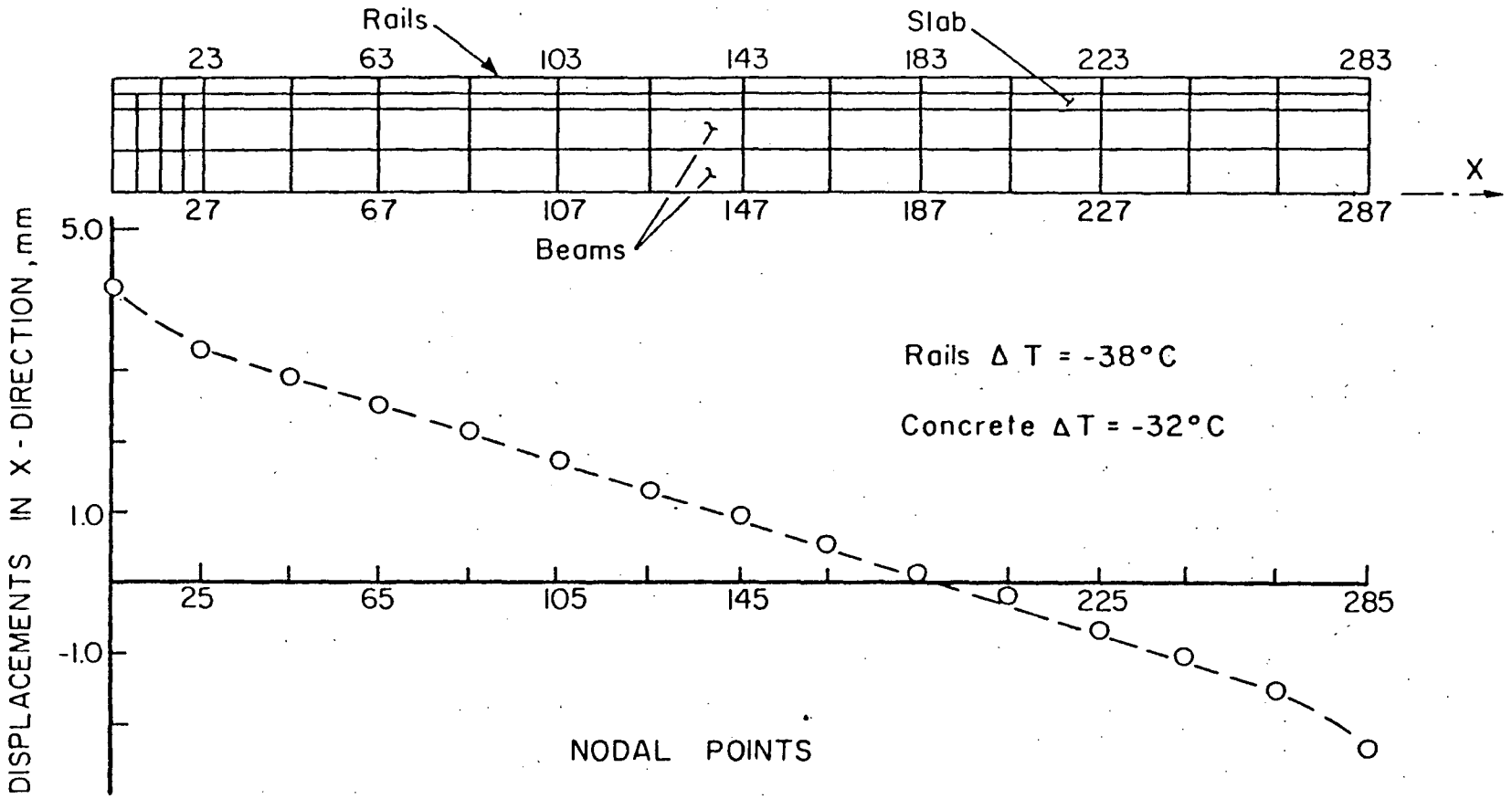

Fig. 31 Longitudinal Displacements of the Bottom of the Slab in Span 6 of Collingswood Viaduct as Computed by the One-Span Model

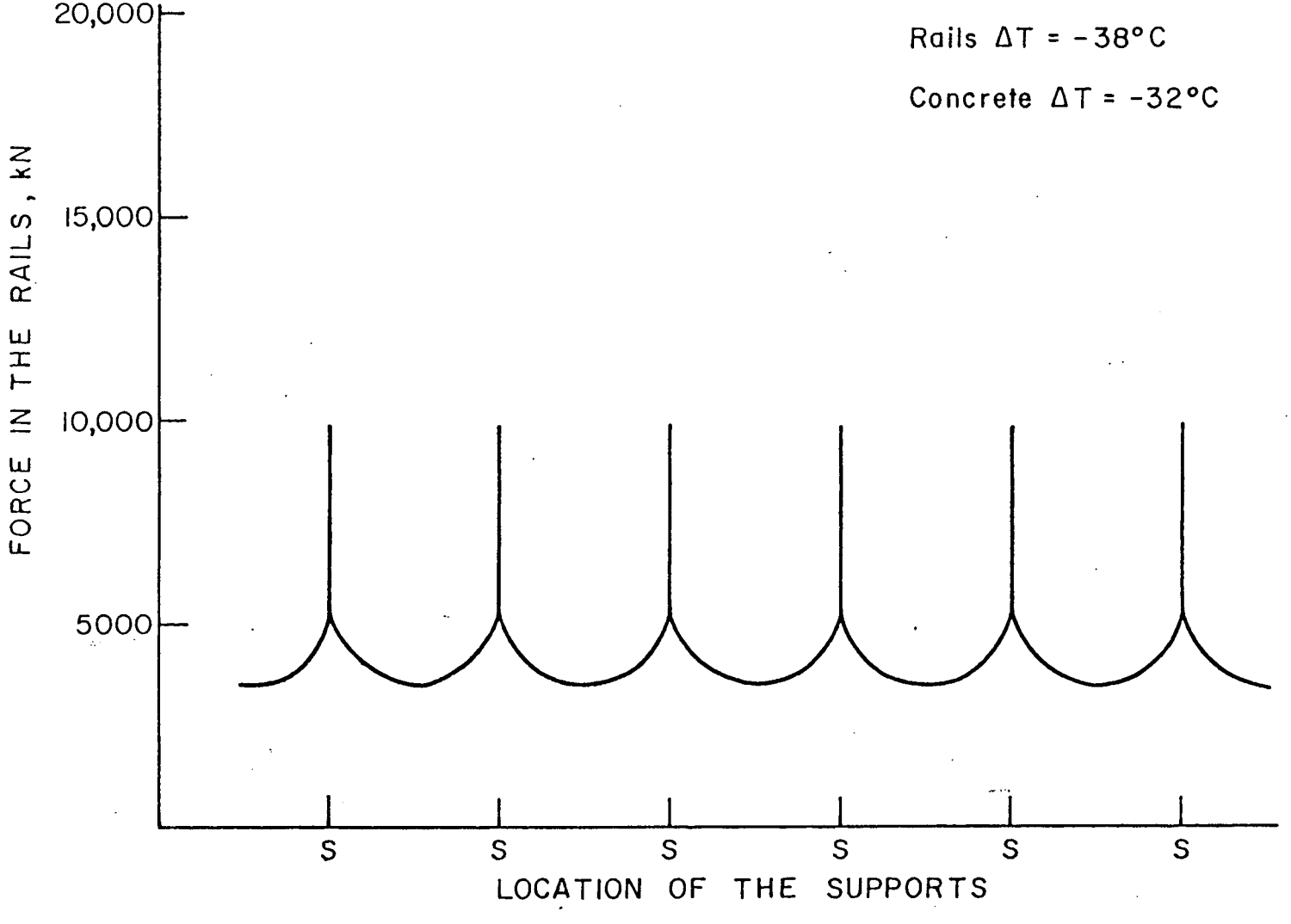

Fig. 32 Computed Variation of Forces in the Rails on the Collingswood Viaduct

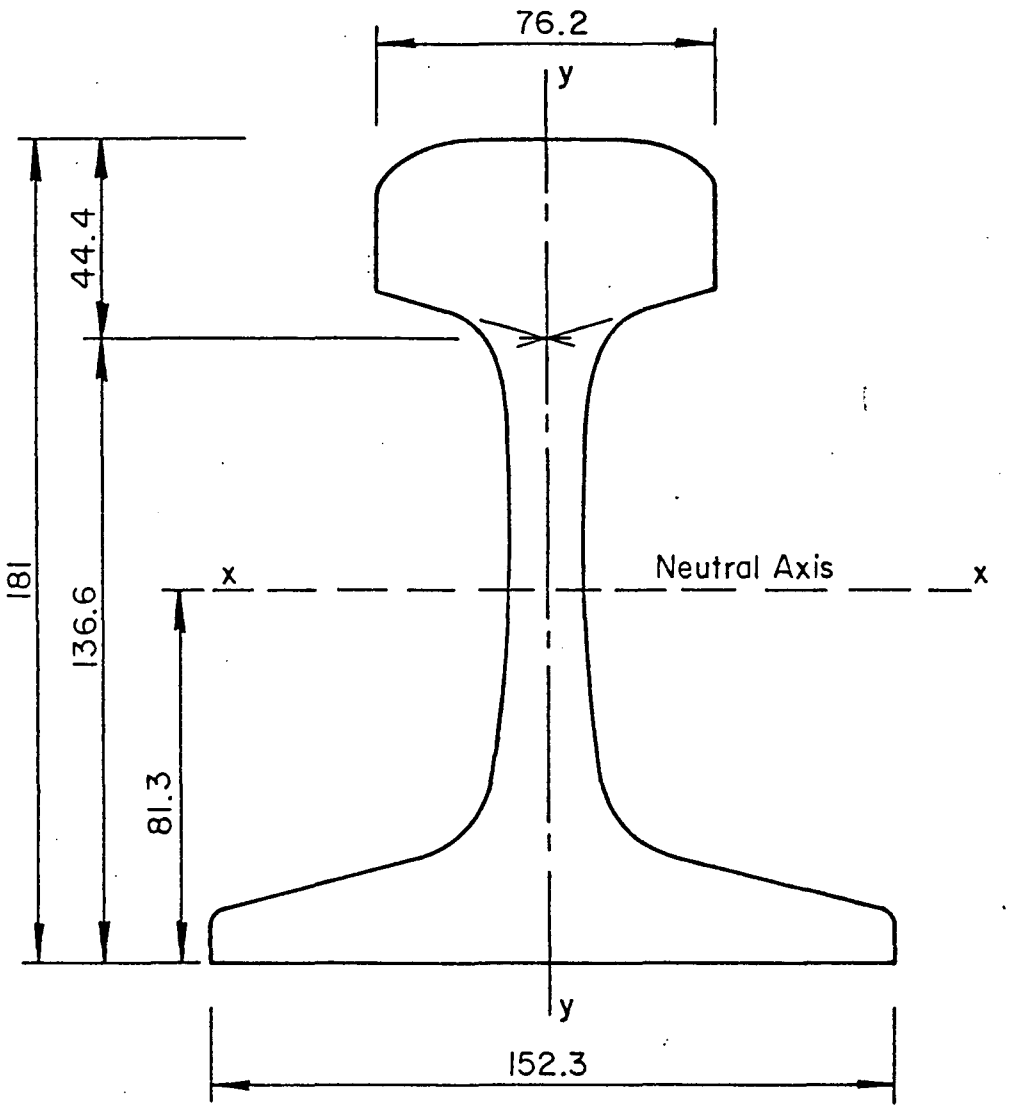

Area = 83.54 cm^2

Moment of Inertia : I_{xx} = 3670.6 cm^4

I_{yy} = 756.3 cm^4

Fig. 33 132 RE Rail

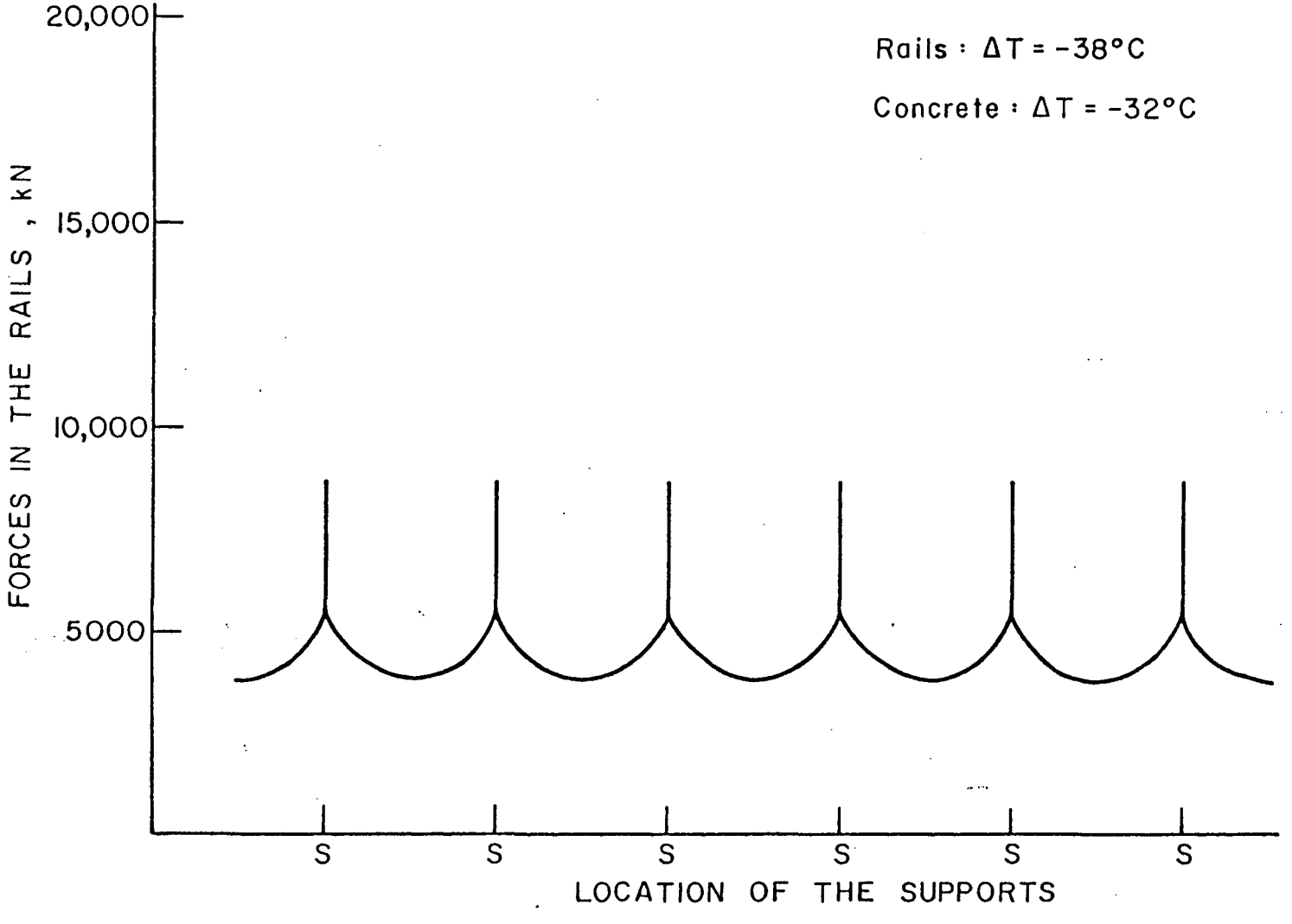

Fig. 34 Computed Variation of Forces in the Rails on the Westmont Viaduct

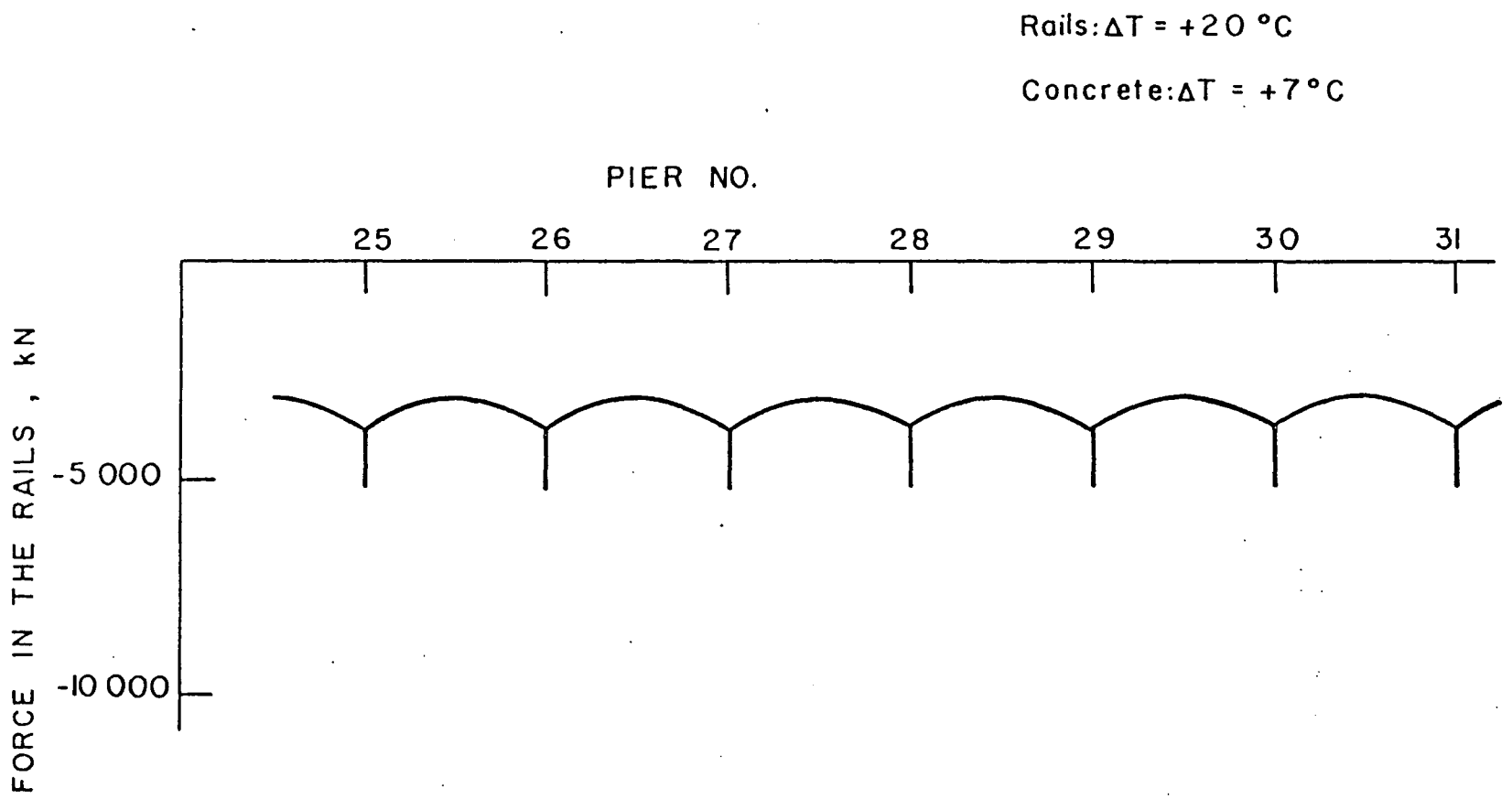

Fig. 35 Computed Variation of Forces in the Rails on the Collingswood Viaduct under Increase of Temperature

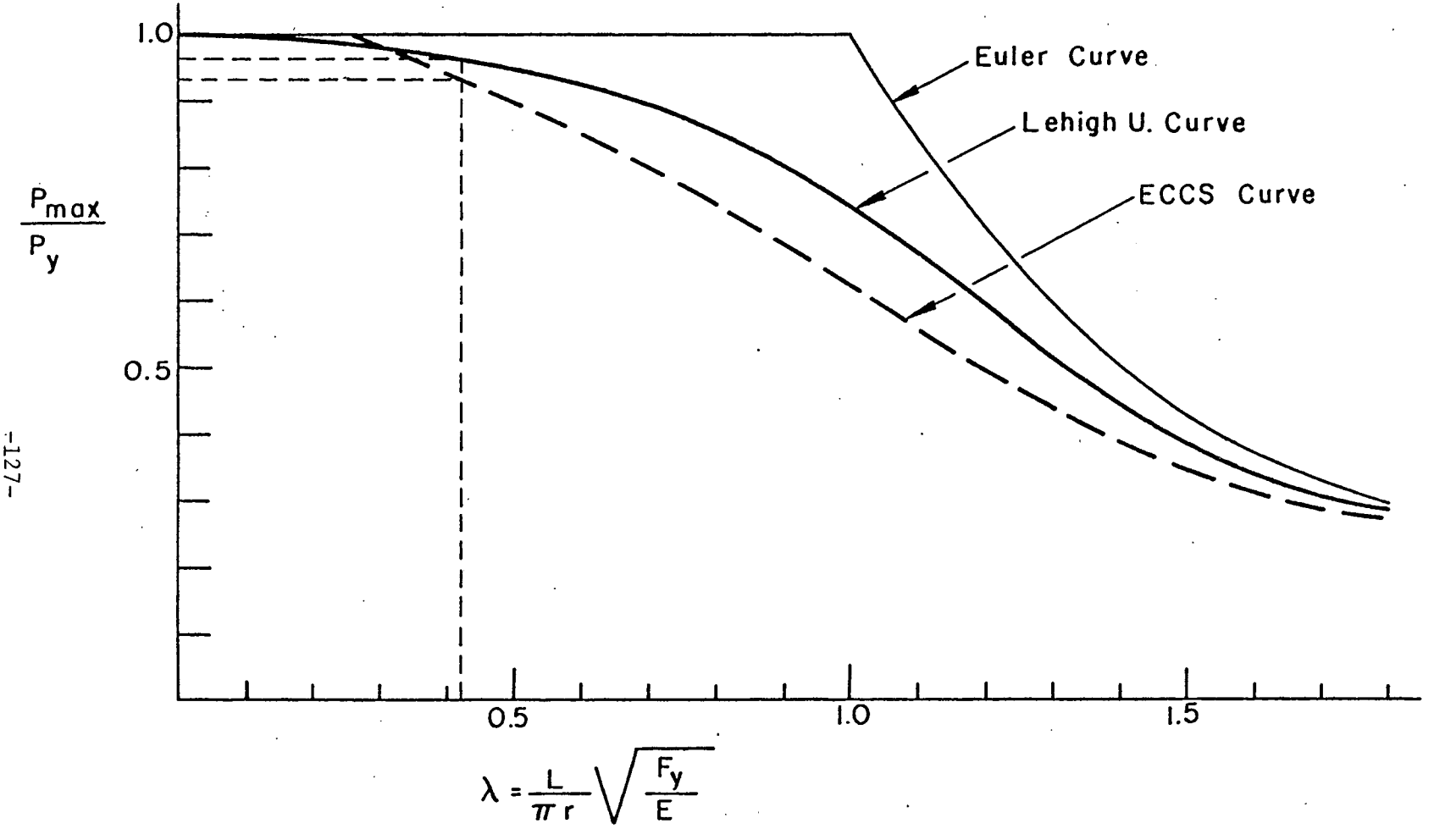

Fig. 36 Column-Strength Curves Developed at Lehigh University and by the European Convention of Constructional Steelwork (ECCS)

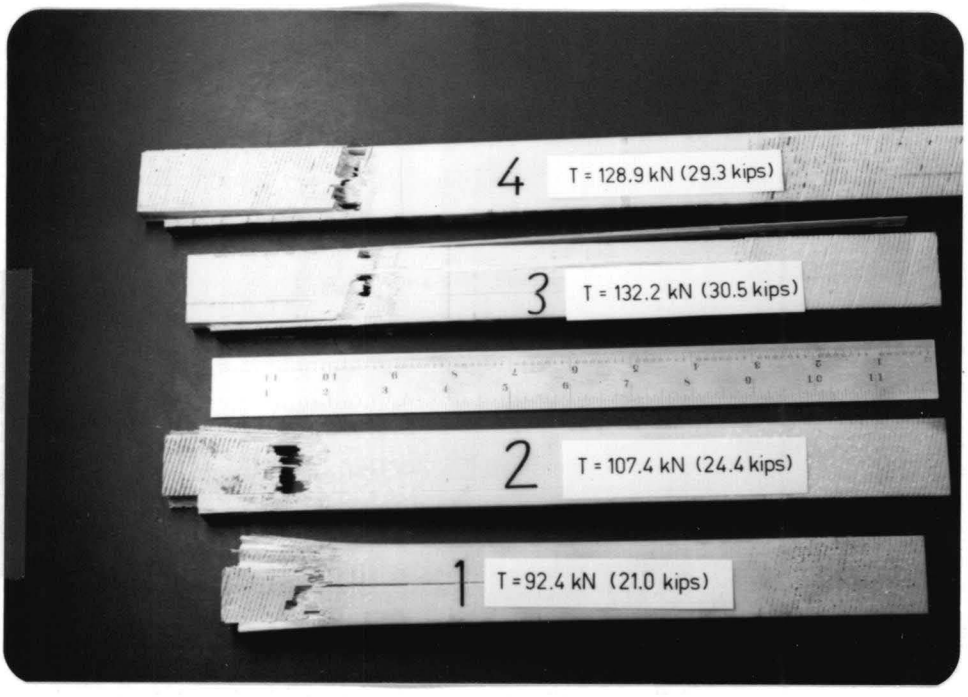

Fig. 37 Fiberglass Bars Tested under Tension after Failure

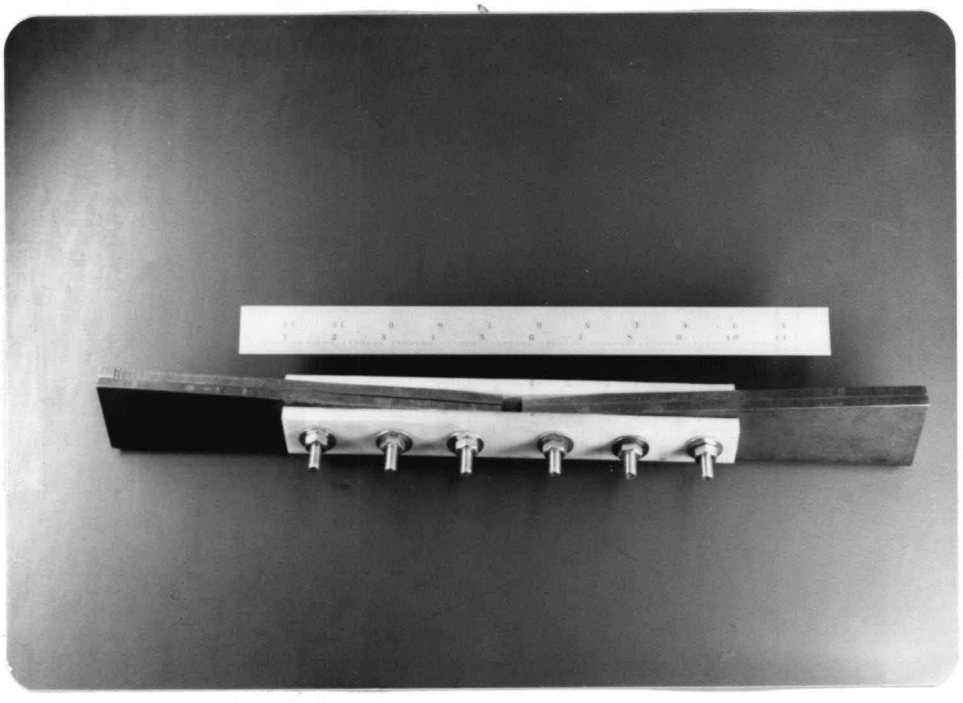

Fig. 38 Fiberglass Joint Model Tested in Tension

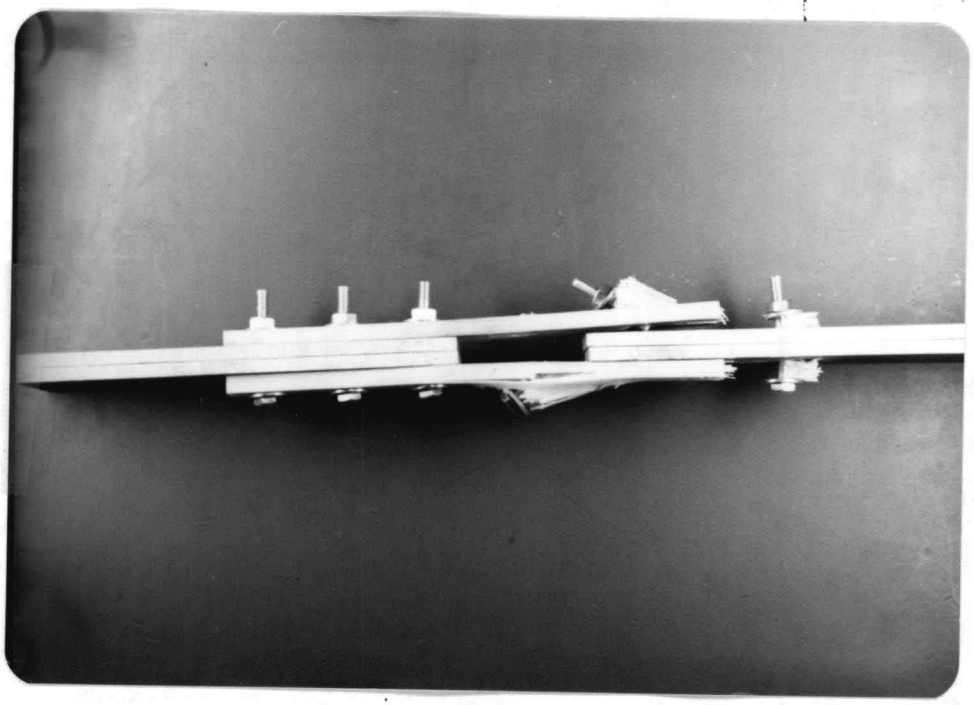

Fig. 39 Fiberglass Strips After Testing

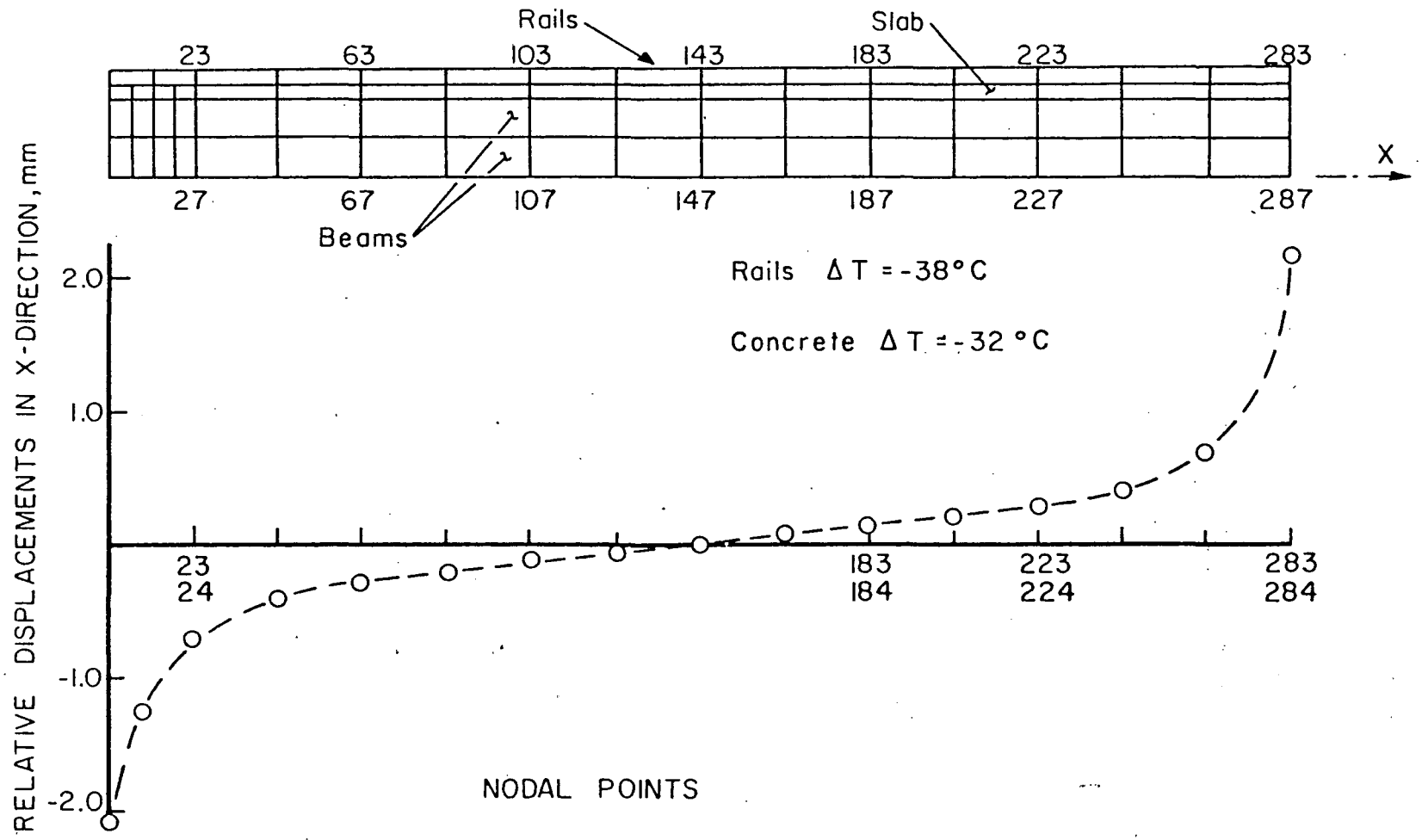

Fig. 40 Computed Relative Displacements Between the Rails and the Slab of Span 6 in the Collingswood Viaduct

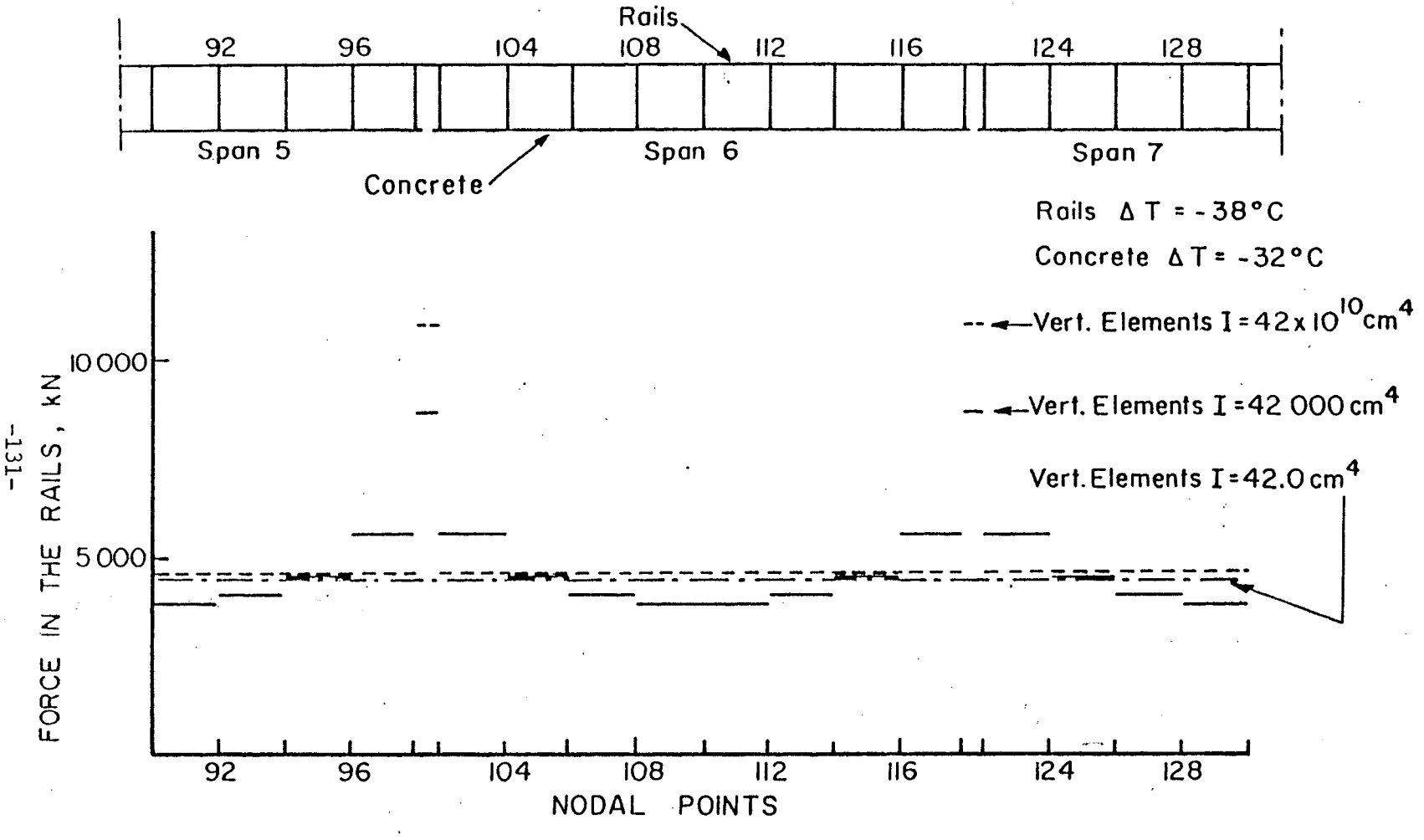

Fig. 41 Computed Axial Force in the Rails in Spans 5, 6 and 7 of Westmont Viaduct

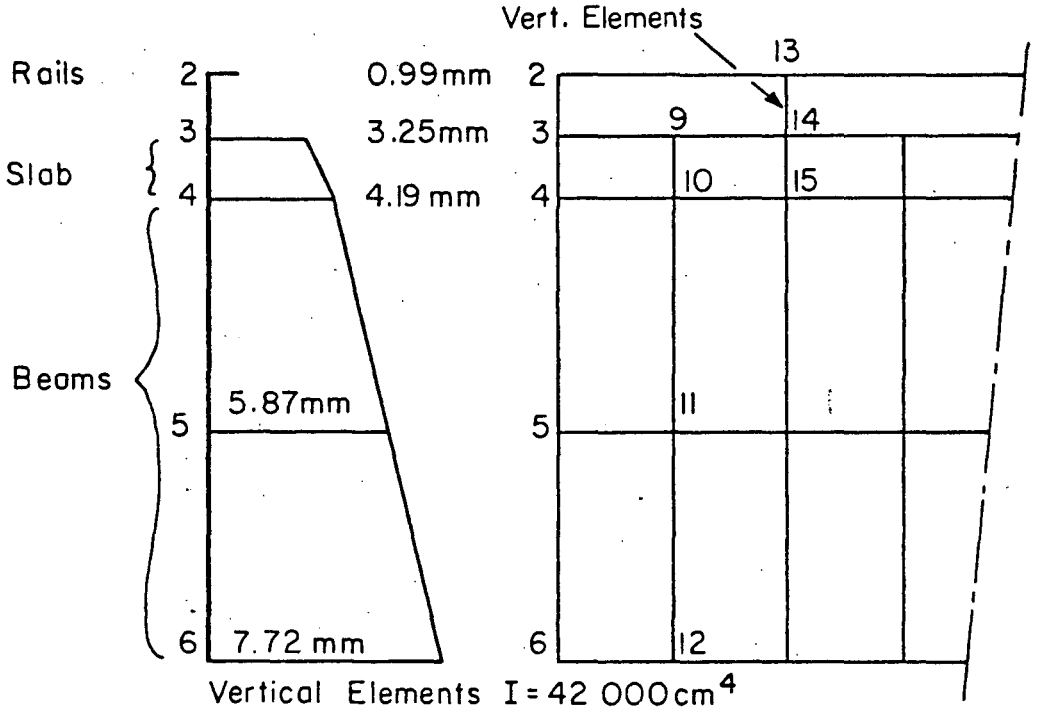

Fig. 42 Longitudinal Displacements of the End of Span 6 of Collingswood Viaduct under Winter Conditions given by One-Span Model

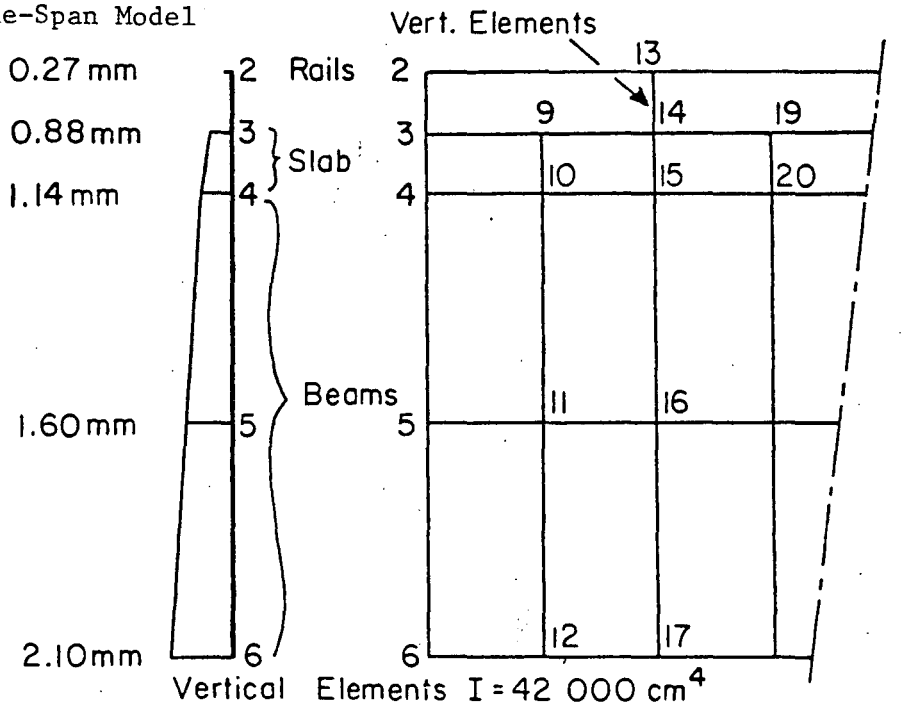

Fig. 43 Longitudinal Displacements of the End of Span 6 of Collingswood Viaduct under Summer Conditions given by the One-Span Model

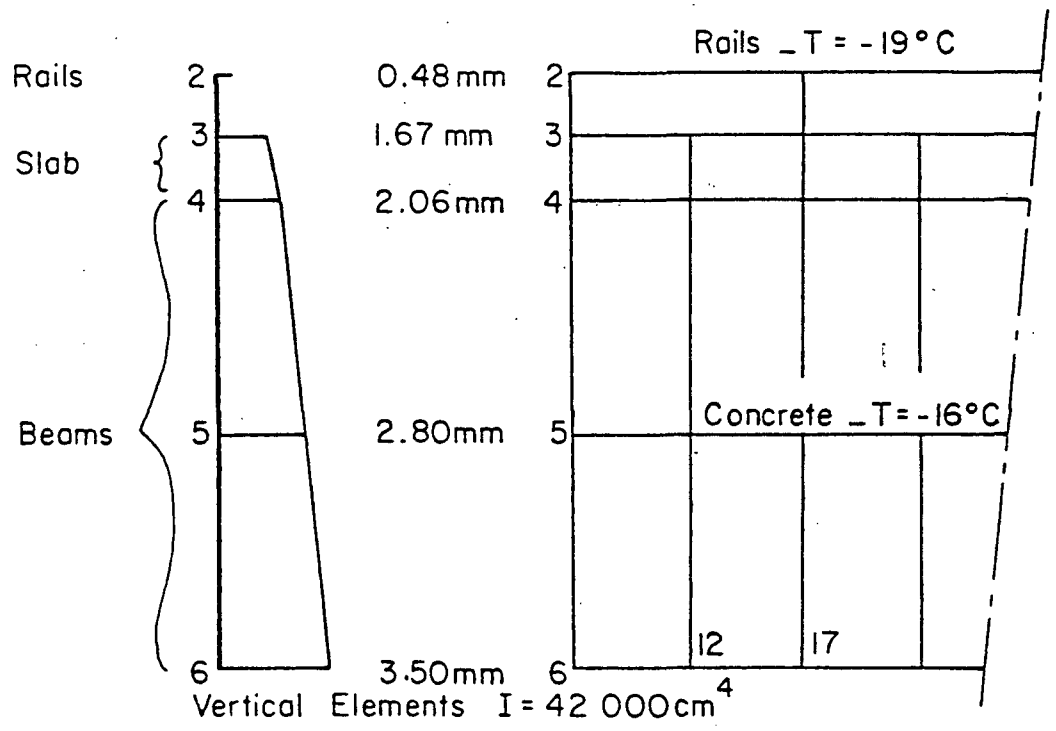

Fig. 44 Longitudinal Displacement of the End of Span 6 of Collingswood Viaduct under an Intermediate Temperature Change

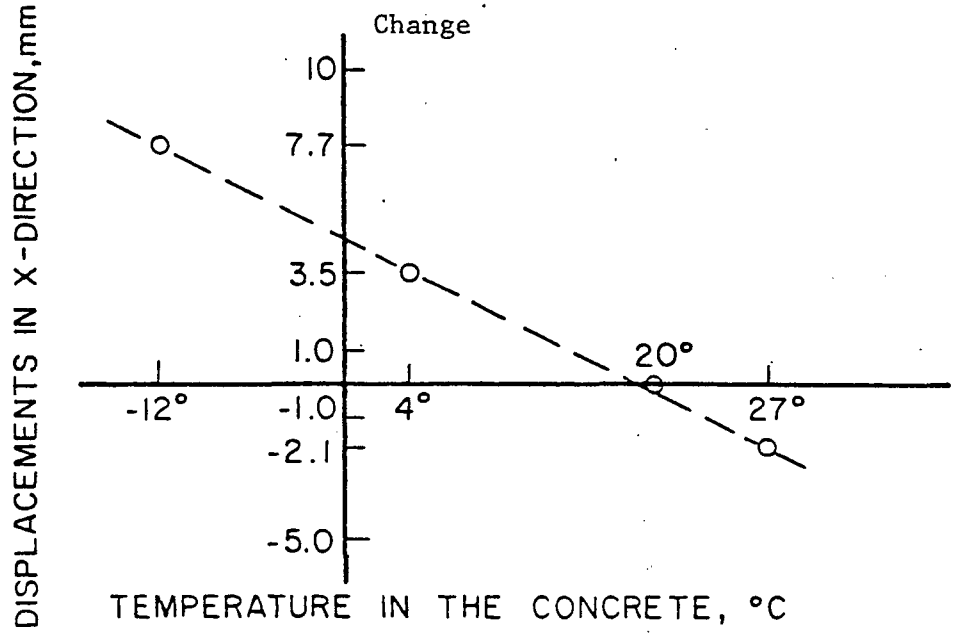

Fig. 45 Displacements of the Bottom of the I-beams in Function of Temperature in the Concrete Computed by the One-Span Model

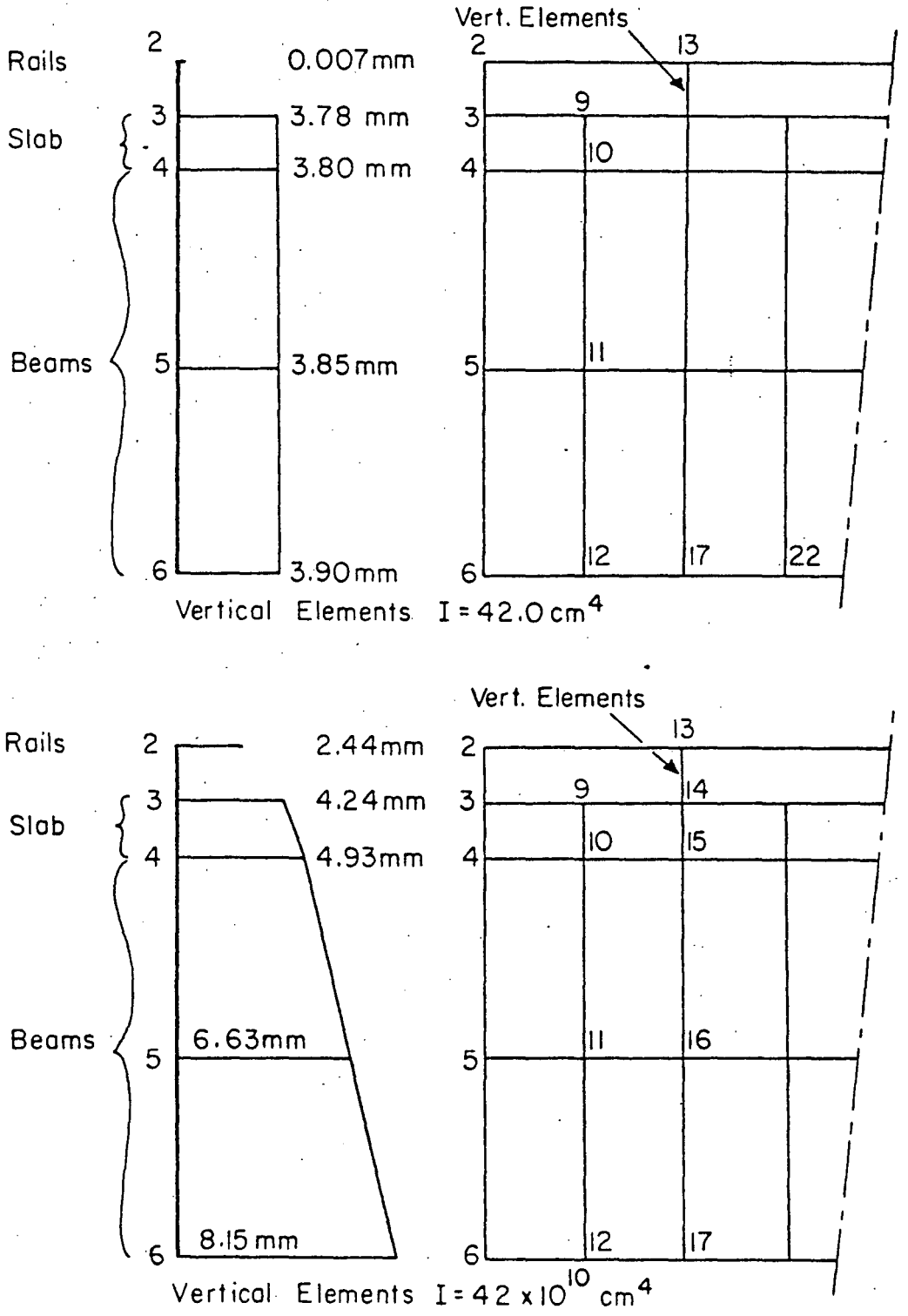

Fig. 46 Longitudinal Displacements of the End of Span 6 of Collingswood Viaduct under Winter Temperature Change with Different Characteristics of the Vertical Elements Given by the One-Span Model

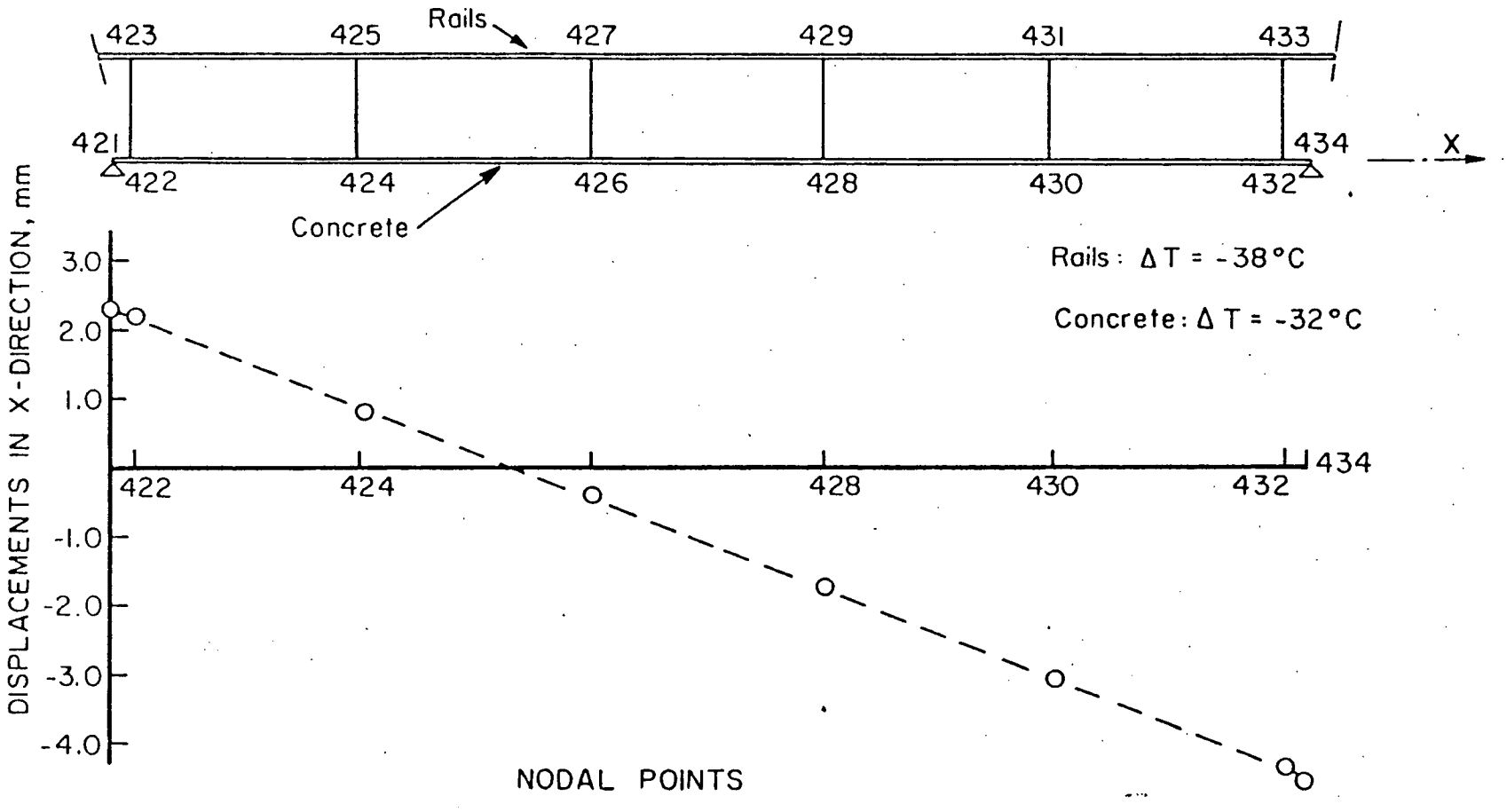

Fig. 47 Longitudinal Displacements of the Concrete Centroid in Span 31 of Collingswood Viaduct as Computed by the E-E Viaduct Model

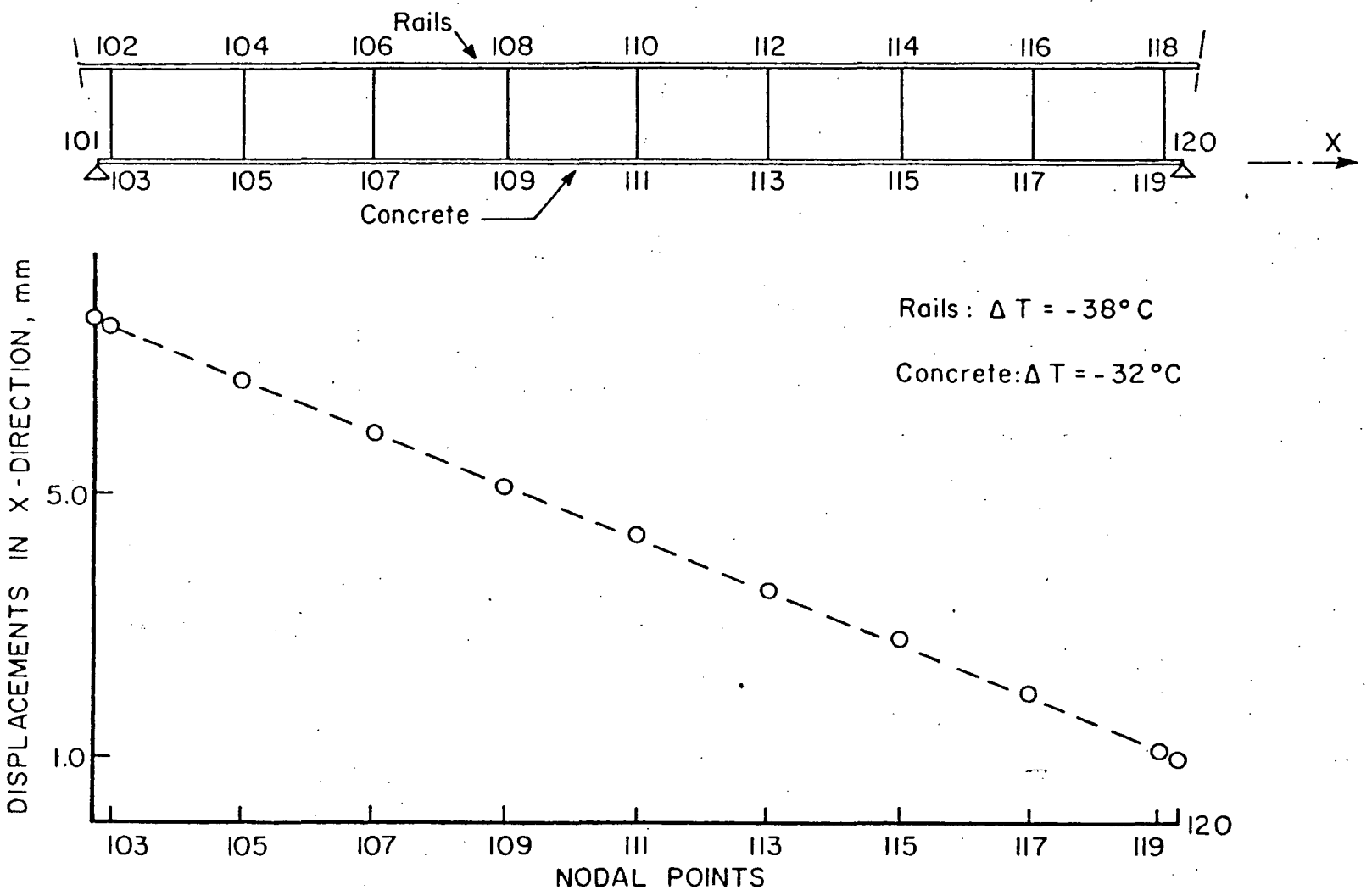

Fig. 48 Longitudinal Displacements of the Concrete Centroid in Span 6 of Westmont Viaduct as Computed by the E-E Viaduct Model

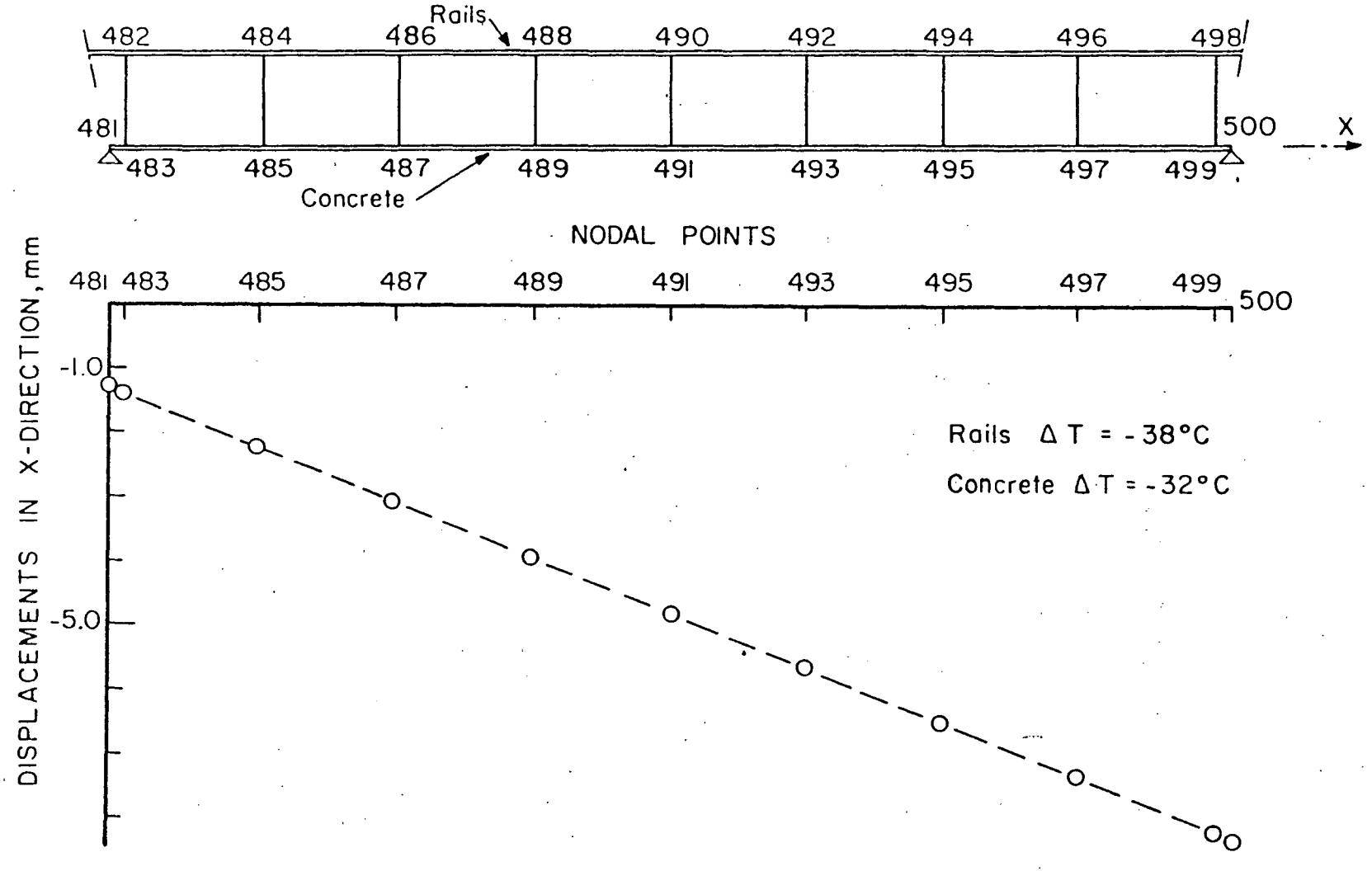

Fig. 49 Longitudinal Displacements of the Concrete Centroid in Span 25 of Westmont Viaduct as Computed by the E-E Viaduct Model

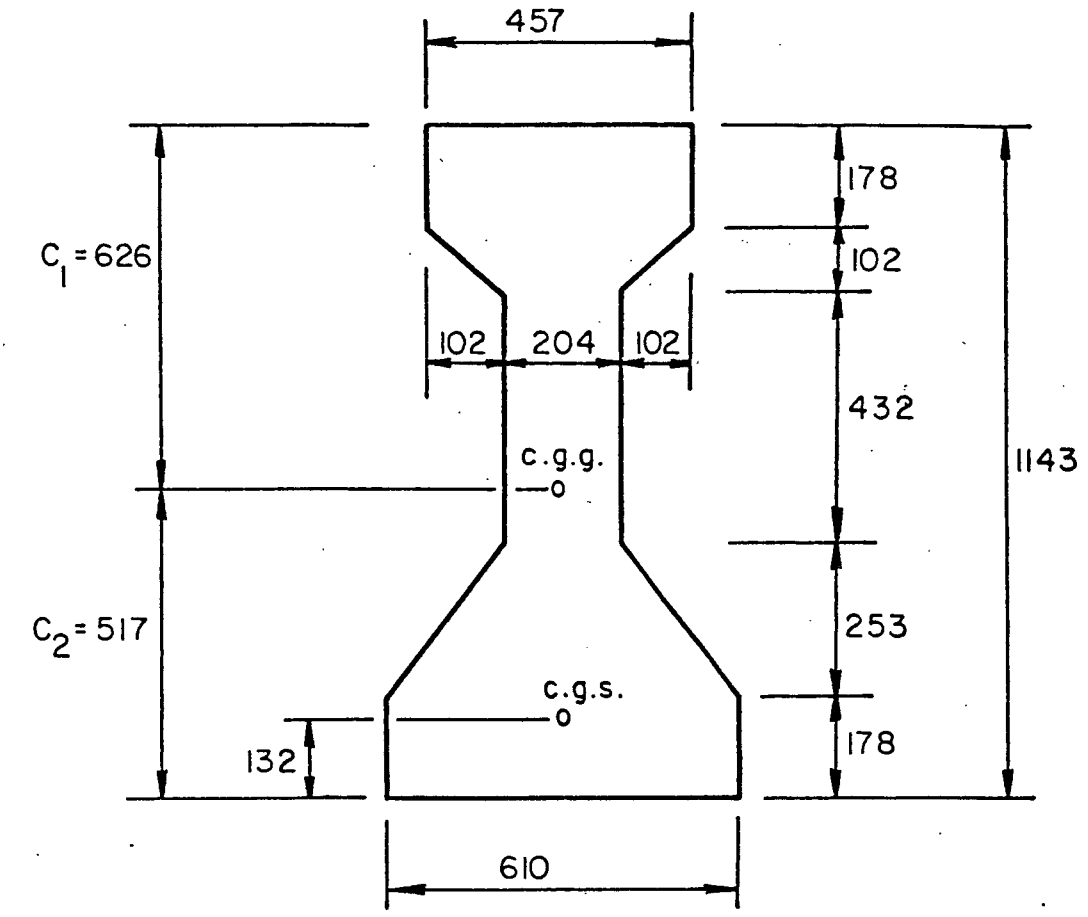

Fig. 50 Cross-Section of the Prestressed I-beam used in the Computation of the Concrete Stresses

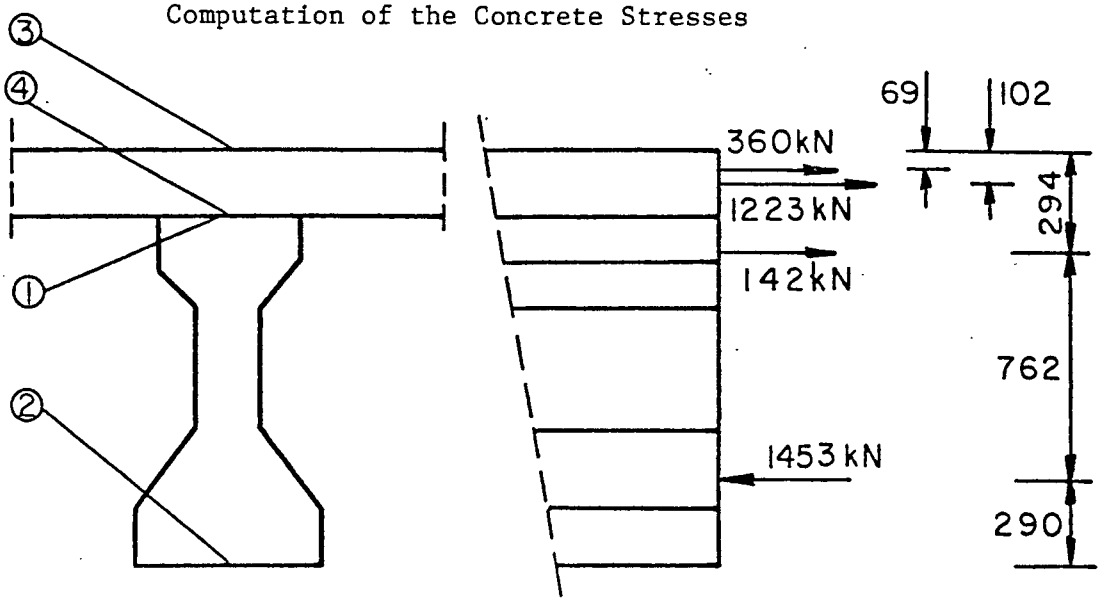

Fig. 51 Internal Forces in the Midspan Section of Span 6 of Collingswood Viaduct due to Winter Temperature Change

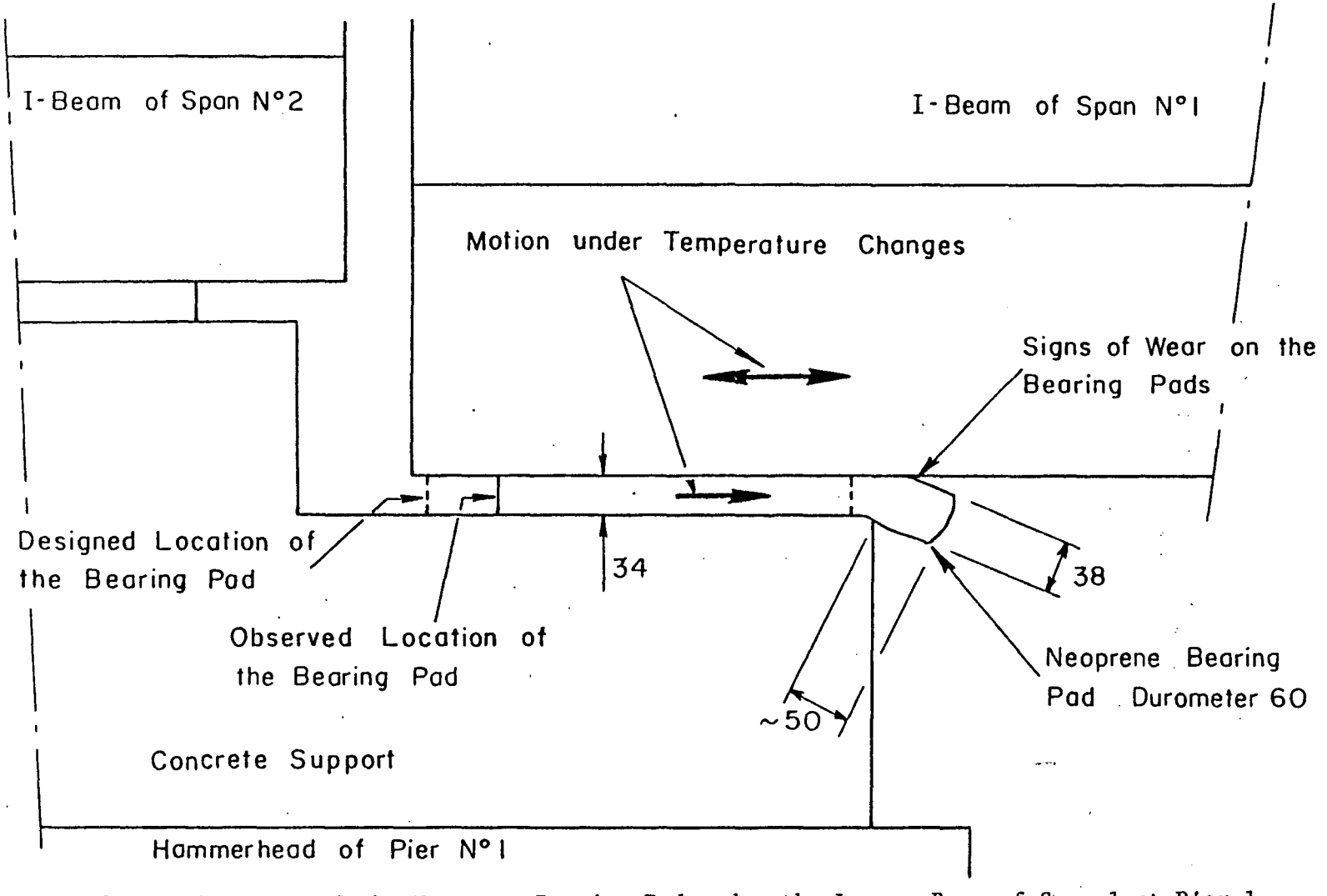

Fig. 52 Displacement of the Neoprene Bearing Pad under the Longer Beam of Span 1 at Pier 1 of Collingswood Viaduct

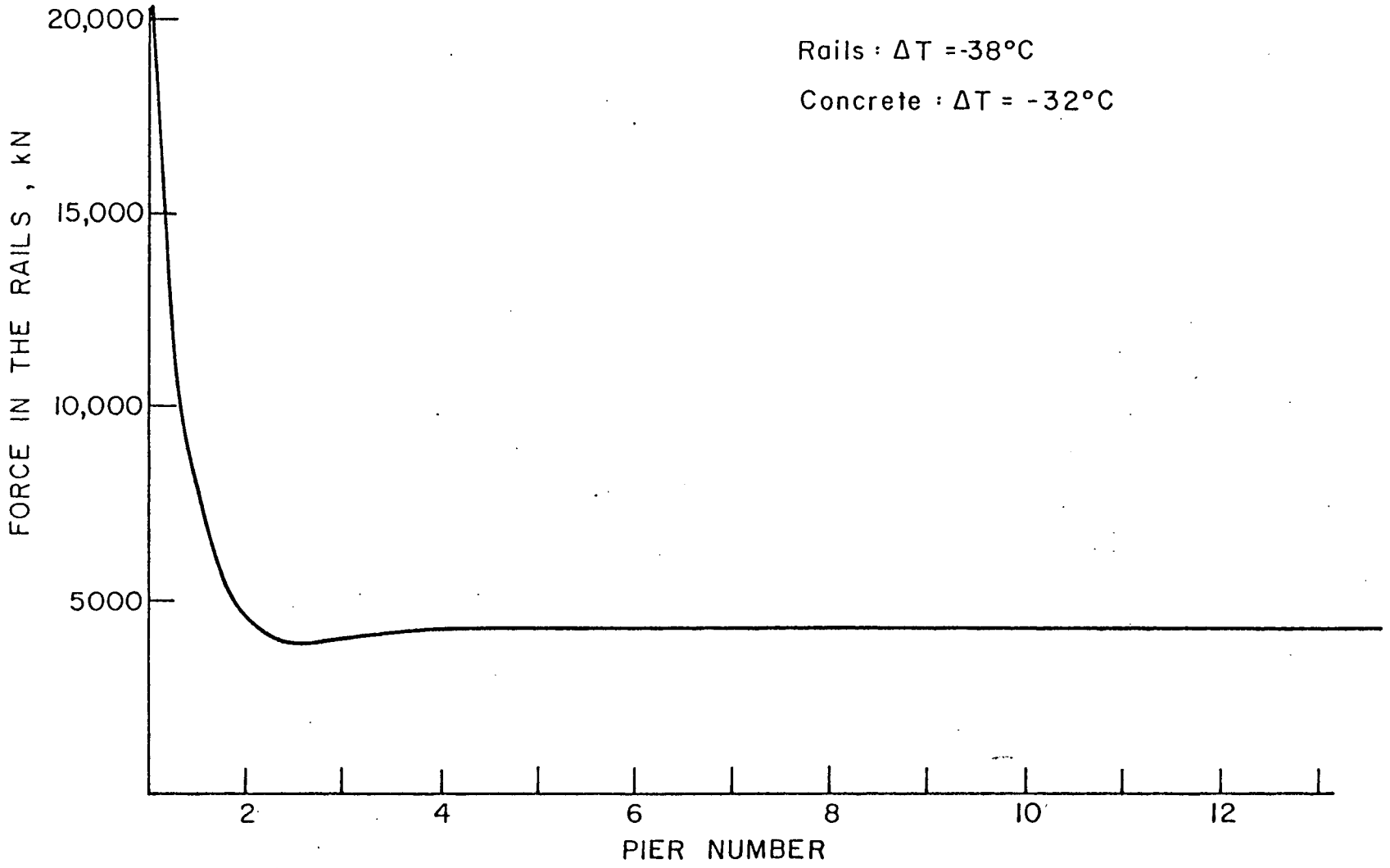

Fig. 53 Variation of the Force in the Rails in a Continuous Viaduct with One Fixed Support

11. REFERENCES

1. Tayabji, S. D., Thompson, M.
   CONSIDERATIONS IN THE ANALYSIS OF CONVENTIONAL RAILWAY TRACK SUPPORT SYSTEM,
   Transportation Engineering Journal, ASCE, Vol. 103, No. TE2, pp. 279-292, March 1977.

2. Middleton, W. D.
   SEOUL CALLS IN PRIVATE ENTERPRISE TO EXPAND THE METRO,
   Railway Gazette International, Vol. 135, No. 11, pp. 1011-1014, November 1979.

3. Wheeler, W. L.
   STATE-OF-ART OF BALLASTLESS TRACK AT-GRADE,
   Transportation Engineering Journal, ASCE, Vol. 102, No. TE1, pp. 131-145, February 1976.

4. Takahara, K.
   JNR EXPERIMENTS WITH CONCRETE TRACK BED,
   The Railway Gazette, Vol. 125, No. 7, pp. 260-262, April 1969

5. Lucas, T. C., Lindsay, D. and Aitken, W. K.
   EXPERIMENTAL CONCRETE TRACK-BED AT RADCLIFFE,
   The Railway Gazette, Vol. 125, No. 14, pp. 547-549, July 1969.

6. Birmann, F.
   GERMAN FEDERAL RAILWAY EXPERIMENTS WITH CONCRETE TRACK BEDS, The Railway Gazette, Vol. 125, No. 8, pp. 308-310, April 1969.

7. Anonymous
   RAILROAD BUILDS "MAINTENANCE FREE" TRACK,
   Engineering News-Record, Vol. 203, No. 8, p. 20, August 1979.

8. Anonymous
   SHIN KANSEN: BUILDING THE FIRST 1000 kM,
   Railway Gazette International, Vol. 127, No. 1, pp. 27-29, January 1971.

REFERENCES (continued)

9. Prud-homme, A.
BUILDING THE WORLD'S FASTEST RAILWAY,
Railway Gazette International, Vol. 127, No. 1,
pp. 51-56, January 1979.

10. DeKalbermatten, G. and Ryser, R.
BRIDGE OVER THE CHANDELARD (in French),
Bulletin Technique de la Suisse Romande, Vol. 99,
No. 9, pp. 138-140, April 1973.

11. Gannett Fleming Corddry and Carpenter, Inc.
DESIGN DRAWINGS OF COLLINGSWOOD AND WESTMONT VIADUCTS,
20 drawings.

12. Gaylord, Edwin H., Jr. and Gaylord, Charles N.
STRUCTURAL ENGINEERING HANDBOOK, pp. 18-31; 18-32,
2nd Ed., McGraw-Hill, New York, 1979.

13. American Railway Engineering Association (AREA)
MANUAL FOR RAILWAY ENGINEERING, p. 4-1-5, AREA,
Chicago, March 28, 1979.

14. Bathe, K. J., Wilson, E. L. and Peterson, F. E.
SAP IV--A STRUCTURAL ANALYSIS PROGRAM FOR STATIC AND
DYNAMIC RESPONSE OF LINEAR SYSTEMS,
Report EERC-73-11, University of California, 1973,
revised April 1974.

15. PATCO-Port Authority Transit Corporation
TEMPERATURE OF THE RAILS WHEN THE RAILS WERE LAID,
2 pages of data, 1968, revised 1978.

16. U. S. Department of Commerce
CLIMATOLOGICAL DATA, Vol. 28, No. 13, Asheville, 1978.

17. Martens, John
RESULTS OF LAST 10 YEARS OF RAIL TESTS,
unpublished results furnished by Mr. John Martens of the
Rail and Truckwork Sale Operation of Bethlehem Steel
Corporation, Bethlehem, PA, 1980.

18. Mareck, Pavel J. and Daniels, Hartley J.
BEHAVIOR OF CONTINUOUS CRANE RAILS,
Journal of Structural Division, ASCE, Vol. 97, No. ST4,
pp. 1081-1095, April 1971.

REFERENCES (continued)

19. Bjorhovde, R. and Tall, L.
MAXIMUM COLUMN STRENGTH AND THE MULTIPLE COLUMN CURVE CONCEPT, Fritz Engineering Laboratory Report 337.29, Lehigh University, 1972.

20. Bjorhovde, R.
DETERMINISTIC AND PROBABILISTIC APPROACHES TO THE STRENGTH OF STEEL COLUMNS, Ph.D. Dissertation, Fritz Engineering Laboratory Report 337.0, Lehigh University, 1972.

21. Sfintesco, D.
EXPERIMENTAL BASIS OF THE EUROPEAN COLUMN CURVES, Journal de la Construction Metallique, No, 3, p. 5, 1970.

22. Beer H. and Schultz, G.
THEORETICAL BASIS OF THE EUROPEAN COLUMN CURVES, Journal de la Construction Metallique, No. 3, p. 58, 1970.

23. Johnston, Bruce G.
GUIDE TO STABILITY DESIGN CRITERIA FOR METAL STRUCTURES FROM THE STRUCTURAL STABILITY RESEARCH COUNCIL, p. 71, John Wiley and Sons, New York, 1976.

24. Boresi, A. P., Sidebottom, O. M., Seely, F. B. and Smith, J. O.
ADVANCED MECHANICS OF MATERIALS, 3rd Ed., John Wiley and Sons, New York, 1978.

25. Fisher, John W., Struik, John H. A.
GUIDE TO DESIGN CRITERIA FOR BOLTED AND RIVETED JOINTS, pp. 84-88, John Wiley and Sons, New York, 1974.

26. Fisher, John W., Daniels, Hartley, J., Slutter, Roger G.
DEVELOPMENT OF DESIGN CRITERIA FOR CONTINUOUS COMPOSITE STEEL-CONCRETE BRIDGES, Fritz Engineering Laboratory Report 359.6, Lehigh University, 1972.

27. American Association of State Highways (AASHTO)
STANDARD SPECIFICATIONS FOR HIGHWAY BRIDGES, AASHTO, 1977.

28. Prestressed Concrete Institute (PCI)
MANUAL FOR STRUCTURAL DESIGN OF ARCHITECTURAL PRECAST CONCRETE, pp. 2-68; 2-70, PCI, Chicago, 1977.

29. Pauw, A.
STATIC MODULUS OF ELASTICITY OF CONCRETE AS AFFECTED BY DENSITY,
Journal ACI, Vol. 32, No. 6, pp. 679-687, December 1960.

30. Nilson, Arthur H.
DESIGN OF PRESTRESSED CONCRETE, Chapter 7
Composite Beams, pp. 241-254, John Wiley and Sons,
New York, 1977.

APPENDIX A - STRESS IN CONCRETE

1. Material Properties

1.1 Prestressed I-Beam

a) Concrete

The concrete compressive cylinder strength given by the designer of the viaducts (11) is f'_{ci} at transfer and f'_c at 28 days:

$$f'_{ci} = 34.47 \text{ MPa } (5000 \text{ psi})$$

$$f'_c = 41.37 \text{ MPa } (6000 \text{ psi})$$

The elastic modulus of the concrete E_c can be computed with reasonable accuracy from the equation proposed by Pauw (29):

$$E_c = 33\, w^{3/2}\sqrt{f'_c} \qquad (A.1)$$

where:

w = unit weight of concrete in pcf

f'_c = compressive cylinder strength in psi.

For normal weight concrete (w = 145 pcf)

$$E_c = 57000\sqrt{f'_c} \qquad (A.2)$$

By introducing the compressive cylinder strength at transfer and at 28 days in Eq. A.2 the elastic modulus at transfer E_{ci} and at 28 days E_c are found:

$$E_{ci} = 27786 \text{ MPa } (4030 \text{ ksi})$$

$$E_c = 30475 \text{ MPa } (4420 \text{ ksi})$$

b) Prestressing Steel

The minimum ultimate strength of the prestressing steel f_{ps} is:

$$f_{ps} = 1860 \text{ MPa } (270 \text{ ksi})$$

The elastic modulus for steel E_s for all steels is about the same (30):

$$E_s = 200000 \text{ MPa } (29000 \text{ ksi})$$

c) Modular Ratios

The modular ratio at transfer n_i and at 28 days n_e are defined:

$$n_i = \frac{E_s}{E_{ci}} = 7.0$$

$$n_e = \frac{E_s}{E_c} = 6.5$$

1.2 Reinforced Concrete Slab

a) Concrete

The concrete compressive cylinder strength at 28 days f'_{cs} is:

$$f'_{cs} = 20.68 \text{ MPa } (3000 \text{ psi})$$

The modulus of elasticity E_{cs} is computed by Eq. A.2

$$E_{cs} = 21526 \text{ MPa } (3122 \text{ ksi})$$

b) Reinforcing Steel

The minimum yields strength of the reinforcing steel f_y is:

$$f_y = 413 \text{ MPa } (60000 \text{ psi})$$

c) Modular Ratios

The modular ratio n_s is defined:

$$n_s = \frac{E_s}{E_{cs}} = 9.0$$

For the computation of the composite section the modular ratio n is defined:

$$n = \frac{E_{cs}}{E_c} = 0.707$$

2. Section Properties

2.1 Gross Section

a) Prestressed I-Beam

The prestressed I-beam used in the computation of concrete stresses is shown in Fig. 50. In the figure c.g.g. is the center of gravity of the concrete gross section and c.g.s. is the center of gravity of the prestressing steel. Gross section properties are as follows:

Gross concrete area	$A_g = 4141.6 \text{ cm}^2$ (642 in^2)
Gross moment of inertia	$I_g = 573.14 \text{ dm}^4$ (137,720 in^4)

Location of c.g.g. $C_1 = 626$ mm (24.6")

Location of c.g.s. $g = 132$ mm (5.2")

Area of prestressing steel $A_{ps} = 28.9$ cm^2 (4.48 in^2)

(39-7/16" strands)

b) The Slab

The dimensions of the slab connected with one beam are taken as b = 2000 mm (78.75") and t = 203 mm (8") where b is the width and t is the thickness.

The composite section with two grades of concrete is modified in one equivalent transformed homogeneous section. The transformed width of the slab b_{tr} is given by:

$$b_{tr} = b \times n = 2000 \times 0.707 = 1414 \text{ mm } (55.68")$$

2.2 Net Prestressed Section

Net prestressed concrete area

$$A_n = 642 - 4.48 = 637.52 \text{ in}^2 \ (4112.7 \text{ cm}^2)$$

Location of the center of gravity of the net prestressed section

$$C_1 = \frac{642(24.63) - 4.48(39.82)}{637.52} = 24.52" \ (622.7 \text{ mm})$$

The prestressing steel eccentricity e measured from the concrete centroid

$$e = 45 - 24.52 - 5.18 = 15.3" \ (389 \text{ mm})$$

The moment of inertia of the net prestressed section

$$I_n = 137720 - 4.48(15.3)^2 + 642(24.63-24.52)^2$$

$$= 136{,}679 \text{ in}^4 \ (568.8 \text{ dm}^4)$$

The section modulus of the net prestressed section are S_{1n} for the top fiber and S_{2n} for the bottom fiber

$$S_{1n} = \frac{136679}{24.52} = 5574 \text{ in}^3 \ (91.33 \text{ dm}^3)$$

$$S_{2n} = \frac{136679}{20.48} = 6674 \text{ in}^3 \ (109.35 \text{ dm}^3)$$

2.3 Transformed Prestressed Section ($n_i = 7$)

Transformed prestressed concrete area

$$A_t = 637.52 + 7(4.48) = 668.88 \text{ in}^2 \ (4315 \text{ cm}^2)$$

Location of the center of gravity of the transformed prestressed section

$$C_1 = \frac{24.52(637.52) + 7(4.48\text{x}39.82)}{668.88} = 25.24" \ (641 \text{ mm})$$

The prestressing steel eccenticity e measured from the concrete centroid

$$e = 45 - 25.24 = 5.18 - 14.58" \ (370 \text{ mm})$$

The moment of inertia of the transformed prestressed section

$$I_t = 136679 + 637.52(25.24-24.52)^2 + 7(4.48\text{x}14.58^2)$$

$$= 143676 \text{ in}^4 \ (597.9 \text{ dm}^4)$$

The section modulus of the transformed prestressed section are S_{1t} for the top fiber and S_{2t} for the bottom fiber

$$S_{1t} = \frac{143676}{25.24} = 5692.4 \text{ in}^3 \ (93.3 \text{ dm}^3)$$

$$S_{2t} = \frac{143676}{19.76} = 7271.1 \text{ in}^3 \ (119.1 \text{ dm}^3)$$

2.4 Transformed Composite Section ($n_e = 6.5$, $n_s = 9$)

Transformed composite concrete section

$$A_{tc} = 637.52 + 6.5(4.48) + 55.68 \times 8 + 8(3.1)$$

$$= 1136.9 \text{ in}^2 \ (7334 \text{ cm}^2)$$

Location of the center of gravity of the transformed composite section

$$C_1 = \frac{24.52(637.52)+6.5(4.48\text{x}39.82)-55.68\text{x}8\text{x}4-8(3.1\text{x}4)}{1136.9}$$

$$= 13.12" \ (333 \text{ mm})$$

The prestressing steel eccentricity e measured from the concrete centroid

$$e = 45 - 13.12 - 5.18 = 26.7" \ (678 \text{ mm})$$

The moment of inertia of the transformed composite section

$$I_{tc} = 136679 + 637.52(13.12-24.52)^2 + 6.5(4.48\text{x}26.7^2)$$

$$+ 55.68 \times 8 \times 17.12^2 + 8 \times 3.1 \times 17.12^2 =$$

$$= 378115 \text{ in}^4 \ (1573.5 \text{ dm}^4)$$

The section modulus of the transformed composite section are S_{1tc}, S_{2tc} and S_{3tc} at the points 1, 2 and 3 shown in Fig. 51.

$$S_{1tc} = \frac{378115}{13.12} = 28819.8 \text{ in}^3 \ (472.2 \text{ dm}^3)$$

$$S_{2tc} = \frac{378115}{31.88} = 11860.5 \text{ in}^3 \ (194.3 \text{ dm}^3)$$

$$S_{3tc} = \frac{378115}{21.12} = 17903 \text{ in}^3 \ (293.3 \text{ dm}^3)$$

3. The Loads

3.1 Prestressed Force

The value of the initial prestressed force P_i is given by the designer of the viaducts (11).

$$P_i = 846.3 \text{ kips } (3765 \text{ N})$$

The prestressed losses are evaluated at 15% (30). The prestressed force after losses P_e is then:

$$P_e = 719.4 \text{ kips } (3200 \text{ N})$$

3.2 Temperature Change

The internal forces computed by the E-E viaduct model in the mid-span section of span 6 of the Collingswood viaduct under the winter conditions are shown in Fig. 51. The positive sign indicates a tension, the negagive sign a compression. These forces are from the top to the bottom of the composite section:

360 kN = 81.0 kips

1223 kN = 275.0 kips

142 kN = 32.0 kips

1453 kN = 326.6 kips

3.3 Self Weight

a) Prestressed I-Beam

Weight per unit length w_o is

$$w_o = A_g \times w = \frac{642}{12^3} 145 = 53.87 \text{ plf } (786.4 \text{ N/m'})$$

The bending moment at mid-span M_o for a simple span beam with a length of 70' (21.34 m) is

$$M_o = \frac{1}{8} \times 0.05387 \times 70^2 \times 12 = 396 \text{ kips-in } (44.75 \text{ kN.m})$$

b) The Slab

Weight per length unit w_d is:

$$w_d = b \times t \times w = \frac{78.75 \times 8}{12^3} 145 = 52.86 \text{ plf } (771.7 \text{ N/m'})$$

The bending moment at mid-span M_{dp} due to the self weight of the slab is:

$$M_{dp} = \frac{1}{8} \times 0.05286 \times 70^2 \times 12 = 388.6 \text{ kips-in } (43.3 \text{ kN.m})$$

The self weight of the beam and the slab are applied to the transformed prestressed section.

3.4 Dead Load

A dead load of 100 psf (4.79 kN/m^2) is applied on the slab. This load represents the weight of the rails, the handrails and other equipment. This load creates a bending moment M_{dc} at mid-span of:

$$M_{dc} = 4824 \text{ kips-in } (545.1 \text{ kN.m})$$

This bending moment is applied to the transformed composite section only.

4. The Stresses in Concrete

4.1 Definitions

The stresses are computed in the four points of the composite concrete section shown in Fig. 51. The equations developed for their computation are based on the usual prestressed concrete theory (30).

The stress in the top fiber of the prestressed I-beam f_1 is given by:

$$f_1 = -P_e\left(\frac{1}{A} - \frac{e}{S_1}\right)_n - \frac{M_o + M_{dp}}{S_{1t}} - \frac{M_{dc}}{S_{1tc}} + \Sigma\ F_T\left(\frac{1}{A} + \frac{a}{S_1}\right)_{tc} \qquad (A.3)$$

where

F_T = the internal forces due to the temperature change

a = distance between the centroid of the composite section and the point of application of F_T.

The stress in the bottom fiber of the prestressed I-beam f_2 is given by:

$$f_2 = -P_e\left(\frac{1}{A} + \frac{e}{S_2}\right)_n + \frac{M_o + M_{dp}}{S_{2t}} + \frac{M_{dc}}{S_{2tc}} + \Sigma\, F_T\left(\frac{1}{A} + \frac{a}{S_2}\right)_{tc} \qquad (A.4)$$

The stress in the top fiber of the slab f_3 is given by:

$$f_3 = \left[-\frac{M_{dc}}{S_{3tc}} + \Sigma\, F_T\left(\frac{1}{A} + \frac{a}{S_3}\right)_{tc}\right] x\ n \qquad (A.5)$$

The stress in the bottom fiber of the slab f_4 is given by:

$$f_4 = \left[-\frac{M_{dc}}{S_{1tc}} + \Sigma\, F_T\left(\frac{1}{A} + \frac{a}{S_1}\right)_{tc}\right] x\ n \qquad (A.6)$$

4.2 Computation

From Eq. A.3:

$$f_1 = -719.4\left(\frac{1}{637.52} - \frac{15.3}{5574}\right) - \frac{396 + 388.6}{5692.4} - \frac{4824}{28820}$$
$$+ 81.0\left(\frac{1}{1136.9} + \frac{15.82}{28820}\right) + 275.0\left(\frac{1}{1136.9} + \frac{17.12}{28820}\right)$$
$$+ 32.0\left(\frac{1}{1136.9} - \frac{9.55}{28820}\right) - 326.6\left(\frac{1}{1136.9} - \frac{20.45}{28820}\right)$$

$$= 1.02 \text{ ksi } (7.03 \text{ MPa})$$

From Eq. A.4

$$f_2 = -719.4\left(\frac{1}{637.52} + \frac{15.3}{6674}\right) + \frac{396 + 388.6}{7271} + \frac{4824}{11860}$$
$$+ 81.0\left(\frac{1}{1136.9} + \frac{15.82}{11860}\right) + 275.0\left(\frac{1}{1136.9} + \frac{17.12}{11860}\right)$$

$$+ 32.0\left(\frac{1}{1136.9} + \frac{9.55}{11860}\right) - 326.6\left(\frac{1}{1136.9} + \frac{20.45}{11860}\right)$$

$$= -2.25 \text{ ksi } (-15.5 \text{ MPa})$$

From Eq. A.5

$$f_3 = 0.707\left[-\frac{735}{17903} + 81.0\left(\frac{1}{1136.9} - \frac{15.82}{17903}\right)\right.$$
$$+ 275.0\left(\frac{1}{1136.9} - \frac{17.12}{17903}\right) + 32.0\left(\frac{1}{1136.9} - \frac{9.55}{17903}\right)$$
$$\left. - 326.6\left(\frac{1}{1136.9} - \frac{20.45}{17903}\right)\right] = 0.024 \text{ ksi } (165 \text{ kPa})$$

From Eq. A.6

$$f_4 = 0.707\left[-\frac{735}{28820} + 81.0\left(\frac{1}{1136.9} + \frac{15.82}{28820}\right)\right.$$
$$+ 275.0\left(\frac{1}{1136.9} + \frac{17.12}{28820}\right) + 32.0\left(\frac{1}{1136.9} - \frac{9.55}{28820}\right)$$
$$\left. - 326.6\left(\frac{1}{1136.9} - \frac{20.45}{28820}\right)\right] = 0.323 \text{ ksi } (2.23 \text{ MPa})$$

APPENDIX B NOMENCLATURE

A	Area of the cross-section
A_g	Area of the gross concrete section
A_n	Area of the net prestressed section
A_{ps}	Area of prestressing steel section
A_t	Area of the transformed prestressed concrete section
A_{tc}	Area of the transformed composite concrete section
a	Distance between the centroid of the composite section and the point of application of the force
b	Width of the reinforced concrete slab or length of bearing pad
b_{tr}	Transformed width of the reinforced concrete slab
c_1	Distance between the center of gravity of the concrete section and the top of the prestressed I-beam
E	Expansion support or modulus of elasticity of the material
E_c	Elastic modulus of the concrete at 28 days
E_{ci}	Elastic modulus of the concrete at transfer
E_{cs}	Elastic modulus of the reinforced concrete slab at 28 days
E_s	Elastic modulus of the steel
E_1, E_2	Elastic modulus of the materials
e	Prestressing steel eccentricity or longitudinal displacement of bearing pad

F	Fix support
F_a	Axial stress that would be permitted if axial force alone existed
F_b	Compressive bending stress that would be permitted if bending alone existed
F_T	Internal forces due to temperature change
F_u	Ultimate tensile strength of the rails
F_y	Yield point of the steel
f_a	Computed axial stress
f_b	Computed compressive bending stress at the point under consideration
f'_c	Concrete compressive cylinder strength at 28 days
f'_{ci}	Concrete compressive cylinder strength at transfer
f_{ps}	Minimum ultimate strength of the prestressing steel
f_y	Minimum yield strength of the reinforcing steel
f_1, f_2, f_3 f_4	Stresses in the concrete at points 1, 2, 3 and 4
G	Shear modulus of elasticity
g	Distance between the center of gravity of the prestressing steel and the bottom fiber of the prestressed I-beam
I	Moment of inertia of the cross-section
I_g	Moment of inertia of the gross concrete section
I_n	Moment of inertia of the net concrete section

I_t	Moment of inertia of the transformed prestressed concrete section
I_{tc}	Moment of inertia of the transformed composite concrete section
K	Effective length factor
L	Length of the column centrally loaded or length of the span
M	Bending moment
M_{dc}	Bending moment at midspan created by the dead load
M_{dp}	Bending moment at midspan due to the self weight of the reinforced concrete slab
n, n_e, n_i, n_s	Modular ratios
P	Concentrated load
P_e	Prestressed force after losses
P_i	Initial prestressed force
P_{max}	Maximum strength allowable on a centrally loaded column
P_y	Yielding strength
r	Radius of gyration
S_{1n}, S_{2n}	Section modulus of the net prestressed concrete section
S_{1t}, S_{2t}	Section modulus of the transformed prestressed concrete section

$S_{1tc'}$, S_{2tc}, S_{3tc}	Section modulus of the transformed composite concrete section
T	Shearing force at bearing
t	Thickness of the reinforced concrete slab
w	Unit weight of the concrete or width of bearing pad
w_o	Weight of the prestressed I-beam per unit length
w_d	Weight of the reinforced concrete slab per unit length
α_1, α_2	Coefficients of thermal expansion of the material
ΔT_1, ΔT_2	Temperature change applied to the materials
λ	Nondimensional slenderness ratio

Abbreviations

AREA	American Railway Engineering Association
BR	British Railways
CRC	Column Research Council (since 1976 Structural Stability Research Council)
CRTSS	Conventional Railway Track Support System
DB	German Federal Railways
ECCS	European Convention for Construction Steelwork
JNR	Japanese National Railways
JRA	Japanese Railroad Association
JRM	Japanese Railroad Maintenance

LIRR	Long Island Railroad
PATCO	Port Authority Transit Corporation
PCI	Prestressed Concrete Institute
SI	International System of Units
SNCF	French National Railways
SSRC	Structural Stability Research Council

Units

As general rule the SI units are used in this thesis. In the text the stresses are given in both systems, SI and American. In the figures only the SI units are used. The following rules have been adopted:

1. All the lengths are in millimeters (mm) for the lengths smaller than 10 m.
2. The lengths are in meters (m) for the lengths longer or equal to 10 m.

In the table below are given conversion factors for used units:

SI	AMERICAN
.1 mm	0.03937 in.
1 m	3.2808 ft.
1 mm^2	0.00155 $in.^2$

SI	AMERICAN
1 N	0.2248 lbf
1 kN	0.2248 kips
1 kN/m^2 = 1 kPa	20.8855 psf
1 MN/m^2 = 1 MPa	0.145 ksi

Abbreviations for Units

^oC	Degree Celsius (centigrade)
cm	Centimeter
dm	Decimeter
^oF	Degree Fahrenheit
ft	Foot
in	Inch
ksi	Kips per square inch
lb	Pound
lbf	Pound force
mm	Millimeter
N	Newton
Pa	Pascal
psi	Pounds per square inch

VITA

The author, son of Henri Lavanchy and Marie-Louise (Rebuz) Lavanchy, was born in Geneva, Switzerland on February 7, 1953.

After graduating from Calvin College in Geneva in 1974, the author enrolled at the Swiss Federal Institut of Technology (E.P.F.) in Lausanne where he completed the civil engineering studies in January 1979.

In August 1979, the author entered graduate school in the Department of Civil Engineering, Lehigh University where he studied toward a Master of Science Degree.